Pumping and tracer test in a limestone aquifer and model interpretation

Akacievej, Hedehusene

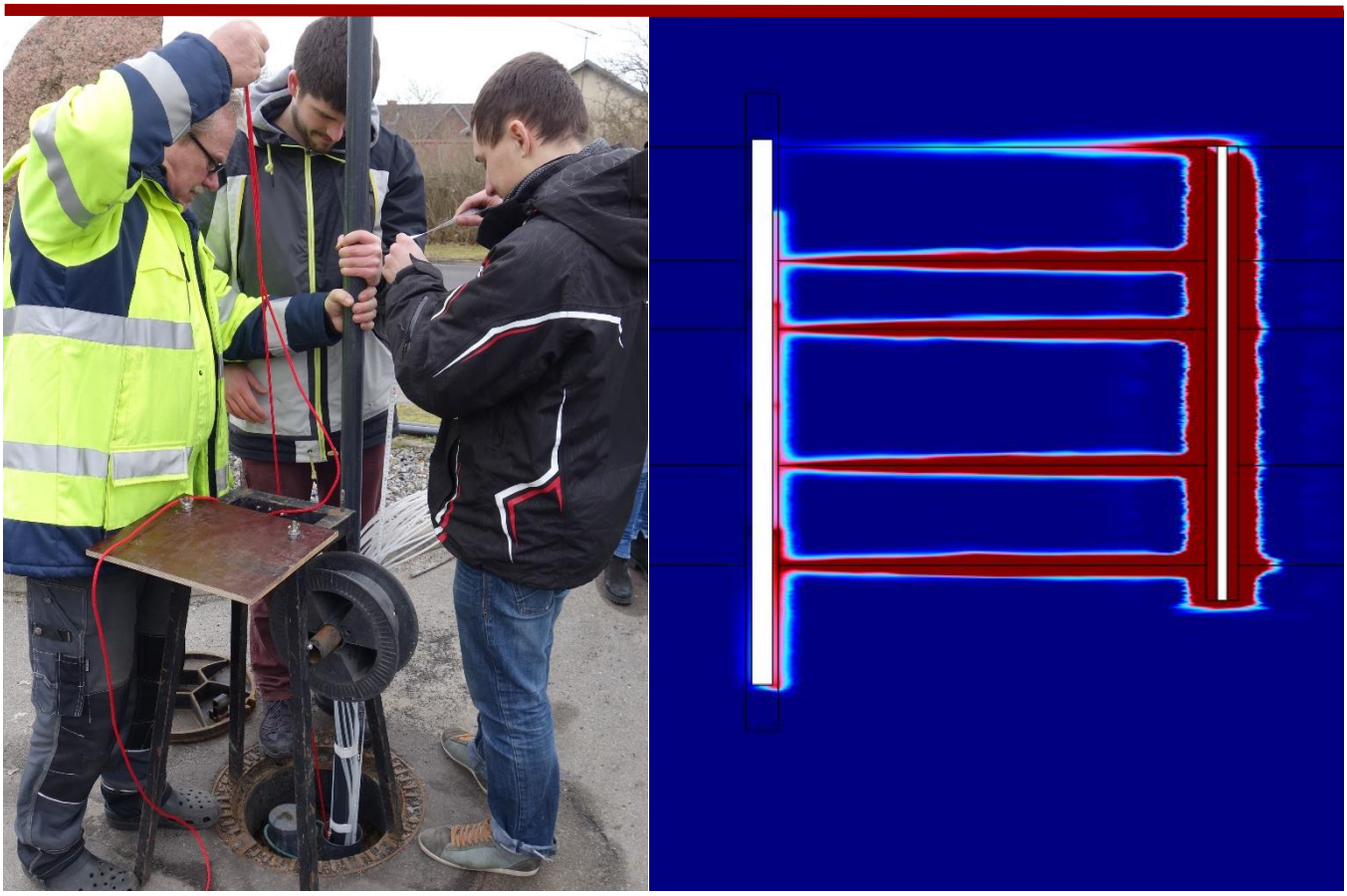

Klaus Mosthaf, Bentje Brauns, Mette M. Broholm, Poul L. Bjerg, Magnus M. Rohde, Christian Helweg, John U. Bastrup and Philip J. Binning

DTU Environment, November 2016

DTU Environment
Department of Environmental Engineering

GEO SUBSURFACE EXPERTISE
REGION H
The Capital Region of Denmark

DTU Environment

Report
November 2016

By Klaus Mosthaf, Bentje Brauns, Magnus M. Rohde, Christian Helweg, John U. Bastrup, Mette M. Broholm, Poul L. Bjerg and Philip J. Binning

Published by: Department of
Environmental Engineering, Bygningstorvet

Preface

This report is part of the Region H Limestone Project, a collaboration between DTU Environment at the Technical University of Denmark (termed DTU) and Region H about the fate of contaminants in fractured limestone aquifers. The limestone project aims at improving our understanding of contaminant transport in limestone aquifers. The project involves a combination of field and lab work, and modeling of field data. The work was conducted at Akacievej, Hedehusene, a former dry cleaning facility, where there is now a major chlorinated solvent contaminant spill and plume.

The field work was conducted by DTU and GEO, with GEO being subcontracted to assist in conducting the pumping test, including measurements and the geological characterization of the site. DTU was responsible for the remainder of the field and lab work, including the tracer tests and chlorinated solvent contaminant sampling at the site. The pumping test was planned by DTU and GEO, with GEO being responsible for executing the test and evaluating the data in collaboration with DTU. The modelling of the pumping and tracer test data was conducted by DTU.

This report describes the pumping and tracer test and the data interpretation, including modeling of results. Most of the report was written by DTU. Chapters 3 and 4 describe the outcomes of the pumping test and were written by GEO and are in Danish.

In the framework of this project, several other reports and student theses have been written which are relevant for the work presented in this report:

- Pedersen et al. (2014), *Overblik over lokaliteter i værkstedsområderne*
  Provides an overview and evaluation of six contaminated sites that are suitable for investigation of flow and transport processes in limestone.
- Geo/GEUS (2014), *Strømning og stoftransport i kalklagene på den Københavnske Vestegn*.
  Explains the overall geology in the area southwest of Copenhagen.
- Geo (2015), *Geologisk og hydrogeologisk undersøgelse – Resultater og konceptuel model*
  Describes the hydrogeological details at the Akacievej study site employed for the pumping and tracer test.
- Broholm et al. (2016b), *Sammenligning af niveauspecifikke prøvetagningsmetoder for vurdering af koncentrationsfordeling i kalkmagasin*
  Describes and compares different sampling techniques in limestone aquifers. The report discusses the contaminant distribution and dynamics at the Akacievej site and includes the contaminant measurements collected before, during and after the pumping and tracer test.
- An online wiki, https://limestone.env.dtu.dk, will be published by the beginning of 2017 with the following contents:
  - Data acquisition and field methods
  - Development of a conceptual model for a field site (example: Akacievej)
  - Modeling objectives and guideline
  - Model types and modeling tools

- Model setup for fracture flow and transport in a limestone aquifer
- Field data and model calibration
- Practical outcomes of the models and methods
- Links to existing tools, reports and literature

Three short notes describe the properties of the selected tracers, and evaluate the risk of the tracer injection and the remedial pump stop at the Akacievej site:

- Mosthaf et al. (2015a), *Tracer selection for the pump and tracer test at the Akacievej site*
  Mosthaf et al. (2015b), *Risk assessment of the tracer injection at the Akacievej site*
- Mosthaf et al. (2015c), *Effects of remedial pump stop for 6 months at the Akacievej site*

Three student theses were written related to the pumping and tracer test in the Akacievej project, providing additional details:

- Jørgensen, *Bestemmelse af hydrauliske parameter i sprækket kalkmagasin ved simple slugtest*, Bachelor Thesis, Jan. 2016.
- Besora, *Design and verification of tracer injection test for contaminant transport characterization of a fractured limestone aquifer*, Master Thesis, July 2016.
- Tsitseli, *Conceptual understanding of the impacts of pumping on the distribution dynamics of PCE in limestone*, Master Thesis, June 2016.

The following researchers from DTU Environment have been involved in the limestone project: Klaus Mosthaf, Bentje Brauns, Annika S. Fjordbøge, Mette M. Broholm, Poul L. Bjerg and Philip J. Binning.

Technical assistance at DTU was provided by Bent Skov, Jens S. Sørensen, Flemming Møller, Satomi Matsuura, Hanne Bøggild and Mikael Olsson. The students Pau Besora, Theodora Tsitseli and David Collet assisted with the fieldwork.

The following people from GEO have been involved in the limestone project:
Johanne Aaberg Andersen, Magnus M. Rohde, Christian Helweg, John U. Bastrup and Remi Chalmas.

Project participants from Region H were:
Henriette Kern-Jespersen, Niels Døssing Overheu and Anna Toft.

Copenhagen, 2016

Contents

1. Background and introduction

1.1 Background

This report presents the results of a pumping and tracer test, conducted as part of the Region H Limestone project. The project aims to improve the understanding of the transport and fate of contaminants in fractured limestone aquifers and to identify and develop appropriate tools for the assessment and remedial planning of contaminated sites.

The overall goals of the Region H Limestone project are:

- To enhance the **conceptual understanding** of the behavior of contaminants in fractured limestone aquifers, which are one of the major drinking water resources in Denmark
- To develop and test appropriate **mathematical models** for the quantitative description of processes, e.g. for risk assessment or the planning of a remediation strategy
- To test and evaluate **field methods** for the determination of relevant hydraulic data and transport properties, which are a prerequisite for modeling
- To test and compare **sampling and analysis methods** for the characterization of contaminants (distribution in the aquifer, localization of DNAPL)
- To contribute to the development and evaluation of contaminant **remediation methods**

Modeling is an integrated part of the project. Modeling was employed at an early stage of the project to plan measurements and fieldwork and was based on preliminary site knowledge. The models helped to develop a conceptual understanding of the site (see Figure 1.1). After collection of the field data, modeling was used to interpret the data and further improve a site conceptual model.

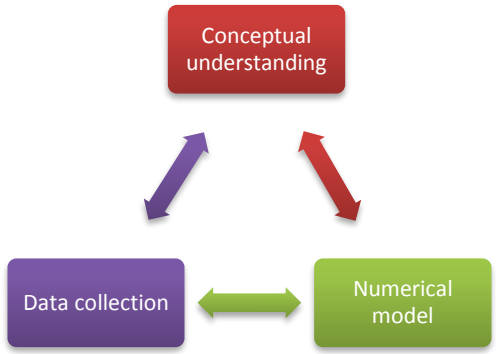

Figure 1.1: Close link between model development, fieldwork and measurements, and update of the conceptual understanding.

To achieve the project goals, a contaminated site in Denmark was chosen as a representative test case. Selection criteria were a short depth to the limestone and a location with prioritized drinking water interests. Pedersen et al. (2014) contains a discussion of different potential sites and the criteria. Based on that, the site located at Akacievej 2 in Fløng, Hedehusene (southwest of Copenhagen) was

chosen for further investigations. It is referred to as the Akacievej site in the following.

1.2 Aims of the pumping and tracer test

To characterize the contaminant hydrogeology at the Akacievej site and to obtain model parameters that can be used for the testing of different model concepts, a long-term pumping test combined with six tracer injections and simultaneous PCE sampling was conducted in spring 2016.

The pumping and tracer test combined with PCE sampling served several goals:

- To provide data which can be used to **obtain and test a fundamental understanding of the mechanisms of contaminant transport in limestone aquifers**, and thereby improve risk assessment, contaminant plume management and selection of remediation alternatives
- Improve the basis for **developing conceptual models** of limestone contaminated sites
- To obtain **field data to test several modeling concepts** for contaminant transport in limestone, namely the equivalent porous medium (EPM) model, the discrete fracture model (DFM) and the dual continuum model (DCM)
- To test methods for obtaining relevant **hydraulic and transport parameters** for contaminant transport models
- To determine the PCE distribution at the site using **concentration measurements** (see Broholm et al. 2016b)
- To develop **predictive tools** and provide **guidance** for future contaminated site investigations

1.3 Site history

At the Akacievej site, a dry cleaning facility was operating in the period 1973-2003. In 2002, the site was screened for contamination. This revealed high concentrations of PCE and TCE in the pore air close to where a dry cleaning facility operated in the years between 1973 and 1975. Most of the contamination is likely to be from the operation of the dry cleaning facility and a release during a fire at the site in 1975. The contamination was evaluated to pose a potential risk for the drinking water extraction at the Fløng waterworks, which has its closest extraction well about 600 meters north of the Akacievej site.

In 2007, the most contaminated soil containing PCE as DNAPL was removed and extensive remedial activities were started. The following actions were taken:

- Removal of contaminated soil in the source area 0-6 m bgs. Local excavation down to the limestone surface at about 8 m bgs. (limestone is found below ca. 7.5 m bgs.)
- Establishment of venting pipes at the excavated surface 6 m bgs.
- Establishment of a drainage pipe at the deepest excavated area 8 m bgs.
- Remedial pumping to establish hydraulic control
- Activated carbon filtering of the pumped water and reinfiltration of the purified water through infiltration cassettes with an overflow connected to a deep borehole
- Construction of a building for the activated carbon filter system

The goal of the remedial activities was to remove the hotspot and to achieve hydraulic control of the groundwater contamination. An overview of the excavated area, the contamination hotspot and the PCE concentration isolines in 2006 are shown in Figure 1.2.

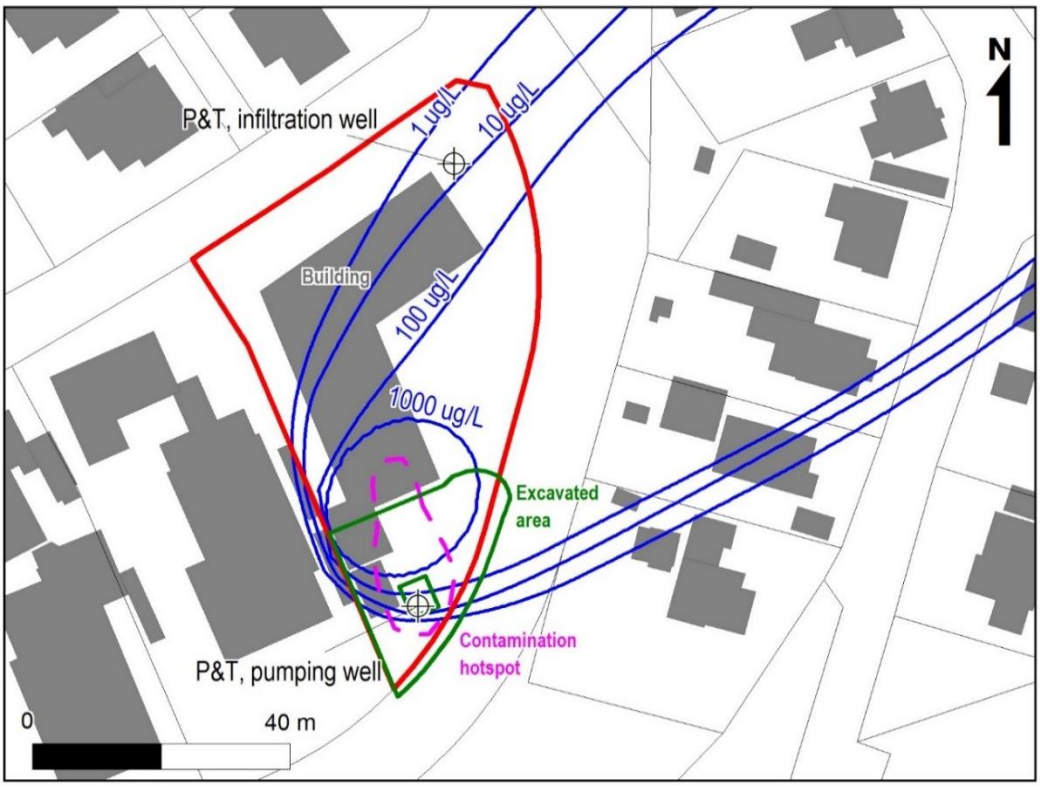

Figure 1.2: Overview map with the source zone (hotspot, pink dashed line) before the remedial activities started. The red line delineates the property boundary and the green line shows the area that was excavated. The blue contours show the PCE concentration isolines in 2006 before the start of remedial activities.

The remediation system was started in 2007 and continuously removes PCE. Before the installation of the remediation system, a dissolved PCE plume had evolved with a length of about 500 m in a northeastward direction (see Figure 1.3). Model simulations have shown that the infiltration system partly pushes the plume southeastwards. This has been confirmed by field measurements in monitoring wells at the site.

1.4 Previous investigations

Previous investigations at the site can be subdivided into two phases. The investigations in the first phase had the goal of identifying and delineating the contamination, of identifying the risk for the groundwater resource and forming a basis for the remedial activities. These investigations were conducted in the period between 2004 and 2008 (Geo 2005a, Geo 2005b, Geo 2006, Geo 2008).

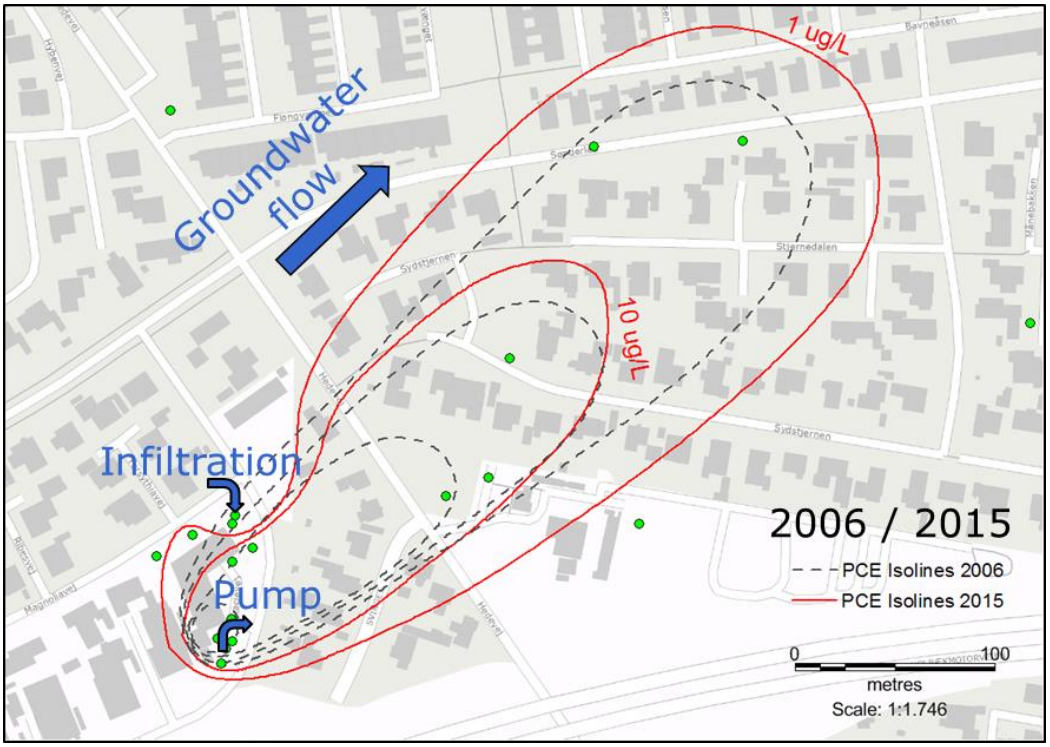

Figure 1.3: Contaminant plume at Akacievej in 2006 (before remediation), and 2015. The concentration isolines are based on the maximum concentrations found in the limestone (predominantly in crushed limestone or top of fractured limestone). The green dots indicate the location of monitoring wells. The location of the remedial pump and infiltration well are also shown. The reinfiltration of the remediated water pushed parts of the plume southeastwards.

The second phase of the investigations began in 2014 and had a goal of improving the knowledge about the fate of the contamination in limestone. It included the development and testing of detailed models, as well as a comparison of sampling techniques (Broholm et al. 2016b). This report contains data and results from the investigations in the second phase (Geo & GEUS 2014, Geo 2015). Broholm et al. (2016b) presents contaminant data of the Akacievej site.

1.5 Geology and hydrogeology

In the course of the project, a geologic model of the Akacievej site was created based on borehole data and prior knowledge (Geo and GEUS, 2014). It is further described in Geo (2015). Figure 1.4 depicts a geologic cross section at the Akacievej site. The location of the cross section is shown in Figure 1.5.

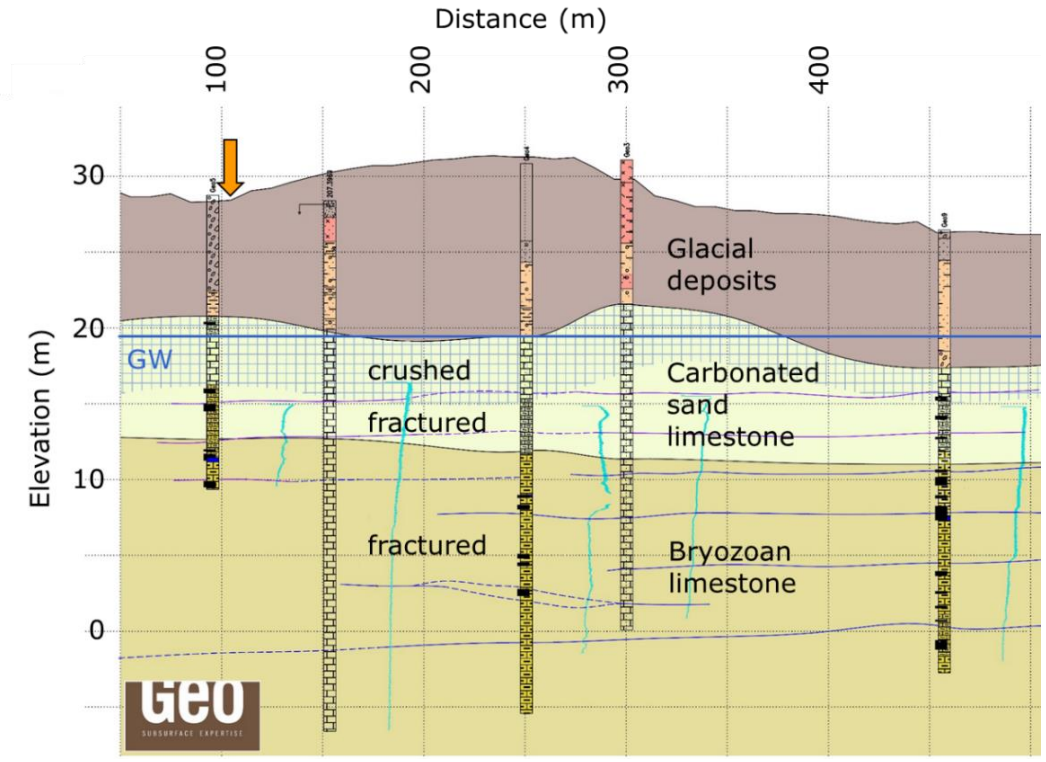

Figure 1.4: Geologic cross section (SW-NE) at the Akacievej site, showing the major geologic layers and the approximate location of the groundwater table. The orange arrow indicates the location of the Akacievej site.

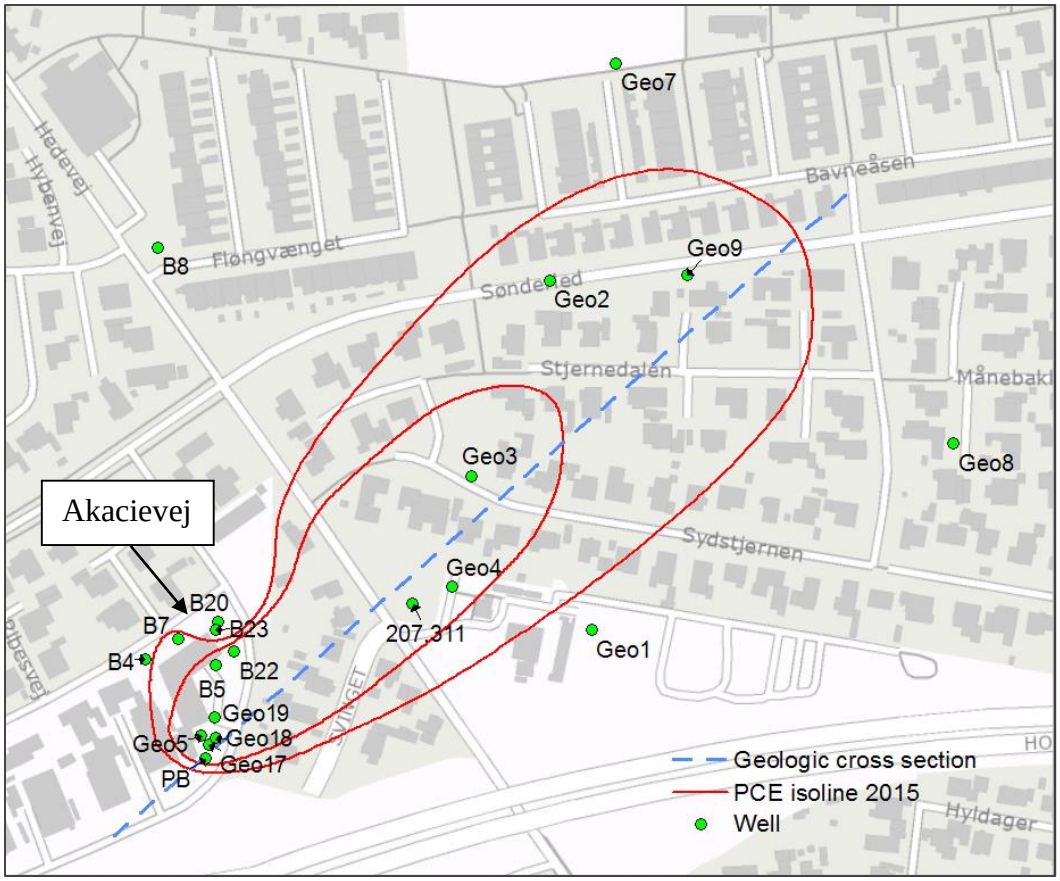

Figure 1.5: Overview of boreholes, location of geologic cross section (dashed blue line) and extent of contaminant plume without pumping in the upper limestone (2015), see Broholm et al. (2016b).

The top layer consists of tertiary glacial deposits with mainly fine material. Below about 8-10 m bgs., a carbonated sand limestone also known as Copenhagen chalk is found. The discovery of the Copenhagen chalk at the site was unexpected and changed the prevailing knowledge of the geology in the area. Below the Copenhagen chalk is a bryozoan limestone layer. Due to glacial activity, the uppermost 1-5 meters of the limestone are crushed. The crushed limestone is mainly in the Copenhagen limestone, but the crushed layer penetrates in some parts of the investigation area into the bryozoan limestone.

The limestone below the crushed layer is fractured with many chert inclusions and nodules (see Figure 1.6 which shows some core samples from the site). With a strong conductivity contrast between fractures and matrix (several orders of magnitude difference in the hydraulic conductivities), flow predominantly occurs in the fractures. However, transported substances diffuse into the matrix, which provides a relatively high porosity and a large storage capacity. Investigations in this project (flow logs) showed that groundwater flow occurs down to about 36 m bgs. (-7 m asl.), with only very little flow below that. This indicates that there are very few fractures below this depth.

Figure 1.6: Borehole core samples from previous investigations (Geo4 and Geo9) showing crushed and fractured limestone with flint inclusions. Note that most of the fractures seen in the core samples were caused by the drilling.

The hydraulic heads in the area around the site were determined in a synchronous sounding round by DTU and Geo in the spring of 2015. Figure 1.7 shows the head measurements and the isopotential map based on that sounding round. The average hydraulic gradient at the site is approximately 0.7 to 1 ‰ towards ENE. The water table at the site was at about 19 m asl., leaving the upper part of the crushed limestone layer unsaturated. However, close to the site confined conditions can also be found. The unsaturated part is quite small compared to the estimated aquifer thickness of 21 meters and drawdowns during the pumping test are small, so the aquifer can be considered to be confined.

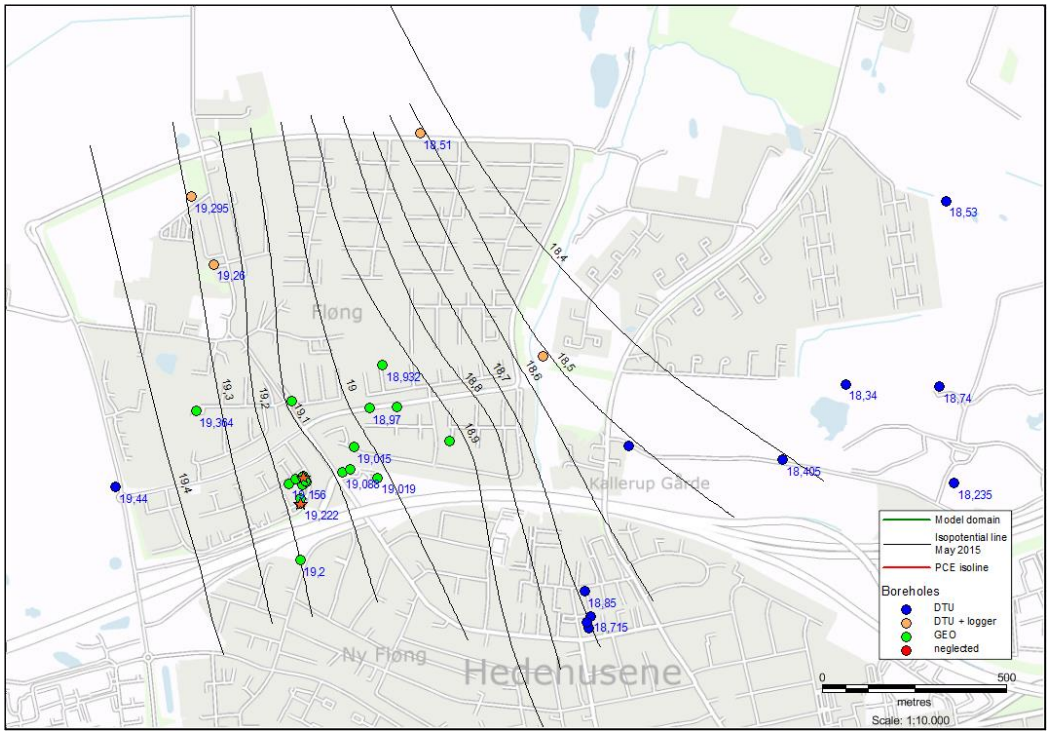

Figure 1.7: Isopotential map including boreholes and head measurements from May 2015. The two stars indicate the remediation and infiltration wells.

2. Methodology: Combined pumping and tracer test

Section 2.1 describes the pumping test methodology, sections 2.2-2.5 the tracer test setup and section 2.6 the PCE contaminant monitoring conducted during the pumping test.

2.1 Pumping test

The goals of the pumping test were to determine the hydraulic properties of the fractured limestone and the dual-porosity properties of the fracture-matrix system. For the design of such a pumping test, existing boreholes at the site and in the surrounding area were considered as potential pumping wells, while also considering whether suitable observation boreholes were available in their vicinity.

Key design questions for the pumping test were:

- Which borehole should be used for pumping? In which boreholes should heads be monitored?
- How long should the pumping test be, and how long should heads be monitored?
- Could existing boreholes be used or were new ones needed?

The **requirements** to the pumping well were:

- To have screens for pumping in the fractured limestone
- To have a borehole with a sufficiently large diameter (minimum 110 mm for the installation of a SP14 pump, which can yield 14-18 m^3/h)
- To have monitoring wells close to the pumping well to allow for the measurement of the drawdown, ideally with screens at the same depth as the pumping well
- Ideally, the pumping well should be located in the plume or source zone, to allow for the simultaneous measurement of the development of PCE concentrations

As a first step, the existing infiltration well (B23, DGU no. 207.3969) was identified as a possible pumping well. A short-term pumping test was conducted in the infiltration well and was reported in Geo (2015). The test showed that the borehole was not suitable (well screen too long, too little drawdown, very low PCE concentrations due to continuous infiltration from the remediation system).

Other existing boreholes previously located at the site had drawbacks with respect to the pumping and tracer test for several reasons:

1. The distance between the boreholes was too large (drawdown could not be measured),
2. The well screens were mainly in the crushed limestone, hence the determined parameters would mainly be representative for the crushed limestone,
3. The well screens were located at various depths (different units of the limestone) making the interpretation difficult,
4. Some of the well screens were only partially below the groundwater table.

2.1.1 Pumping and monitoring wells

The pumping test setup consists of a new central pumping well (Geo17) with a 6 m long screen in the fractured limestone (the existing remediation well PB has its screen mainly in the crushed limestone, see Figure 2.1). The new pumping well was placed in the PCE contaminated area next to two wells (PB and Geo5) located 6.5 m (Geo5) and 8 m (PB) from the new pumping well (Table 2.1). The idea was to place the new pumping well so that three boreholes surrounding the pumping well can be used for head monitoring and tracer injections from different directions. For this design, the drilling of two new boreholes was necessary, Geo17 (the new pumping well) and Geo18 with two screened wells 5 m away from Geo17. The shallow screen of the Geo18 was chosen to be at the same depth as the screen of the new pumping well.

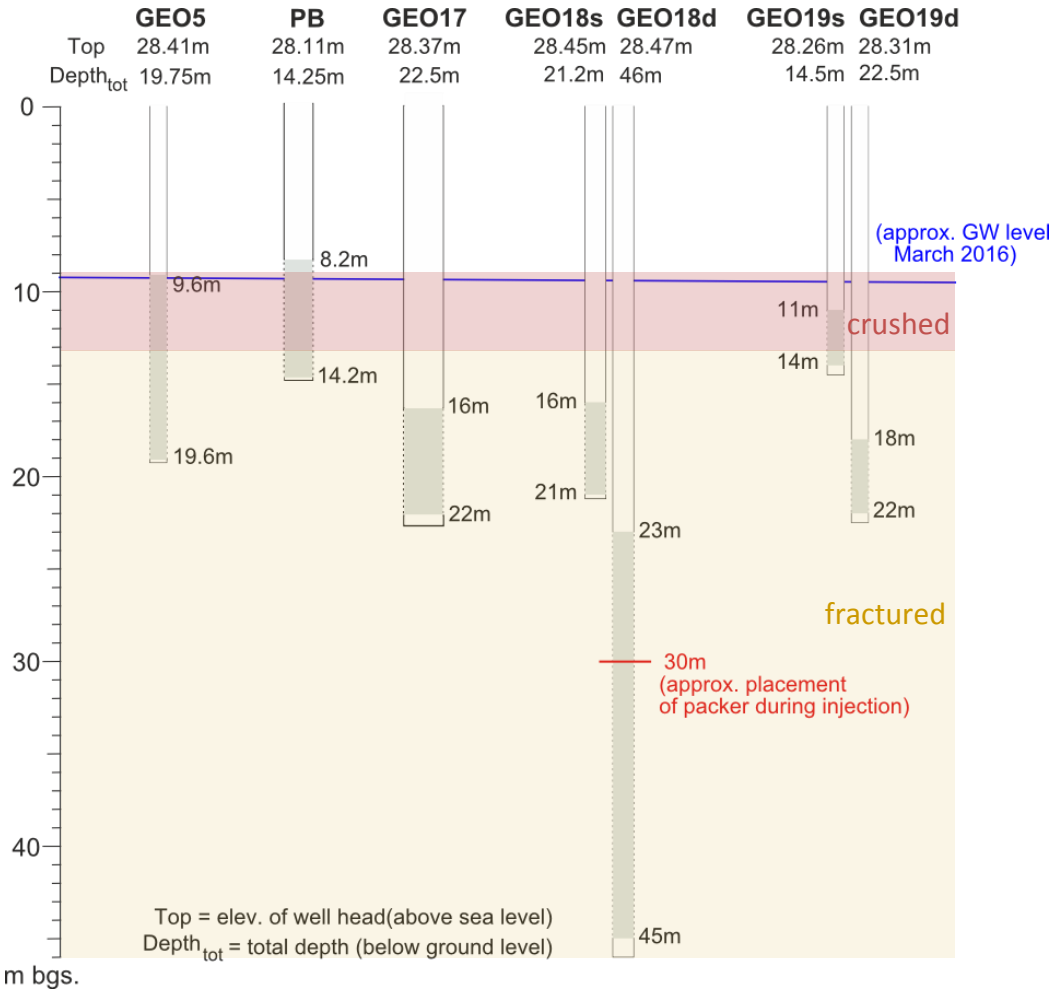

Figure 2.1: Borehole depths and location of screens. Geo5, Geo18s and Geo19d have a screen at a similar depth as the pumping well Geo17. PB and Geo19s are mostly located in the crushed limestone.

In addition to the two new wells, Geo19 was drilled with two screened wells at a distance of 15 m for the sampling for PCE close to the building, under which the contaminated soil was not excavated. With two already existing wells close to the Akacievej building (B5 and B22 at a distance of 43 and 52 m from Geo17), six boreholes were located close to the pumping well and could be exploited as observation wells for the drawdown created by the pumping test. Model simulations indicated that the drawdown was expected to be within a measureable range.

A pumping rate of 19.6 m^3/h was chosen with a pumping duration of several weeks. The extracted water was filtered through an activated carbon treatment system (Figure 2.2) and then discharged to the local sewage system. The pumping rate was chosen to be as high as practically possible, so that the pumping test could measure the different stages of the drawdown (fractures drain first, followed by fracture-matrix interflow and finally matrix flow, see Nielsen, 2007). Higher pumping rates could not be employed because of practical constraints (pump requires an even bigger borehole diameter; the large volume of pumped water has to be discharged to the sewage system).

Well name	Horizontal distance [m]	Elevation of well top [m asl.]	Screen depth [m bgs.]	Diameter [mm]
Geo17	0	28,37	16-22	225
Geo18s	5	28,45	16-21	110
Geo18d	5	28,47	23-45	110
Geo5	6.5	28,41	9.6-19.6	90
PB (207.4059)	8	28,11	8.2-14.2	165
Geo19s	15	28,26	11-14	90
Geo19d	15	28,31	18-22	90
B5	43	28,34	10.5-14.5	63
B22	52	28,32	10-14	

Table 2.1: Horizontal distances of the boreholes to the new pumping well (Geo17). For the location of the wells, see Figure 2.3.

The remediation system at Akacievej was switched off before the three new boreholes were drilled (October 9th, 2015) and remained off until the end of the pumping and tracer test (April 27th, 2016). The remediation system extracts water from PB and infiltrates it through B23. The effects of the remedial pump stop were evaluated before it was switched off (Mosthaf et al., 2015a).

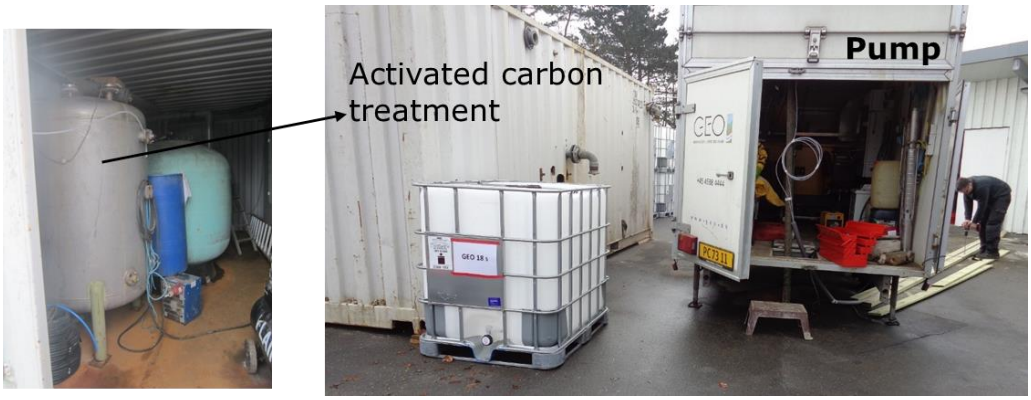

Figure 2.2: Trailer containing the pump and container with the activated carbon treatment system for the extracted water from the pumping test.

2.1.2 Overview of new boreholes

In total, three additional boreholes (Geo17 – Geo19) were drilled at the site for the pumping and tracer test at the end of 2015. Figure 2.3 provides an overview of the existing boreholes at the Akacievej site, highlighting in orange the new boreholes. A cross section showing the well screen locations is depicted in Figure 2.1. The distances between the boreholes are listed in Table 2.1. The borehole reports of the new boreholes and the flow logs for Geo17 and the deep screen of Geo18 can be found in Appendices A and B. For the shorter screens in Geo18 (upper screen) and Geo19, flow logging was not possible. All wells are screened to prevent a collapse of the borehole walls. The following paragraphs provide details on the new boreholes and their purpose.

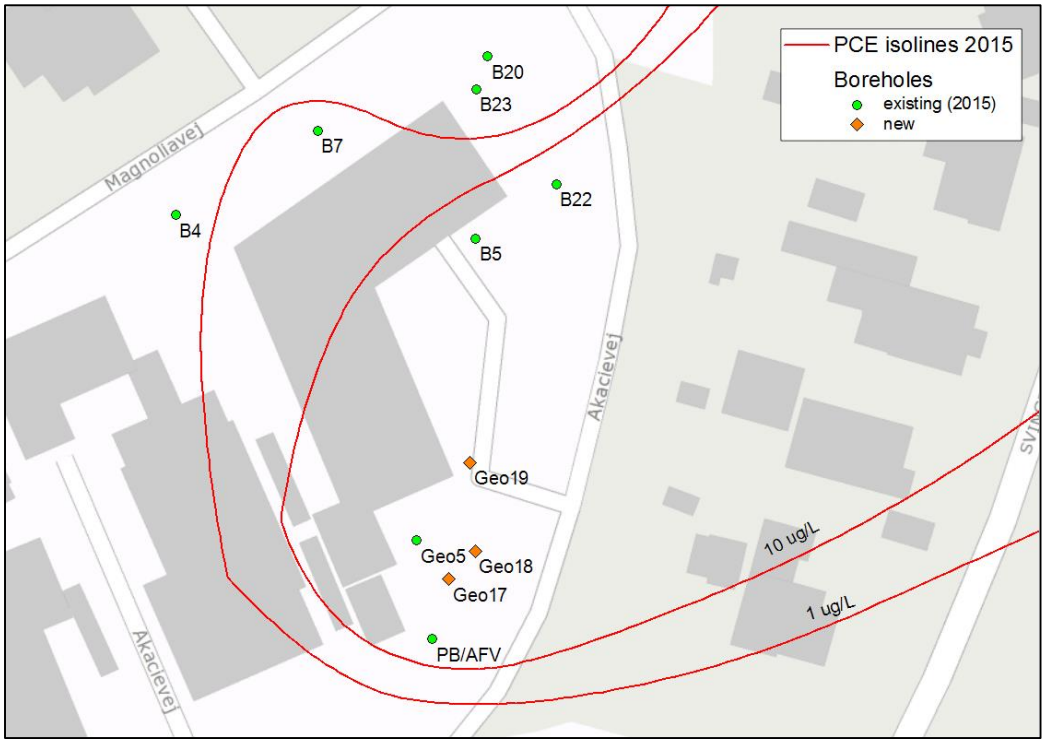

Figure 2.3: Overview of boreholes at the Akacievej site. The new boreholes drilled in November 2015 are marked in orange. The red lines indicate the PCE distribution in 2015 without pumping.

Geo17: Central borehole for pumping, drawdown measurements, PCE sampling and tracer detection, one screen completely in fractured limestone.
Depth and screens: 22.5 m deep, down to 8 m asl.; 6 m screen in the fractured limestone (6.5-12.5 m asl.); Diameter: 225 mm to allow the installation of a big pump and loggers for the tracer test.

Geo18: One borehole with two screened wells. The shallow well (Geo18s) was equipped with a 5 m screen at the same depth as the extraction well, so tracer could be injected and flow horizontally to the extraction well. It was also used for head monitoring.
The deeper well (Geo18d) was drilled down to 46 m bgs. (-17.5 m. asl.) and had the purpose of determining the depth of the conductive limestone aquifer and of detecting the lower bound of the dissolved contaminant plume with multilevel sampling. The Geo18d was also used for head monitoring and tracer injection to shed light on the properties of the deeper part of the aquifer.
Depth and screens: The shallow well is 21.2 m deep and has a 5 m screen located at the same depth as the screen of the extraction well Geo17 (7.5-12.5 m asl., mainly in Copenhagen limestone). The deep well is 46 m deep. The deeper part of it (-16.5 m to 5.5 m asl.) was kept unscreened for additional measurements (optical televiewer, packer tests etc.). After these measurements were finished, a screen was installed (-16.5 m to 5.5 m asl.) to allow for multilevel sampling of the contaminant. Relatively small diameter (110 mm).

Geo19: One borehole with two relatively shallow screened wells. The upper well screen (Geo19s) is located in the crushed limestone, whereas the lower screen (Geo19d) is located in the top of the fractured limestone. The main purpose of Geo19 was to examine whether PCE contamination is found below the Akacievej

building, where the contaminated soil was not excavated. It was also employed for head monitoring, tracer injection and slug tests in both screens to analyze the hydraulic parameters in the crushed and in the fractured limestone.
Depth and screens: Shallow borehole: 14.5 m deep with a screen in the crushed limestone (14-17 m asl.). Deeper borehole: 22.5 m deep with a screen in the fractured limestone (6-10 m asl.). Small diameter (90 mm).

2.1.3 Preparatory tests

Slug tests

To obtain an approximate measurement of the hydraulic conductivities and its spatial variation in the aquifer, several slug tests (relatively quick and easy single-borehole aquifer tests, where a slug of water is released and the pressure response measured) were conducted. Because the aquifer is very permeable and the water table responds very quickly, a slug test with a vacuum system was employed to pull the water table up at the borehole (Figure 2.4). The raised water table was then released and the heads recorded with a pressure transducer with a short measurement interval (0.5 s). The hydraulic head measurements were taken approximately 1 m below the water table in the well. The measurements were then evaluated with the software Aqtesolv and approximate hydraulic conductivity values were determined. Different solution schemes were applied to interpret the slug tests, namely the Bouwer-Rice solution, the Kansas Geological Survey solution (KGS) and the Springer-Gelhar solution. Some of these solution schemes are especially developed for an oscillating water table, which was observed in some of the slug tests, particularly when the well screen was located in a highly conductive zone. More details are described in the student theses of Besora (2016) and Jørgensen (2015).

Figure 2.4: Slug test using a conventional vacuum cleaner (left). Slug test device installed in a borehole (right).

The slug tests in the shallow and deep screen of Geo19 indicated a lower hydraulic conductivity in the crushed layer (upper screen) than in the fractured limestone (lower screen). The determined hydraulic conductivity for the crushed limestone (shallow screen) was in the range of 2×10^{-4} to 4×10^{-4} m/s, whereas the conductivity in the fractured limestone (deep screen) was about 8×10^{-4} m/s. Note that slug tests

are very local measurements and the measured values are possibly influenced by the sand or gravel packs that surround the wells.

Further slug tests were conducted in Geo4, Geo7 and Geo9 (see Figure 1.5 for location). They show a strong variation of the aquifer hydraulic conductivity, both spatially and with depth (location of the screen), see Table 2.2 and Jørgensen (2015).

Well	Screen location [m asl.]	Screen length [m]	Hydraulic conductivity [m/s]	Limestone condition
Geo4	-5.5 - 18.5	24	2×10^{-4}	crushed + fractured
Geo7d	14 - 16	2	5×10^{-6}	crushed
Geo9	-3.5 - 17.5	21	1.2×10^{-4}	crushed + fractured
Geo19s	14 - 17	3	3×10^{-4}	crushed
Geo19d	6 - 10	4	8×10^{-4}	fractured

Table 2.2: Hydraulic conductivities in Geo4, Geo7 and Geo9 determined by slug tests. The location of the boreholes is shown in Figure 1.5.

Poroperm tests of limestone core samples

A steady state gas permeameter and porosimeter (Poroperm) was used to determine the hydraulic conductivity and porosity of intact limestone core samples from Geo4, Geo5 and Geo9. The determined values are very low (Table 2.3) and are representing mainly the properties of the limestone matrix.

Well	Depth [m bgs.]	Hydraulic conductivity [m/s]	Porosity [%]	Grain density [g/cm^3]	Bulk density [g/cm^3]
Geo5	12.50-12.72	5.17×10^{-9}	15.9	2.71	2.28
Geo4	20.28-20.40	1.05×10^{-6}	46.1	2.73	1.47
	20.55-20.74	1.50×10^{-9}	11.5	2.70	2.38
	21.51-21.66	3.00×10^{-9}	12.0	2.70	2.38
	23.06-23.28	2.68×10^{-8}	28.4	2.69	1.92
	31.05-31.35	3.20×10^{-10}	9.9	2.71	2.44
Geo9	17.06-17.15	1.03×10^{-6}	45.2	2.72	1.49
	17.37-17.52	4.40×10^{-9}	14.4	2.70	2.31
	17.93-18.15	5.88×10^{-10}	10.8	2.70	2.41
	22.93-23.10	1.46×10^{-9}	12.0	2.71	2.38
	25.79-26.00	5.21×10^{-11}	7.2	2.72	2.52

Table 2.3: Hydraulic parameters measured by poroperm tests with relatively intact borehole core samples from Geo4, Geo5 and Geo9. Most of the values represent the limestone matrix.

Evaluation of water works data and drawdown caused by the remediation well

Water works have often automated head measurements in their extraction wells. The Fløng waterworks are the water works closest to the Akacievej site. They are extracting drinking water from four wells, situated between 600 and 1700 m north of the Akacievej site. They are operating an alternating pumping scheme, which distributes the water extraction to the four wells according to the demand by

switching pumps on/off or by regulating the pumping rate of the wells. This leads to a sequence of pumping-test like events, which can be evaluated. The pumping rates and the hydraulic heads in the pumping wells are automatically monitored. For the evaluation, the measurement interval was set to 30 s. The evaluation of the recorded drawdown curves allowed estimating hydraulic conductivity values for the wells of the water works. The results are presented in Table 2.4. The determined conductivity values vary considerably between the different wells that have screens with a different length and at different depth. This indicates a strongly heterogeneous aquifer. The fourth well is an open borehole and furthest away from the Akacievej site. It was not further considered.

Well (DGU no.)	Screen location [m asl.]	Screen length [m]	K fractures [m/s]	K matrix [m/s]
200.5539	-29.4 - 7	36.4	0.03	2.5×10^{-9}
200.5375	1.1 - 13.1	12	4.2×10^{-4}	1×10^{-10}
207.2699	9 - 16	7	1.75×10^{-5}	1×10^{-9}

Table 2.4: Screen location and conductivity values estimated with Aqtesolv (Moench solution).

2.2 Overview of tracer tests

In total, six forced-gradient tracer tests were planned and successfully completed in the spring of 2016. Model simulations guided the design of the tracer test and lead to the final design. Key design questions for the tracer tests were:

- Natural gradient vs. forced gradient tracer test, or both sequentially?
- Which tracers to use? How to detect and analyze the tracers (loggers, tracer samples)? Where to monitor the tracers?
- In which boreholes and at which depths should the tracer be injected?
- How long should the tracer be injected? Should the tracer be injected as a pulse followed by injection of water or should it be injected continuously? Mixing in the borehole?
- Same injection rate as the pumping rate or lower injection rate?
- Simultaneous injection of several tracers with different diffusion and sorption coefficients in one borehole?
- Which injection concentration of the tracers should be used?

The four wells next to the pumping well were selected for tracer injections (the existing wells Geo5 and PB, and the two new wells, Geo18 and Geo19) and were expected to be within the capture zone of the pumping well (at a distance of 5 to 15 m). The distance between injection and extraction well was kept short to reduce the required breakthrough time and to ensure a high tracer recovery. More distant wells were excluded as possible locations for tracer injection because of the risk that the tracer would not be drawn to the pumping well.

Two fluorescent tracers (fluorescein and sulforhodamine-B) and a salt tracer (lithium bromide) were selected for the tracer test after conducting a risk assessment, which showed that they could be injected at measurable concentrations with little risk to the groundwater aquifer (Mosthaf et al. 2015b). The tracer concentrations were monitored in the pumped water of the extraction well (Geo17). The fluorescent tracers were continuously monitored with a flow-through spectrophotometer at the site. Additionally, a series of water samples were

collected with the help of a sampling carousel. The flow-through measurements guided the sampling frequency. The samples were stored so that they were protected from light and heat, and later analyzed in the lab for their tracer concentrations. Figure 2.5 shows the an example of the tracer test setup.

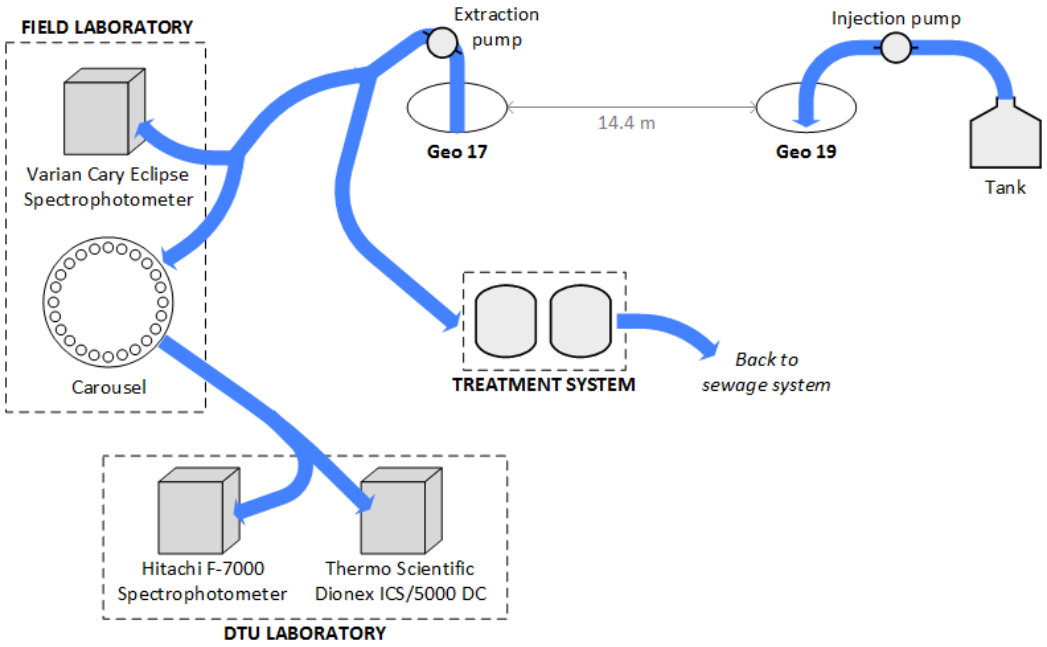

Figure 2.5: Schematic setup of the tracer test with Geo19 as example borehole for the injection system (Besora, 2016).

The locations of the injection wells and the extraction well are depicted in Figure 2.6. Figure 2.7 depicts a side view of the tracer test setup showing the expected transport of the tracers in the aquifer.

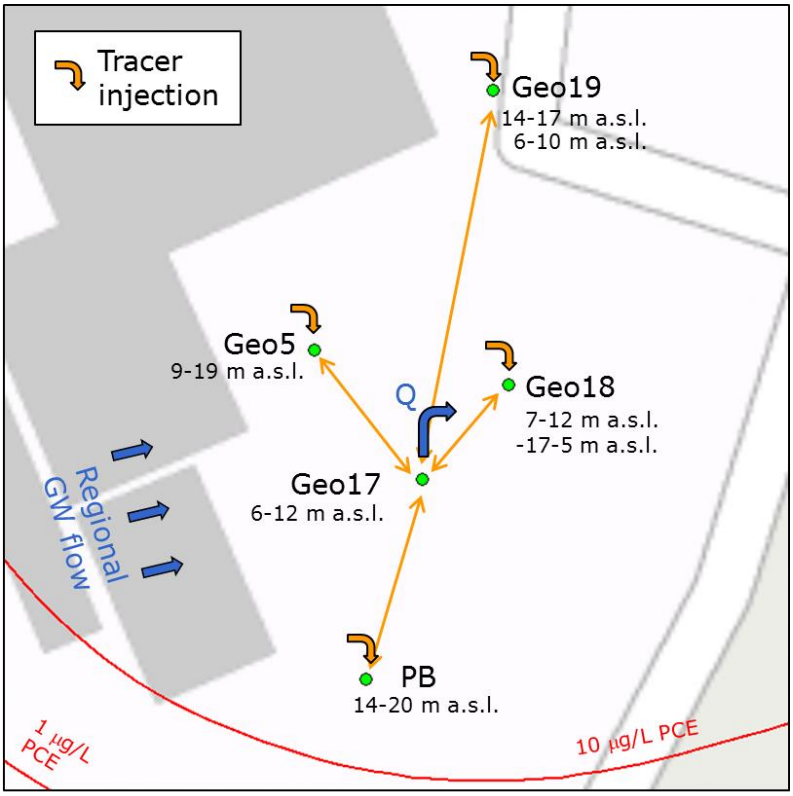

Figure 2.6: Overview of boreholes and tracer injection wells with depths of the screens. Geo18 was used for three tracer injections: before the pump was started, while pumping and an injection into the deep screen. Only the shallow screen of Geo19 was used for an injection.

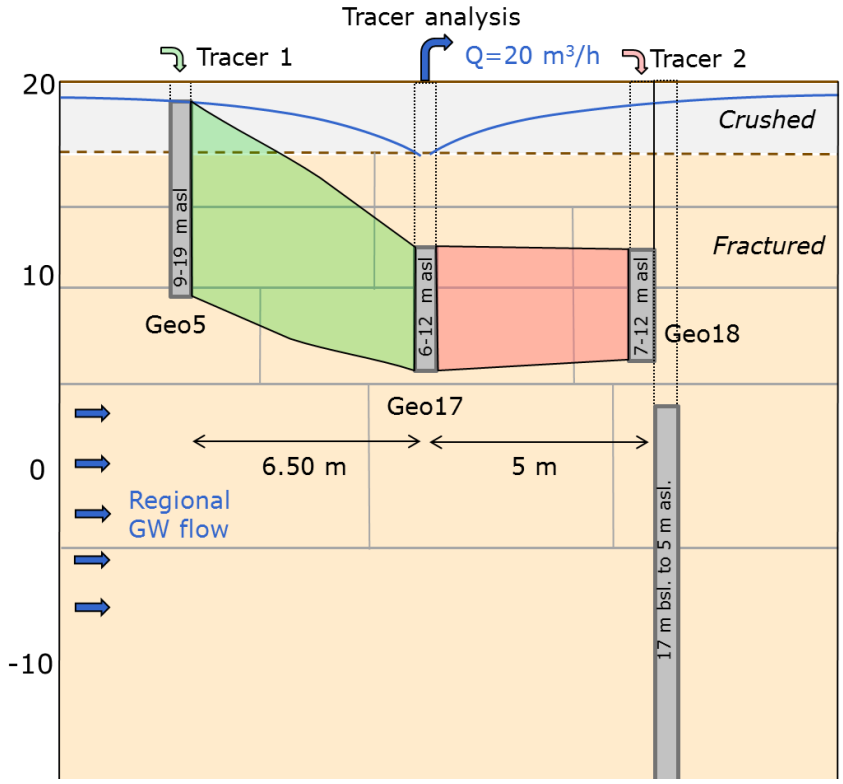

Figure 2.7: Side view of the tracer test setup for the injections conducted in Geo5 and Geo18s. The gray lines are a simplified representation of the horizontal and vertical fractures.

2.3 Tracer selection and properties

Two different kinds of tracers were selected: fluorescent tracers and ionic (salt) tracers. Criteria for the tracer choice were the following:

- Non-toxic to humans and harmless to the aquifer
- Easily detectable (e.g. with loggers) and low detection limits
- Contrast to background concentrations (particularly for salt tracers)
- No detection interference with other aquifer substances or tracers
- Predictable sorption characteristics (preferably non-sorbing to limestone and used materials)
- Differing diffusion behavior of the individual tracers
- Used in (limestone) aquifers before
- Availability and moderate costs

Based on these criteria, lithium bromide was chosen as salt tracer. Other salt ions had a too high background concentration (Na, Cl) or other detection issues (f.e. iodide may sorb to the limestone). Both lithium and bromide ions were used as a tracer and individually analyzed.

For the fluorescent tracers, fluorescein (disodium-fluorescein, or uranine), sulforhodamine B and amino-g acid were considered (Figure 2.8). They are widely used in groundwater, have very low detection limits and can be simultaneously monitored with a flow-through cell at the site (complementary to lab measurements). The three fluorescent tracers have non-overlapping color spectra, so the tracers can be easily distinguished. Fluorescein emits in the green spectrum, whereas sulforhodamine B emits in the red spectrum. Amino-G is a tracer emitting in the blue spectrum. All three tracers have been used in other studies in limestone with good results (Riley et al. 2001, Hartmann et al. 2007, Bottrell et al. 2010). A risk evaluation document and a tracer selection document provide more details about the tracers (Mosthaf et al. 2015b,c).

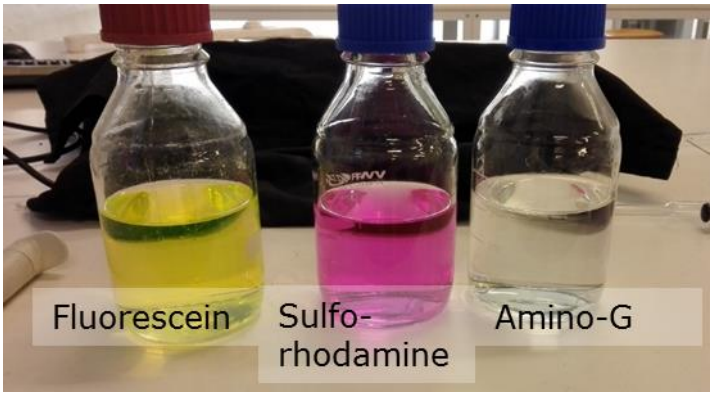

Figure 2.8: Fluorescein, sulforhodamine and amino-g acid at high concentrations. Amino-g acid is visible under UV light.

An injection of the degradable amino-g acid was planned, but the tracer could not be delivered in time for the tracer test. Hence, fluorescein and sulforhodamine B were used. Approximate diffusion coefficients are presented in Table 2.5.

	Diffusion coefficient [m^2/s]	Source
Fluorescein	$3{,}2\times10^{-10}$	Calculated
Sulforhodamine B	$2{,}3\times10^{-10}$	Calculated
Lithium	1×10^{-9}	Tanaka & Nomura, 1987
Bromide	$1{,}3\times10^{-9}$	Calculated

Table 2.5: Molecular diffusion coefficients of the tracers.

2.4 Tracer injection and mixing in the borehole

Model simulations suggested that a pulse injection with a high injection rate of 1000 L/h and a relatively short injection interval of approximately 1 hour for the tracer injections would be optimal to obtain a good tracer breakthrough curve, while keeping the time for the tracer test short and the influence of the injection on the flow field limited.

The tracer amounts were selected based on the detection limits of the instruments and the anticipated dilution of the injected tracer from the injection to the pumping well. To estimate the dilution of the injected tracer concentration, discrete-fracture model simulations of the tracer tests were used. The tracer test aimed to inject as little tracer as possible to obtain a well detectable breakthrough curve. A further constraint on the injection concentration, particularly for the salt tracer, was to avoid density effects. For natural gradient conditions, density effects can occur at concentrations higher than 300 mg/L (e.g. the tracer may sink to the bottom of the borehole). However, with the strong hydraulic gradient due to the pumping and the used injection method, density effects were not expected. The injected tracer concentrations decrease fast due to the mixing with the aquifer water after the injection.

The tracers were injected as one-hour pulse injections. To obtain a relatively uniform injection over the entire screen length, two different methods were considered:

1) Mixing the concentrated tracer in the borehole by recirculating the water using a pump, as described in Hartmann, Odling, and West (2007).
2) Injecting diluted tracer with a relatively high injection rate through multiple injection ports (tubes) distributed along the well screen.

For a recirculation in the borehole, it would be necessary to lower a pump into the borehole, which would occupy part of the space in the well and lead to a considerable heat production. This may result in unfavorable density effects in the borehole and effect the fluorescence of the fluorescein tracer.

Hence, a method with a high injection rate of 1000 L/h through several injection ports along the well screen was developed. This has the advantage that it does not have any heating effects, that the tracer is pushed out from the borehole and it is easier to control the injection concentration. It was tested beforehand how many PE tubes were required for the planned tracer injection rate of 1000 L/h and 20 injection tubes were required. In order to have a similar injection rate in all boreholes and injections, the same number of tubes was used for all injections.

A long PVC pipe with 20 PE tubes (4 mm diameter) was installed in the injection borehole. The ends of the PE tubes were fixed at intervals of 20 to 50 centimeters (depending on the length of the well screen) in order to cover the entire well screen. Nozzles were fixed at the ends of the tubes to provide the same discharge in each tube (see Figure 2.9). The upper ends of the tubes were fastened to a flow distributor that was connected to the tracer injection tank via a jet pump.

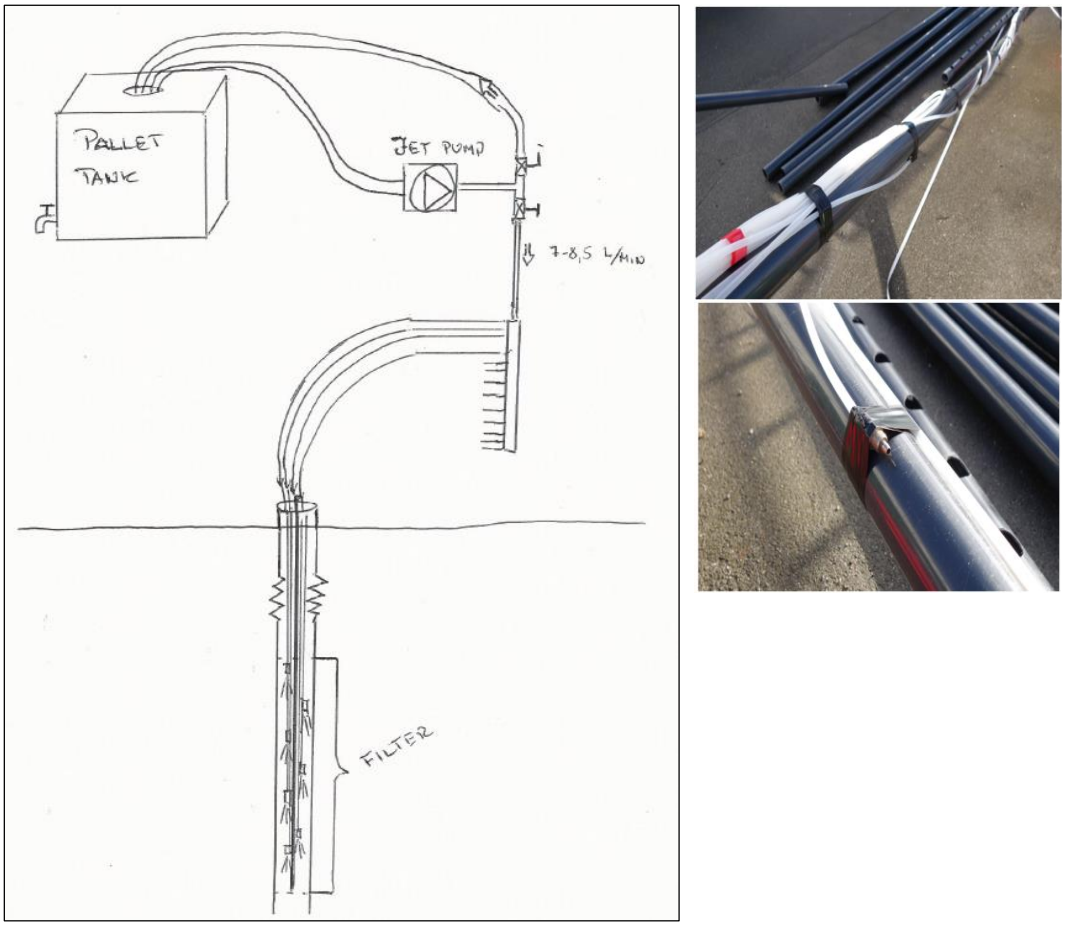

Figure 2.9: Schematic setup of the injection system (left). Injection tubes attached to PVC pipes (top right). The nozzles were fixed at the end of the injection tubes (bottom right).

For each injection, groundwater was extracted at the site before the pumping and tracer test began and stored in 1000 L tanks at the site. A concentrated tracer solution was mixed, and immediately before the injection transferred into the 1000 L tanks containing the groundwater (see Figure 2.10). When fluorescein and lithium bromide were simultaneously used for an injection (Geo18s_pre, Geo19d), two separate concentrated tracer solutions were made and transferred into the same tank. A recirculation pump homogenized the tracer concentration in the tanks for about 30 minutes before the injection. The water temperature in the tanks was measured and adjusted (heated) to the approximate aquifer temperature of 9° C. Each tracer (mix) was injected as a pulse injection over 1 hour. Right after the tracer injection, 120-200 L of chasing groundwater was injected to clean the equipment and to flush the tracer partly out of the borehole. The equipment was removed from the borehole and adjusted for the next tracer injection.

Figure 2.10: Concentrated fluorescein solution (left). 1000 L tank with diluted fluorescein (20 mg/L) and lithium bromide solution (1000 mg/L) before injection at borehole Geo19d (right).

Due to the instability of the limestone and its varying hardness (from soft limestone to very hard flint), all injection wells were completed as screened wells, where the well screen is surrounded by a gravel or sand pack. The gravel packs were later shown to influence the tracer distribution.

Testing of injection method and mixing in borehole

To test the developed injection method and the mixing in the borehole, blue food-grade dye was injected in the DTU lab in a large plastic column (see Figure 2.11). The dye mixed with water in the column within a few seconds.

To test the injection method in the field, a sodium chloride (NaCl) solution at g/L level was injected with a high concentration in a borehole using the developed injection system. The electrical conductivity measured over the borehole depth with an EC logger showed a good mixing in the borehole.

2.5 Tracer sampling and analysis

2.5.1 Tracer sampling procedure

Water samples were collected for the lab analysis of the injected tracers by diverting water pumped from Geo17 to a shed that was equipped with sampling and detection instruments. There, water samples were collected in 500 ml beakers on a specially designed sampling carousel (Figure 2.13), which could collect up to 24 samples (about 120-140 ml each) at predefined time intervals.

Figure 2.11: Lab test of the injection system. Tube with nozzle (left), candy dye injected into the plastic column showing a good mixing behavior (right).

The time intervals were chosen according to the simulated and observed breakthrough behavior. The sampling frequency was between 3 minutes and 2 hours, guided by the concentrations from the flow-through measurements. When the first tracer arrived at the pumping well, the tracer concentrations increased quickly and short sampling intervals were employed (down to 3 minutes). After the tracer breakthrough, intervals were gradually increased to up to two hours. Depending on the sampling intervals, the samples remained between a few minutes to maximum 24 hours on the sampling carousel in the shed with relatively stable temperature conditions and protected from sunlight.

Each of the water samples was distributed from the 500 ml beaker into four different vials. A high-density polyethylene vial (20 ml) was filled with unfiltered water from the sampling beakers for the lab analysis of the fluorescent tracers. Another two 20 ml PE vials were filled with water for the lithium analysis and 2-3 drops of sulfuric acid were added. The sample for the bromide analysis was filtered through a 0.45 µm cellulose syringe filter before injecting it into a 6 ml PE vial. All samples were kept in cooling boxes in the dark before they were transported to DTU, where they were stored protected from sunlight and heat in a 10 degree room until the analysis for the tracer concentrations.

Results showed that the filtered samples for the bromide analysis gave more consistent results for fluorescein compared to the noisy measurements of the unfiltered samples. Probably, the fluorescein interacted with some dispersed particles in the groundwater during storage and lowered the measured concentrations (dependent on the concentration of these particles in the respective sample). If possible, the filtered samples were analyzed for their fluorescein concentrations.

Figure 2.12: Field spectrophotometer (Vary Eclipse) with flow-through cell and peristaltic pump. The spectrophotometer was connected to a computer that continuously measured the tracer emissivities of water diverted from the pumping well.

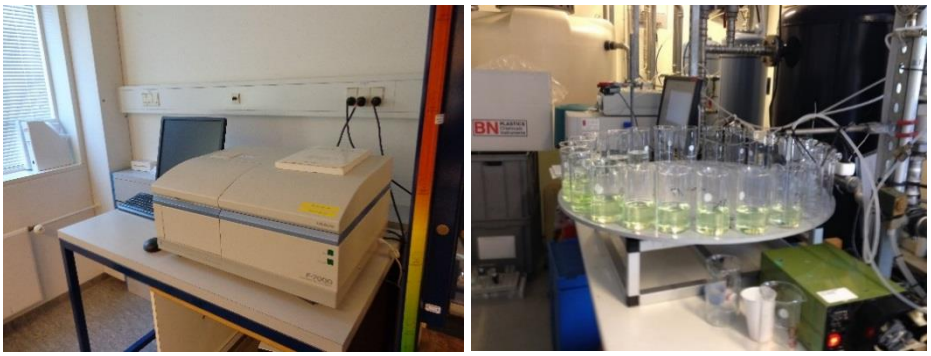

Figure 2.13: Lab spectrophotometer (Hitachi F-7000) and sampling carousel, which took samples of the pumped water at predefined intervals.

2.5.2 Fluorescein and sulforhodamine B

In addition to the samples that were analyzed in the lab, the fluorescent tracers were continuously monitored at the site with a Varian Cary Eclipse fluorescence spectrophotometer (Figure 2.12) equipped with a flow-through cell. A portion of the water from the pumping well was diverted to the shed, where the flow-through spectrophotometer (Figure 2.13) and the sampling carousel were installed. A small tube delivered water with a peristaltic pump (flowrate 1.75 mL/min) to the flow-through cell (volume 40 µL) in the field-spectrophotometer, where the fluorescence of the tracers was continuously measured (time interval 8 seconds). The detector allowed for the simultaneous measurements of three fluorescent tracers with different color spectra. The best measurement wavelength was tested for each tracer. Table 2.6 gives an overview of the excitation and emission wavelengths used for the analysis with both spectrophotometers (lab and field spectrophotometer).

Tracer	Excitation max [nm]	Emission max [nm]
Fluorescein	495	515
Sulforhodamine B	560	583
Amino-G acid	350	450

Table 2.6: Excitation and emission wavelength of the fluorescent tracers used for the Varian Cary Eclipse fluorescence spectrophotometer. The same settings were used for the Hitachi F-7000.

The flow-through measurements guided the sampling frequency of the carousel. The water samples that were taken with the sampling carousel were analyzed in the DTU laboratory with a Hitachi F-7000 fluorescence spectrophotometer (Figure 2.13). The flow-through spectrophotometer has an upper detection limit. When the measured concentration exceeds the upper limit, out-of-range values are measured, which cannot be used for the evaluation. The lab measurements of water samples were considered to be more accurate and flexible than the field measurements. With those, it is possible to dilute the tracers, when the concentration exceeded the measurement range. Furthermore, the detection sensitivity could be adapted by adjusting the photomultiplier tube voltage (usually 700 V were used).

2.5.3 Lithium bromide

Lithium bromide was injected in combination with fluorescein. This had the advantage that the fluorescein measurements with the flow-through spectrophotometer could be used to control the sampling frequency of the sampling carousel. Both ions of the lithium bromide were analyzed for their concentration in the water samples.

Bromide

For the on-site detection of bromide, a bromide-selective electrode was initially selected. However, the detection limit in the high ionic strength groundwater restricted its usage, being unable to detect bromide concentrations in groundwater below 500 µg/L (far above background level, Table 2.7). Hence, it was only used during the first injection and the concentration measurements were done in the lab.

The samples for the bromide analysis were filtered through a 0.45 µm cellulose syringe filter before filling it into a 6 ml PE vial. The bromide concentrations were measured in the DTU lab, using a Thermo Scientific Dionex ICS-5000 DC HPIC (high-pressure ion chromatograph).

Lithium

The samples for the lithium analysis were filled in 20 ml PE plastic vials. Then 2-3 drops of sulfuric acid were added to the water samples, which were stored protected from light and heat until the analysis. The lithium concentrations were analyzed by an accredited laboratory (Eurofins), using an Agilent ICP-MS.

2.5.4 Preparatory tests

The success of a tracer test hinges on careful planning and preparation. Several preparatory tests were performed prior to the first tracer injection to ensure detectability and reliable measurements.

Measurement of background concentrations of ions

Groundwater samples from the site were analyzed for the ion concentrations (Table 2.7 and Table 2.8). The chloride, sodium and calcium ion concentrations showed a surprisingly high variation. The bromide concentrations were below detection limit. The lithium concentrations measured in Geo5 and PB were low and in a narrow range.

Kote [m]	pH	Temp [°C]	Cond. [µS/cm]	O_2 [mg/L]	NO_3^--N [mg/L]	Fe [mg/L]	Mn [mg/L]	SO_4^{2-}-S [mg/L]	Cl [mg/L]	Br [µg/L]
17,5	7,0	10,3	1139	1,8	3,3	0,17	0,03	35	123	<40
16,2	7,0	8,5	1177	2,1	3,7	0,13	0,04	28	131	<40
14,6	7,0	9,7	1206	1,7	2,4	0,12	0,03	27	110	<40
13,5	6,9	10,0	1116	1,2	2,5	0,17	0,03	37	108	<40
12,4	6,9	10,0	1119	1,3	2,6	0,18	0,03	38	114	<40
11,0	6,9	10,4	1124	1,3	1,2	0,12	0,03	30	50	<40
10,5	6,9	10,7	1127	1,3	2,1	0,11	0,03	29	102	<40

Table 2.7: Field parameters and anion concentrations in Geo5 (multilevel sampling) determined by ion chromatography.

Well	Li [µg/L]	Na [mg/L]	K [mg/L]	Ca [mg/L]	Rb [µg/L]
Geo5	11-13	26-49	3,5-4,3	186-197	0.33-1,4
PB	12-13	75-96	4,1-4,8	170-225	0,6-2,4

Table 2.8: Cation concentrations measured in Geo5 and PB determined by ICP-OES analysis (Rb also with ICP-MS). The values show the minimum and maximum values in the wells (multilevel sampling).

Test of detectability and detection limits of tracers

Before conducting a tracer test it is important to test, if the applied tracers can be detected under natural conditions in the groundwater from the site with the prevalent background concentrations. This ruled out several ionic tracers (sodium and chloride), because the background concentration was too high and variable.

Furthermore, the detection limits of the instruments used for the tracer detection and analysis were tested to determine if they were sufficiently low (Table 2.9). This information was also used for the determination of the injected tracer amounts.

Compound	Machine	Detection limit
Bromide	Thermo Scientific Dionex ICS-5000 DC; Bromide-selective electrode	25 µg/L 500 µg/L
Sulforhodamine B	Varian Cary Eclipse fluorescence spectrophotometer (field) Hitachi F-7000 fluorescence spectrophotometer (lab)	0.15 µg/L
Fluorescein	Varian Cary Eclipse fluorescence spectrophotometer (field); Hitachi F-7000 fluorescence spectrophotometer (lab)	0.05 µg/L
Lithium	Agilent ICP-MS (Eurofins labs)	0.5 µg/L

Table 2.9: Used instruments for the tracer detection and analysis and detection limits.

Testing of sorption behavior of tracers
Initial sorption tests were conducted with the equipment (PE tubes for the injections, high-density PE vials for the tracer samples from the sampling carousel) and with limestone samples. They showed that very little sorption to the tested materials occurred. No sorption was observed for bromide. Fluorescein was slightly sorbed. More sorption was observed for sulforhodamine, but with negligible effects on the tracer test results. The sorption behavior of lithium was not tested.

Degradation tests for tracers when storing them protected from light in a 10-degree room
Four test tracer solutions were kept in a 10 degree room without exposure to light for 9 days while measuring their tracer concentrations repeatedly. No significant degradation could be observed.

2.6 PCE sampling

Before, during and after the pumping test, sampling for the PCE concentrations was conducted in several boreholes. Single-depth sampling was conducted in the wells B5, B22 and PB. The PCE concentration was monitored in the pumped water from Geo17. Depth-discrete multilevel sampling was conducted in the wells Geo5, Geo18 and Geo19 by semi-passive slow purge sampling with a bladder pump slowly lowered in the wells. The PCE concentration data as well as a method description and comparison with other methods can be found in Broholm et al. (2016b).

3. Pumpeforsøg

3.1 Forberedende og ledsagende arbejder

I forbindelse med de nye boringer, beskrevet i afsnit 2.1.2, blev der lavet yderligere undersøgelser med geofysiske borehuls logs og korte pumpeforsøg. Formålet med de ledsagende undersøgelser var at kunne dimensionere og tilrettelægge pumpe- og tracerforsøget bedst muligt, samt at opnå supplerende viden om kalken.

I boringerne Geo17 og Geo18 blev der udført geofysisk logging (Table 3.1), boring Geo17 er der udført et kort pumpeforsøg med trinvis stigende pumperate og i Geo18 er der udført pumpesøg i fire 1,5 m intervaller (packerforsøg).

3.1.1 Geofysisk borehulslogging

I boringerne Geo17 og Geo18 er der udført geofysisk borehulslogging. I boring Geo18 er der udført borehulslogging før og efter filtersætningen. Feltarbejdet er udført i overensstemmelse med GEUS kravspecifikation for udførelse af geofysisk borehulslogging.

Undersøgelsen bestod af geofysisk borehulslogging med en kalibersonde, en induktionssonde, en porøsitetssonde, en densitetssonde, en temperatur/fluidresistivitetssonde og en flowsonde.

Målingerne er udført fra top røroverkant til bunden af boringer, naturlig gamma data fra kalibersonden er anvendt ved rapporteringen. Logprogrammet ses i Table 3.1. Den geofysiske logging er i øvrigt udført som beskrevet i Geo (2015). Resultaterne af den geofysiske logging er præsenteret i Appendix B.

Logprogram			
Sondetype	**Måling**	**Geo17**	**Geo18 før/efter filtersætning**
3 arm kaliber *måler også naturlig gamma*	Måler diameter af borehullet	-	+/-
Ledningsevne og temperatur *måler også natulig gamma*	Måler væskens temperatur og elektriske ledningsevne	+	+/+
Induktion *måler også naturlig gamma*	Måler formationens elektriske ledningsevne	+	+/+
Porøsitet *måler også naturlig gamma*	Måler formationens porøsitet	+	+/+
Flow, propel *måler også naturlig gamma*	Måler vertikal flow i borehullet	+	+/+
Densitet *måler også naturlig gamma*	Måler formationens densitet	+	+/+
Optisk televiewer *måler også naturlig gamma*	Optager et billede af borehulsvæggen	-	-/+
Akustisk televiewer *måler også naturlig gamma*	Optager et akustisk billede af borehulsvæggen	-	-/+

Table 3.1: Logprogram, +: udført, -: ikke udført

3.1.2 Korttidspumpeforsøg

Efter filtersætningen i Geo17 er der 2015-12-02 udført et 2-trins pumpeforsøg for at kunne fastlægge pumperaten i det senere langtidspumpeforsøg. Forsøget var planlagt som 3-trinspumpeforsøg, men med den observerede sænkning under forsøget var det ikke muligt at udføre et tredje trin. Dette ville overskride pumpens kapacitet, og det ville heller ikke være muligt at udlede så store vandmængder til kloak. Der blev benyttet 2 stk. Grundfos SQ-7 pumper under forsøget. Pumperaterne var ca. 10 m^3/t i de første 60 min (1 pumpe), og ca. 19 m^3/t de sidste 60 min (2 pumper). Under forsøget var der installeret tryktransducere i boringerne Geo5, Geo18 og DGU nr. 207. 4059. Resultaterne af pumpeforsøget er vist i Appendix D.

Inden filtersætning af Geo18 blev der 2015-11-19 udført 4 korttidspumpeforsøg i den åbne del af boringen. Ved hvert pumpeforsøg blev en strækning på 1,5 m af boringen isoleret med to gummipackere, hvorimellem en pumpe var installeret (packerforsøg). Niveauerne, hvor packerforsøgene blev udført, var udvalgt på baggrund af en foreløbig analyse af resultaterne af den geofysiske logging, særligt flowloggen og den optiske televiewer log. Ved hvert packerforsøg blev der pumpet

20 min. med en pumperate på ca. 10 m^3/t. Der var installeret tryktransducere under den nederste packer, mellem packerne, over den øverste packer, og i boringerne Geo5 og DGU nr. 207.4059. Pumpen var en Grundfos SQ-7. Resultaterne af packerforsøgene er vist i Appendix E.

3.2 Pumpeforsøg

Der er udført et langtidspumpeforsøg med pumpning i boring Geo17.
Geo17 er boret med 12" symmetrix i kvartæret og 10" DTH i kalken. Den er filtersat med Ø 225 mm PVC filter og blindrør. Filterrøret går fra 16 til 22 m.u.t., men der er gruskastet 2 meter over denne strækning, således er der gruskastet 14-22,5 m u.t.

Pumpeforsøget blev udført med en Grundfos SP 17-5 pumpe, forsynet med frekvensstyring således at pumperaten kan holdes konstant. Det oppumpede vand blev ledt gennem et vandbehandlingsanlæg med aktivt kulfilter inden udledning til kloak.

På grund af nedbrud i pumpeudstyret blev forsøget afbrudt og genstartet to gange, således at der i alt blev tre sænkninger og tre stigninger.

Periode	**Pumperate [m^3/t]**	**Pumpeperiode**	**Stigningsperiode**
1	19.6	15-03 10:15 til 25-03 21:14 (ca. 10 dage)	Ca. 10 dage
2	19.6	05-04 10:17 til 15-04 09:20 (ca. 10 dage)	209 min
3	23.7	15-04 12:49 til 15-04 14:41 (ca. 112 min)	4-5 timer

Table 3.2: Pumpeperioder under langtidsforsøget.

Under pumpeforsøget blev vandstanden i boringerne/filtrene angivet i Table 3.3 målt.

Boring/ filter	**Top [m DVR90]**	**Bund [m DVR90]**	**OD/ID [mm]**	**Afstand til Geo17**	**Vandspejlsvariation under pumpeforsøget [m DVR90]**
Geo17	+12,6 (herover 2 m filtergrus)	+6,6	225/ 207.6	0	18.9-19.4 (0,5 m)
PB				7,0	
Geo5	+18,9	+8,9		6,3	19.2-19.4 (0,2 m)
Geo19s	+17,5	+14,5		15,0	19.1-19.4 (0,3 m)
Geo19d	+10,5	+6,5		15,0	19.0-19.4 (0,4 m)
Geo18s	+14,6	+7,4		4,9	19.1-19.4 (0,3 m)
Geo18d	+5,6	-16,4		4,9	19.2-19.4 (0,2 m)
B5	+17,9	+13,9		44.2	
B22	+18,5	+14,5		53,8	

Table 3.3: Boringer og filtre i langtidsforsøget.

3.2.1 Opsamling og behandling af data.

Under pumpeforsøget blev vandspejl i boringerne registreret automatisk af DTU med tryktransducer/dataloggere (herefter benævnt vandspejlsloggere) og pejlet manuelt.

Der er anvendt en høj målefrekvens (en måling pr 0,5 sek.) i vandspejlsloggerne omkring planlagte start og stop af pumpen og lavere målefrekvens i resten af perioden. Vandspejlsloggerne har således været oppe for at blive om-programmeret eller tappet flere gange under forsøget. For hver periode loggeren har været sat ned, er positionen af loggeren (koten) så vidt muligt bestemt ud fra sammenhørende værdier af vandspejlskote opnået ved håndpejling og vandsøjle-højde over loggeren. Herefter er vandspejlskoterne i boringen beregnet ud fra logger positionen og de loggede vandsøjlehøjder over loggeren. Pumpedata er opsamlet med elektronisk flowmåler med datalogger.

3.2.2 Korrektion af data

Under forsøget blev vandspejlet i boringerne påvirket af faktorer, som ikke havde noget med pumpeforsøget at gøre. Derfor blev data så vidt muligt korrigeret for disse faktorer inden tolkning. De væsentligste faktorer var barometereffekt og en generel trend i vandspejlet over tid.

3.2.2.1 Barometereffekt

Vandspejlsdata fra pumpeboringen og fra observationsboringer udviser en tydelig barometereffekt, se f.eks. Figure 3.1. Barometereffekten betyder at vandspejlet i boringen varierer med ændringer i lufttrykket, og at vandspejlet i boringen ikke svarer til vandspejlet i magasinet omkring boringen.

Korrektionen af data var kritisk fordi pumpningen under pumpeforsøget kun inducerer små ændringer i vandspejlet, for de fleste observationsboringer 7-8 cm, mens atmosfæretrykket i samme periode varierer med ca. 60 cm vandsøjle. Således ville en for stor eller lille korrektion kunne få stor indflydelse på tolkningen.

Barometereffekt er normal i spændte magasiner, og kan også optræde i frie magasiner, hvis luftadgangen til vandoverfladen i magasinet er begrænset pga. tætte geologiske lag og hvis boringens vandspejl ligger over top af filter-strækningen, som det er tilfældet med de fleste boringer her.

For spændte magasiner antages effekten at skyldes, at kornskelettet i magasinet bærer en del af ændringen i tryk, mens vandet i magasinet bærer resten. I boringen er det kun vandet, som bærer ændringen i atmosfæretryk. Derfor vil der opstå en trykforskel mellem boring og magasin med deraf følgende flow ind og ud af boringen og forskel i hydraulisk trykniveau.

For frie magasiner kan effekten nærmere forstås som en forsinkelse. Hvis de geologiske lag i den umættede zone er relativt impermeable for luft, vil trykket på vandoverfladen i magasinet kun langsomt ændre sig som følge af en ændring i atmosfæretrykket ved jordoverfladen. Der vil midlertidigt være skabt en

trykforskel, som vil give et flow ind eller ud af boringen og en forskel i hydraulisk trykniveau.

Effekten for frie magasiner afhænger af luftpermeabiliteten i den umættede zone og af boringens kvalitet, mens den for spændte magasiner afhænger af magasinets egenskaber samt af boringens kvalitet. Forholdet mellem ændringen i lufttryk og deraf følgende ændring i vandspejl i boringen benævnes barometrisk effektivitet.

$$BE = \frac{\Delta h}{\Delta\left(\frac{p_a}{\gamma}\right)}$$

Hvor BE er barometrisk effektivitet, Δh er ændringen i hydraulisk trykniveau, p_a er atmosfærisk tryk og γ er specifik vægt af vand (Batu, 1998). $\frac{p_a}{\gamma}$ svarer således til atmosfæretrykket i meter vandsøjle og benævnes herefter B.

Barometrisk effektivitet er specifik for et givent magasin og for en given boring og kan bestemmes ud fra sammenhørende data for atmosfæretryk og vandspejl i boringen. Der findes en lang række forskellige metoder til bestemmelse hvoraf Clarks metode skulle være fordelagtig, hvis der er underliggende trends i data, som ikke skyldes ændringer i atmosfæretrykket (Batu, 1998). Hvis Clarks metode som beskrevet af Batu (1998) anvendes på data fra boring Geo17, og der tages udgangspunkt i de tre perioder, hvor der ikke pumpes, kan man bestemme barometrisk effektivitet til at være mellem 0,20 og 0,25. Hvis der i stedet tages udgangspunkt i den grafiske metode forslået af Gonthier (2007) kommer man også frem til en barometrisk effektivitet på omkring 0,22. Den barometriske effektivitet varierer lidt fra boring til boring, så der er justeret lidt i værdierne for den enkelte boring ud fra en visuel vurdering. De ligger dog alle omkring 0,20.

Vandspejlsdata korrigeres for barometrisk effekt ved følgende formel:

$$h_{t,korr} = h_t - BE \cdot (B_0 - B_t)$$

Hvor h_t er højden af vandspejlet til tiden t, $h_{t,corr}$ er højden af vandspejlet til tiden t korrigeret for barometereffekt, B_t er atmosfæretrykket til tiden t og B_0 er reference atmosfæretryk, begge i meter vandsøjle.

Hvis rådata fra vandspejlsloggeren sammenlignes med data fra barometerloggeren, ses det, at selvom der er en tydelig sammenhæng mellem de to tidsserier, så er svingningerne i de to tidsserier ikke helt synkrone. Der er en forsinkelse mellem trykændringer i atmosfæren og trykændringerne som vandspejlsloggeren oplever. Derfor er korrektionen tidsforskudt med omkring 3 timer.

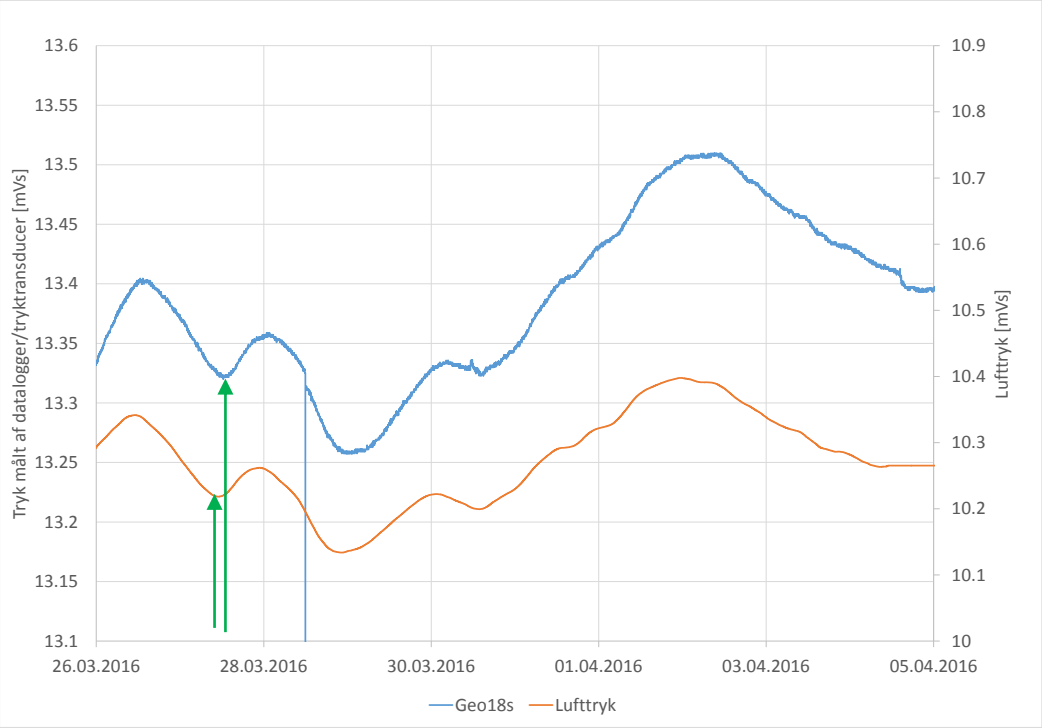

Figure 3.1: Tidsforskydning på omkring 3 timer mellem tryk registreret af vandspejllogger i boring Geo18s og lufttryk. De grønne pile viser forskellen mellem på toppunkter på hhv. vandtryk og lufttryk.

3.2.2.2 Trend

Udover den tydelige effekt at ændringer i atmosfæretrykket, lader der også til at være en generel nogenlunde lineær stigende trend i data. Denne kan kvantificeres til at være omkring 0.1 m/30 dage, og data er også korrigeret herfor.

Data korrigeres for lineær trend ved følgende formel: $h_{t,korr} = h_t - \tau \cdot (t - t_0)$

Samlet ser korrektionen af vandspejlet således ud som

$$h_{t,korr} = h_{total} - B_t - BE \cdot (B_0 - B_t) - \tau \cdot (t - t_0)$$

Efter korrektion for barometrisk effekt og lineær trend er der stadig en systematisk lille sinus formet variation i data. Der er omkring 12-12,5 time mellem toppene, og variationen formodes at skyldes månens og solens tyngdemæssige indvirkning på jorden, hvilket er et kendt fænomen. Der er ikke korrigeret for denne variation, der er mindre end 1 cm.

Figure 3.2: Korrektion af data fra pumpeforsøget. Den øverste, orange graf viser data, der ikke er korrigeret, mens den nederste grå graf viser de korrigerede data. De viste data er korrigeret for barometereffekt (korte udsving, ca. 1-2 cm i amplitude) og lineær trend (generel stigende tendens, ca. 5 cm over den viste tidsperiode).

4. Resultater af pumpeforsøg

4.1 Undersøgelsesmetoder

I de udførte boringer er der udført flere typer undersøgelser for at beskrive kalken geologisk og hydrogeologisk. De kan samlet opsummeres som geofysisk borehulslogging, hydrauliske forsøg og forsøg på kerneprøver. Herudover er der opsamlet vandprøver fra boringerne til kemisk analyse. Generelle brugbare undersøgelses metoder vurderet på opnåede parametre er skematisk opsummeret i Appendix H.

4.2 Geofysisk logging

De geofysiske borehulslogs har overordnet vist sig som alsidige metoder, der både kan anvendes i åbne og filtersatte boringer, dog er det ikke alle log-metoder der giver anvendelige resultater i filtersatte boringer. Det har i denne undersøgelse vist sig, at den optiske televiewer log (OTV) kan give brugbare resultater i DTH-boringer, hvor borevæggen er ujævn. Den akustiske televiewer gav til gengæld ikke gode resultater i en åben DTH-boring. I denne undersøgelse blev der ikke udført logging med NMR-metoden (nuklear magnetisk resonans), der kan give informationer om porøsitet, vandmætning og porestørrelse. Metoden er især

interessant i åbne boringer med lille diameter, f.eks. kerneboringer eller sonicboringer.

I Geo17 viser resultaterne (Figure 4.1) af gammaloggen ikke nogen markante markørhorisonter. Pga. boringens forsegling med bentonit mellem 10 og 12 m u.t. viser resultaterne i dette niveau primært bentonittens egenskaber og ikke kalkformationens. Herunder kan man dog genfinde mønstret i induktionsloggen (formationskonduktivitet) fra de øvrige boringer, hvor der over 20 m u.t. eller ca. kote 10 er tre bølger (markørhorisonterne Geo17-e, -f og –g). Derudover er et skifte i kalkens egenskaber indikeret omkring 20 m u.t. på induktionsloggen, porøsitetsloggen og densitetsloggen. Flowloggen viser at den største del af indstrømningen sker jævnt mellem 18,7 m u.t. og 21,7 m u.t., hvilket er er i overensstemmelse med flowloggen i Geo5, hvor der også sker en betydende indstrømning i dette niveau. Overordnet viser resultaterne af den geofysiske logging i Geo17 god overensstemmelse med de tidligere resultater på lokaliteten (Geo, 2015).

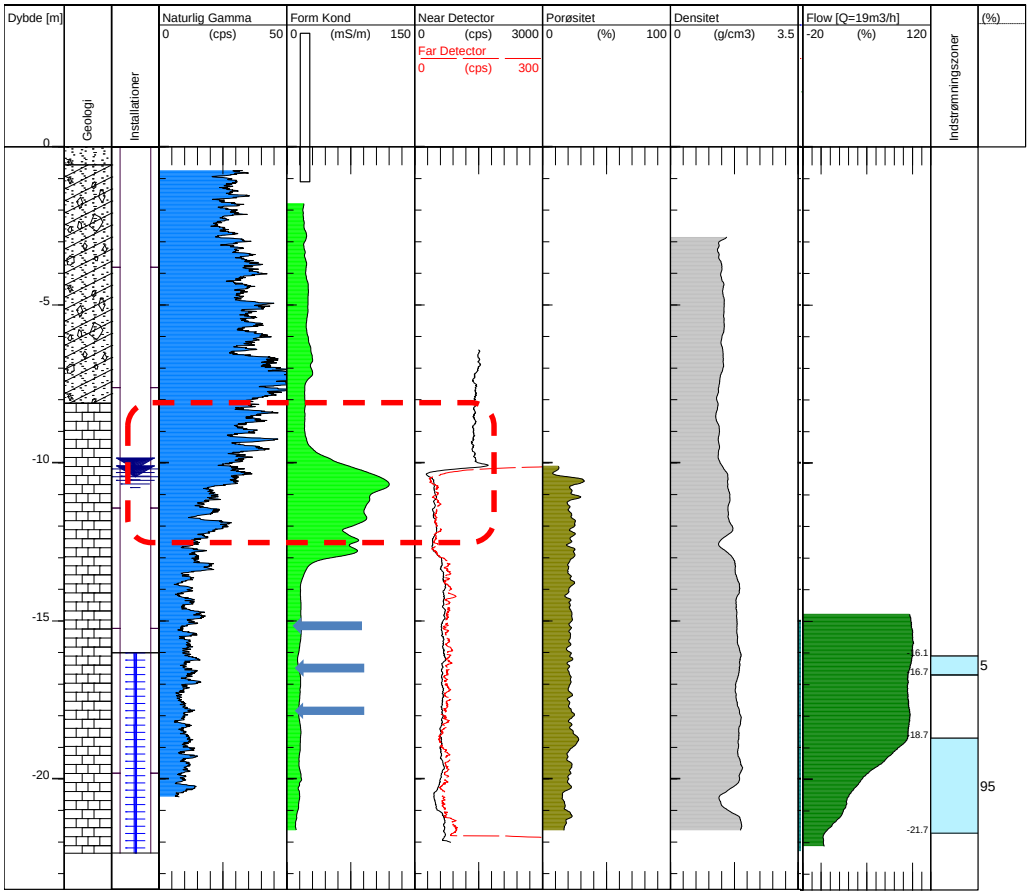

Figure 4.1. Et udsnit af resultaterne af den geofysiske log i Geo17. Påvirkningen fra afpropningen med bentonit er markeret med rød stiplet linje. De tre markørhorisonter Geo17-e, -f og –g er markeret med blå pile. Indstrømningszoner er markereret med lys blå. De fuldstændige resultater findes i Appendix B.

I Geo18 er resultaterne (Figure 4.2) over 28 m u.t. (før filtersætning) og over 23 m u.t. (efter filtersætning) påvirket af forerør og boringens udbygning (det øverste filter). På lokaliteten er der ikke tidligere udført boringer eller geofysisk logging under ca. 32 m u.t. (Geo4). Resultaterne af gamma-, induktions-, porøsitets- og

densitets-loggen viser en relativt ensartet kalk ned til 40 m u.t., hvor der sker en ændring i porøsiteten og induktionsloggen.

Flowloggen i den filtersatte boring viser indstrømning i relativt smalle zoner mellem ca. 25 m u.t. og 37 m u.t. Dette tolkes som indstrømning i sprækkezoner i denne del af kalken. Sprækkezonerne kan genfindes i flowloggen fra den ikke-filtersatte boring, men her er resultaterne forstyrret af turbulent strømning eller ujævnheder i boringsvæggen. Under 37 m u.t er der ganske lille indstrømning.

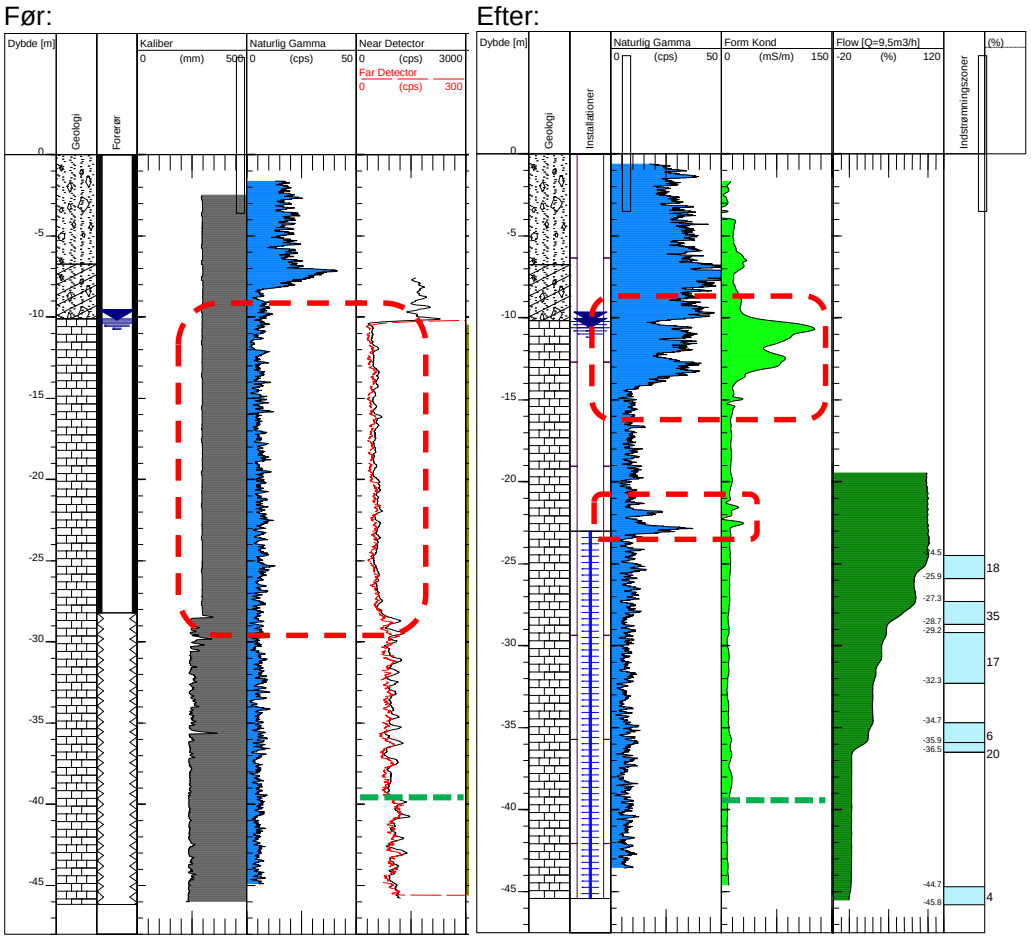

Figure 4.2. Et udsnit af resultaterne af den geofysiske log i Geo18, før og efter filtersætning. Påvirkningen fra afpropningen med bentonit og foringsrør er markeret med rød stiplet linje. Ændringer i porøsitets- og induktionsloggen er markeret med grøn stiplet linje. Indstrømningszoner er markereret med lys blå. De fuldstændige resultater findes i Appendix B.

Den optiske televiewerlog viser et billede af boringsvæggen, og det er muligt at identificere flintknolde og lag i den gennemborede kalk. Flint viser sig som mørke grå områder i den lyse grå til hvide kalk. Boringens væg er ujævn og lyskilden på sonden er derfor ikke i samme relative position i alle retninger og dybder. Der er derfor uens belysning af borevæggen, hvilket kan ses resulteret i lysere og mørkere områder i kalken. Ved 39,3 m u.t. eller ca. kote -10, er der et markant skifte i fordelingen af flint i kalken (Figure 4.3). Over dette niveau forekommer flinten i mange små knolde og enkelte lag. Under dette niveau forekommer flinten i større knolde og flere lag af mindre mægtighed. På lokaliteten er grænsen mellem Mellem og Øvre Danien (Stevns Klint Fm København Kalk Fm) bestemt til ca.

kote 10, og der er således ca. 20 m bryozokalk over den observerede grænse 39,3 m u.t. Stevns Klint Fm er tidligere beskrevet som ca. 60 m tyk og de øverste 20 m bryozokalk på lokaliteten kunne derfor svare til det øverste bankekompleks i bryzokalken (Geo og GEUS, 2014).

I den optiske televiewerlog kan der desuden observeres 8 vandrette sprækker og 1 lodret sprække, et eksempel er vist i Figure 4.4. Sprækkerne er listet i Table 4.1, hvor der også er markeret om der er observeret indstrømning i flowloggen i det pågældende niveau. Der er stor forskel på om der observeres indstrømning i den filtersatte eller ikkefiltersatte boring. I den filtersatte boring kan alle observerede sprækker kædes sammen med en indstrømningszone, mens det kun er tilfældet for den mest markante sprække i den ikke filtersatte boring. Den lodrette sprække er observeret mellem 29,7 og 30,1 m u.t. Den er således ca. 40 cm lang og forbinder to vandrette sprækker.

Pga. af boringens store diameter er det ikke umiddelbart muligt at tolke resultaterne af den akustiske televiewer.

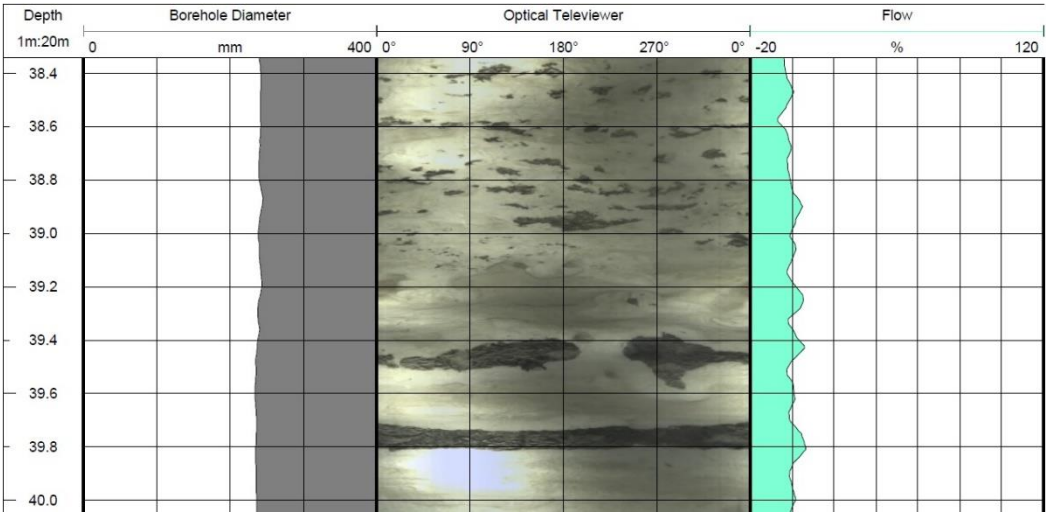

Figure 4.3. Et udsnit af resultaterne af den optiske televiewer log i Geo18. Der sker et markant skifte i fordelingen af flint ved ca. 39,3 m u.t., hvilket ses på billedet (Optical Televiewer). De fuldstændige resultater findes i Appendix C.

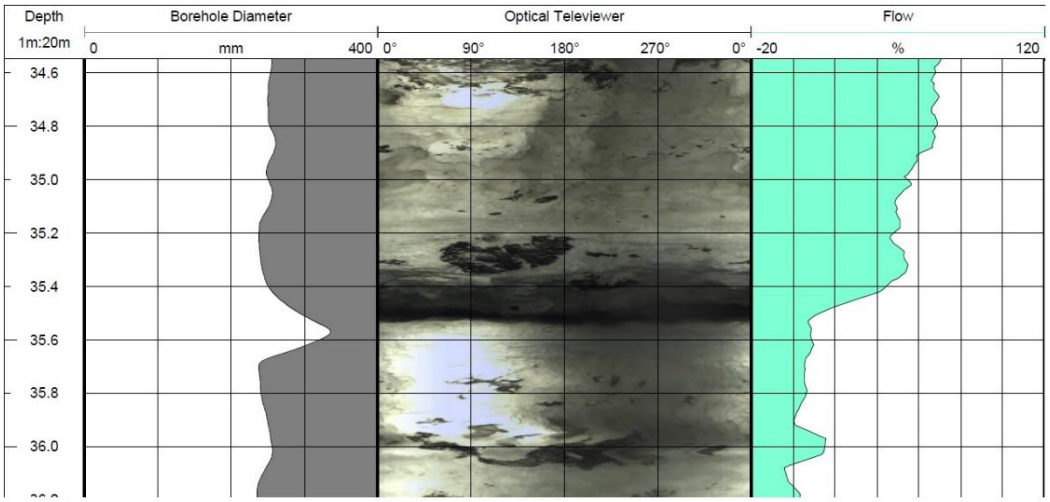

Figure 4.4. Et udsnit af resultaterne af den optiske televiewer log i Geo18. En sprække kan ses ca. ved 35,5 m u.t. og kan identificeres på kaliperloggen (Boreholde Diameter), på billedet (Optical Televiewer) og der sker en indstrømning i dette niveau (Flow). De fuldstændige resultater findes i Appendix C.

Nr.	Dybde af sprække (m u.t.)	Indstrømning i filtersat boring	Indstrømning i ikke filtersat boring
1	29,1	+	-
2	29,3	+	-
3	29,8	+	-
4	30,2	+	-
5	30,5	+	-
6	31,5	+	-
7	34,3	+	-
8	35,5	+	+

Table 4.1: Vandrette sprækker i Geo18.

4.3 Korttidspumpeforsøg

Niveauerne for de enkelte packerforsøg er fastlagt således, at de er udført på enkelte sprækker eller sprækkezoner. De enkelte forsøg er tolket udfra en antagelse om ensartede isotrope forhold i et spændt (porøst) magasin (Theis-løsning). Der er udelukkende benyttet sænkningsdata fra det pumpede interval (ingen observationsboringer), og data fra stigningsperioden er foretrukket, hvor der ikke er overensstemmelse mellem pumpe og stigningsdata. Resultaterne af de enkelte tolkninger er vist i Table 4.2.

Test nr.	Dybde af forsøg (m u.t.)	Transmissivitet (m^2/s)	S (kun tolknings-parameter)	Note	Sprække nr. (fra Table 4.1)
1	34,75 - 36,25	$2,3 \times 10^{-2}$	0,040	Pumpe og stigningsdata	8
2	33,25 - 34,75	$3,0 \times 10^{-4}$	$2,0 \times 10^{-4}$	Pumpedata	7
3	31,5 - 32,65	$2,2 \times 10^{-2}$	-	Stigningsdata	6
4	28,75 - 30,25	$5,2 \times 10^{-2}$	-	Stigningsdata	1, 2, 3, 4

Table 4.2: Resultater af packerforsøg.

Data fra pumpeforsøge er opsamlet og behandlet som beskrevet i afsnit 3.2.1 og 3.2.2, dog er der benyttet en måleinterval på 5 sekunder i pumpeboringen og 10 sekunder i observationsboringerne. Der er ikke korrigeret for trend på grund af pumpeforsøgets korte varighed, og der er ikke korrigeret for magasinets barometereffekt.

En tolkningskurve for trinpumpeforsøget i Geo17 er vist i Figure 4.5. Her er benyttet en Theis-model (isotrope forhold i en spændt, porøst magasin) med varierende pumperate. Resultaterne er i overensstemmelse med et magasin med en transmissivitet på ca. $7,1 \times 10^{-2}$ m^2/s, hvilket er i samme størrelsesorden, men dog lidt højere end de tidligere resultater fra lokaliteten (2×10^{-2} m^2/s til 5×10^{-2} m^2/s).

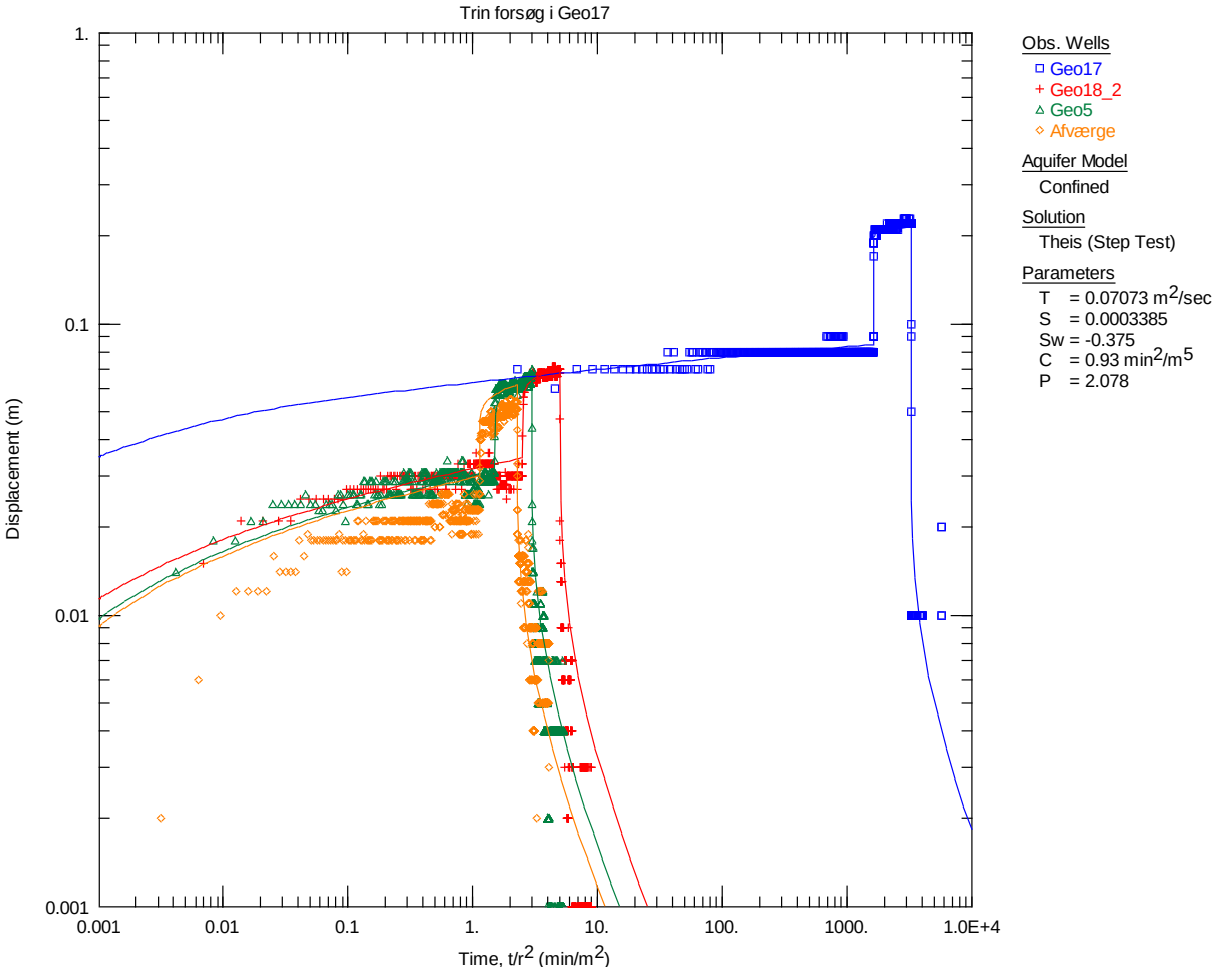

Figure 4.5. Tolkningskurve for trinforsøget i Geo17.

4.4 Pumpeforsøg

For at kunne uddrage magasinparametre til en grundvandsmodel er data fra pumpeforsøget tolket. Det vil sige, at en analytisk model for sænkningen er forsøgt tilpasset til data fra pumpeforsøget ved justering af parametrene i den analytiske model. Da der ved Akacievej er tale om strømning i sprækker, og da der ønskes magasin parametre til en såkaldt dobbeltporøs grundvands model, er det i hovedsagen forsøgt at tolke data under antagelse af, at magasinet kan betragtes som værende dobbeltporøst.

På Akacievej ligger grundvandspotentialet ca. 1-2 m under kalkoverfladen, og grundvandsmagasinet i kalken er således et delvist frit magasin. Der findes ikke umiddelbart en analytisk løsning, der kan beskrive sænkningen i et dobbelt-porøst, frit magasin. For at kunne tolke pumpeforsøget, er det derfor nødvendigt at se bort fra effekten af enten dobbeltporøsiteten eller det frie vandspejl. Sænkningen under pumpeforsøget er op til ca. 0,4 m under pumpeforsøget, og sammenlignet med den totale tykkelse af magasinet (ca. 21 m), vil effekten af det frie vandspejl være lille. Desuden er pumpeboringen og flere observations-boringer placeret 5 m eller mere under grundvandsspejlet (toppen af magasinet). Dette betyder, at effekten af det frie grundvandsspejl er lille, og at den forsinkede frigivelse af vand er påvirket af de dobbeltporøse forhold i magasinet. Samlet vurderes magasinet bedst at kunne beskrives som et spændt dobbeltporøst frem for et frit homogent magasin.

4.4.1 Dobbeltporøst magasin

Et opsprækket magasin med et tæt net af sprækker kan i mange tilfælde betragtes som et dobbeltporøst magasin. Det vil sige at magasinet kan ses som bestående af to domæner. Et sprækkedomæne med stor hydraulisk ledningsevne og lav magasin kapacitet (storage) samt et matrixdomæne med lav hydraulisk ledningsevne og stor magasin kapacitet. I et sådant system sker alt flow til boringen gennem sprækkerne, mens matrixen udveksler vand med sprækkerne. Når der pumpes falder trykket i sprækkerne og matrixen afgiver vand til sprækkerne pga. trykforskellen mellem matrix og sprække (Duffield, 2007).

Et sådant system vil, når det stresses ved pumpning, udvise en sænkningskurve med flere faser. I den første fase (tidlig fase) vil vandtransport gennem sprækkerne være bestemmende for sænkningskurvens udvikling. Herefter vil der være en transitionsperiode, hvor kurveudviklingen bestemmes af udvekslingen mellem matrix og sprækker, og til sidst vil der være en tredje fase (sen fase), hvor sænkningskurvens udvikling bestemmes af kombinationen af matrixens udveksling med sprækkerne og vandtransporten i sprækkerne. Den tidlige og den sene fase følger begge en Theis kurve, og i et log sænkning- tid plot, vil de udvise rette linjer med samme hældning, som svarer til transmissiviteten af sprækkedomænet. Man vil ideelt set kunne observere overgangen mellem den tidlige fase og transitionsfasen som et nedadvendt knæk mod lavere hældning, og overgangen mellem transitionsfasen og den sene fase som et opadvendt knæk mod højere hældning.

Ifølge Nielsen (2007), kan transitionsperioden begynde meget hurtigt i spændte dobbeltporøse magasiner med lav magasin kapacitet. Han nævner få sekunder. Den første fase kan derfor meget vel være maskeret af borehulseffekten.

Specielt i magasiner med små blokke (tæt net af sprækker) og stor hydraulisk ledningsevne af magasinet, vil trykket hurtigt udlignes mellem sprække og matrix, og transitionsperioden vil være kort. Derfor ser man i praksis ofte kun den tredje fase, som ligner en normal Theis kurve. I dette tilfælde er det kun hydraulisk ledningsevne for sprækkerne som kan bestemmes. I andre tilfælde kan der opstå en pseudo steady state i transitionsperioden som så kan vare længere (timer).

Uheldigvis ligner dele af kurveforløbet for et dobbeltporøst magasin forskellige situationer i et almindeligt porøst magasin. De to første faser fra et pumpeforsøg i et dobbeltporøst magasin vil ligne sænkningskurven fra et almindeligt porøst magasin med en positiv grænse eller lækage. Og de to sidste faser vil ligne sænkningskurven fra et almindeligt porøst magasin med negativ grænse.

4.4.2 Borehulseffekt

Når pumpen starter vil der være en kort periode hvor sænkningen i boringen er domineret af at det vand som står i filterrøret tømmes ud.

I denne periode styres sænkningen ikke af hvad magasinet kan yde, men kan fejlagtigt tages for at være den første fase i sænkningskurven fra et dobbeltporøst magasin. Borehulseffekten kan også overlappe og dermed maskere den første fase i sænkningskurven fra et dobbeltporøst magasin. Tidsrummet hvor borehulseffekten styrer sænkningen kan beregnes ud fra:

$$t = \frac{\pi(r_c^2 - r_{rm}^2)s_w}{Q} \qquad (1)$$

I tilfælde hvor der er større sprækker i direkte kontakt med boringen vil disse også kunne bidrage til borehulseffekten og tidsrummet hvor denne er styrende vil være længere end estimeret ud fra formel (1) (Nielsen, 2007).

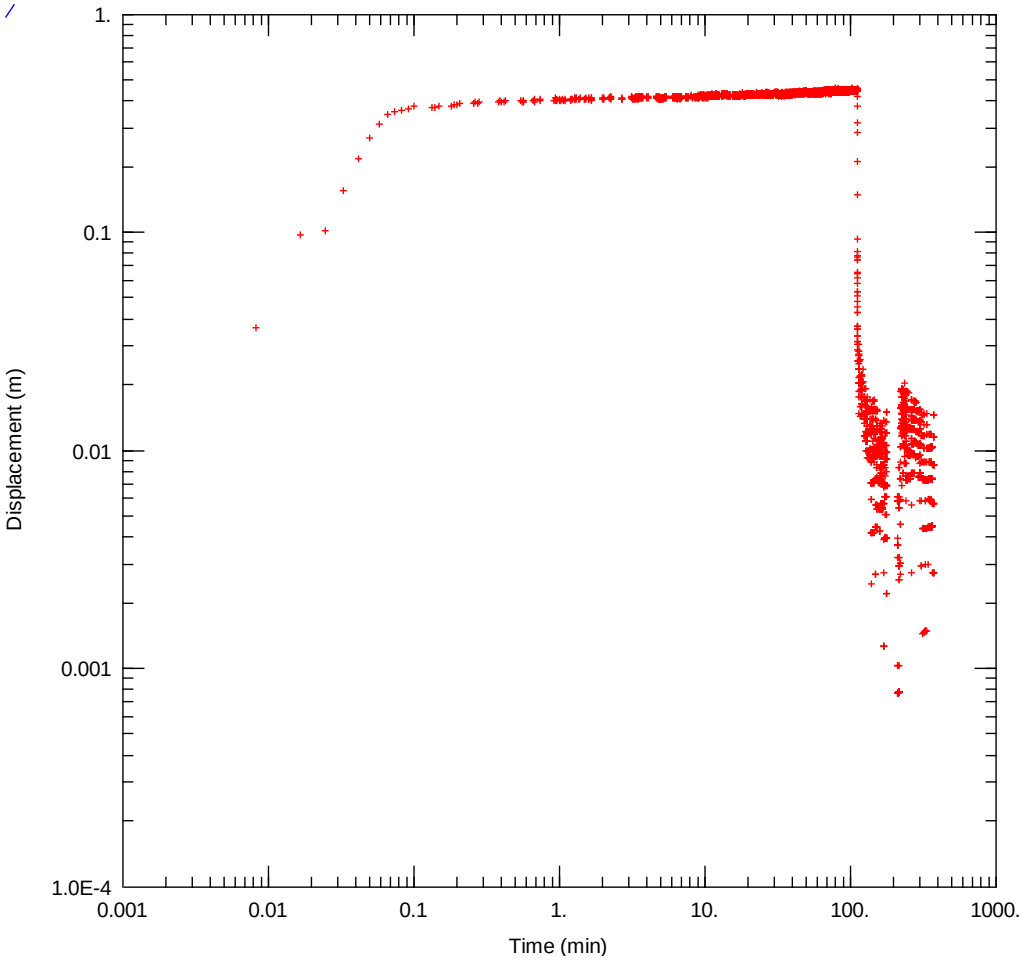

Figure 4.6: log-log plot af sænkningen i Geo17 mod tid for tredje pumpeforsøg. Den blå linje har hældningen 1.

I et log-log plot af sænkning mod tid vil data i perioden hvor borehulseffekten er styrende beskrive en linje med hældningen 1 og i et plot af den afledte (numerisk differentierede) viser borehulseffekten sig som en bule, se Figure 4.6 og Figure 4.7. For tredje pumpeforsøg i boring Geo17 var borehulseffekten styrende i omkring 0.08 min.

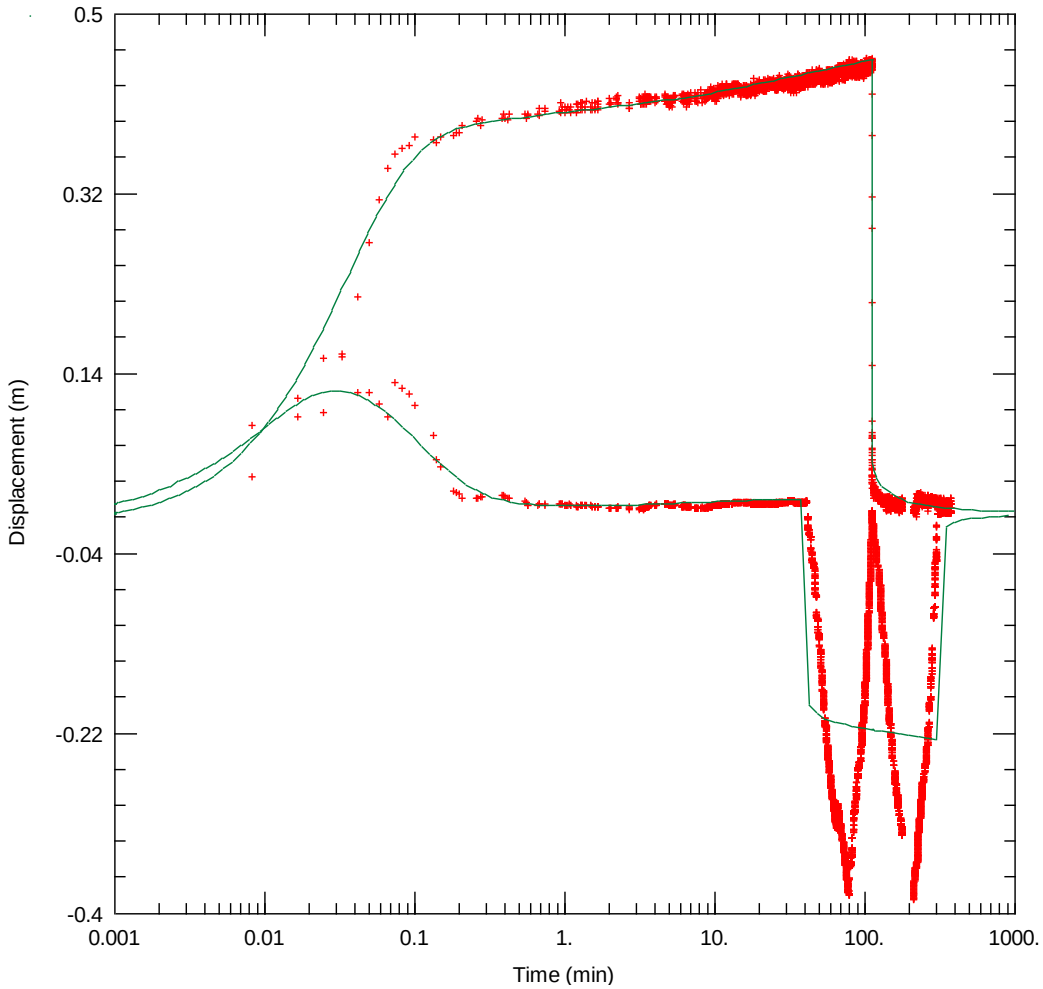

Figure 4.7: Den observerede sænkning (røde kors) i pumpeboringen Geo17 sammen med den afledte heraf (den numerisk differentierede af sænkningen, nederste datasæt, også røde kors). De grønne linjer er en Moench-løsning der svarer til de observerede data.

4.4.3 Tolkning i AQTESOLV

Programmet AQTESOLV for Windows (Duffield, 2007) er anvendt til tolkningen af pumpeforsøget og en Moench dobbeltporøs løsning med slab blocks (Moench, 1984) er forsøgt tilpasset til data. Moench er en dobbeltporøs løsning som kan tage hensyn til borehuls effekt, filtertab og partiel filtersætning. Parametrene som fittes med Moench er:

K: Hydraulisk ledningsevne for sprækkerne
Ss: Specifik magasinkapacitet for sprækkerne
K': Hydraulisk ledningsevne for matrixen
Ss': Specifik magasinkapacitet for matrixen
Sf: Sprække skin (modstand i overgangen mellem sprække og matrix)
s_w: Filtertab
r_w: Boringsradius
r_c: Filterrørs radius

Desuden er der for første periode benyttet Barker dobbeltporøs løsning med slab blocks. Her fittes desuden parameteren n, der beskriver dimensionen af strømningen (1= lineær, 2= cylindrisk, 3 = sfærisk). Modsat Moench, kan Barker

løsningen ikke tage højde for delvis filtersætning af grundvandsmagasinet, dvs. det antages at filtersætningen af pumpe- og observationsboringer er udført i hele magasinets tykkelse.

Data er korrigeret for lineær drift over hele perioden samt barometereffekt som beskrevet. Herudover er der for periode 1 korrigeret yderligere for lineær trend observeret over denne periode. De færdigkorrigerede vandspejlsdata er efterfølgende komprimeret og omregnet til tid siden pumpestart og sænkning inden indførsel i tolkningsprogrammet. Tidspunktet for start og stop af pumpen er fundet ved analyse af data fra pumpeboringen. Pumperatedata er ligeledes komprimeret og omregnet til tid siden pumpestart.

Der er i tolkningen regnet med at grundvandsmagasinet går fra rovandspejlet ca. 9 m.u.t. til 30 m.u.t. og dermed er 21 meter tykt. Boringerne er således kun filtersat i en del af dette magasin og der regnes derfor med partiel filtersætning. Der er regnet med en generel anisotropi Kv/Kh lig 0.1. Der er anvendt en tykkelse af slab blokkene på 2.5 meter, valgt ud fra kendskabet til sprækkefordelingen (Geo, 2015).

Der er tolket på sænkning fra første periode og på stigning og sænkning fra tredje periode. Tilpasningen er i hovedsagen udført manuelt ved justering af parametre og visuel vurdering.

Data fra første periode
På grund af den høje transmissivitet og begrænsning i maksimal pumperate er sænkningerne meget små i forhold til et typisk pumpeforsøg. Dette giver et dårligt signal-støj forhold og betyder samtidig at datakorrektionen får stor betydning. Herudover sker sænkningen meget hurtigt i en række observations-boringer. Det betyder at meget af sænkningen sker i et tidsrum med borehuls-effekt. Den hurtige sænkning betyder også at pumpens opstart får indflydelse på formen af sænkningskurven. Pumpen styres af en frekvensomformer som har en ”ramp-up time” hvilket vil sige at den starter blødt op og når sænkningen sker meget hurtigt påvirker måden pumpen starter på kurvens forløb. Det har ikke været muligt at opsamle pumperatedata med tilstrækkeligt kort interval til at kunne indbygge dette i tolkningsgrundlaget.

Grundvandsmagasinet ved Akacievej er på grænsen mellem at være spændt og frit. Ingen af de analytiske metoder kan beskrive et frit, dobbeltporøst magasin.

Indledningsvis er observationsboringerne grupperet i 5 grupper, på baggrund af deres sænkningsforløb, således at observationsboringer med ensartet respons er samlet. Opdelingen er foretaget på baggrund af et sænknings-afstandsplot, hvor observationsboringerne i de enkelte grupper plotter på en ret linje (Figure 4.8). Grupperingen af observationsboringerne fremgår af Table 4.3.

Den observerede sænkning i hver af de 5 grupper er tilpasset 5 forskellige teoretiske modeller, der hver kan give information om magasinets hydrauliske egenskaber. Indledningsvis er der benyttet en Theis løsning på pumpeperioden og stigningsperioden. I både pumpeperioden og i stigningsperioden ses et knæk op på kurven, mod slutningen af perioden. Dette indikerer at forholdene i magasinet ikke

er i overensstemmelse med antagelserne i den teoretiske model, dvs. at magasinet ikke er spændt, homogent, isotropt eller uendeligt. Knækket kan indikere effekten af dobbeltporøsitet, et frit magasin eller evt. en afgrænsning af magasinet. Ud fra forhåndskendskab til geologien i området, antages det at knækket skyldes dobbeltporøsitet. Der er ikke nogen kendt afgrænsning af magasinet og det vurderes at effekten af det frie grundvandsspejl er lille.

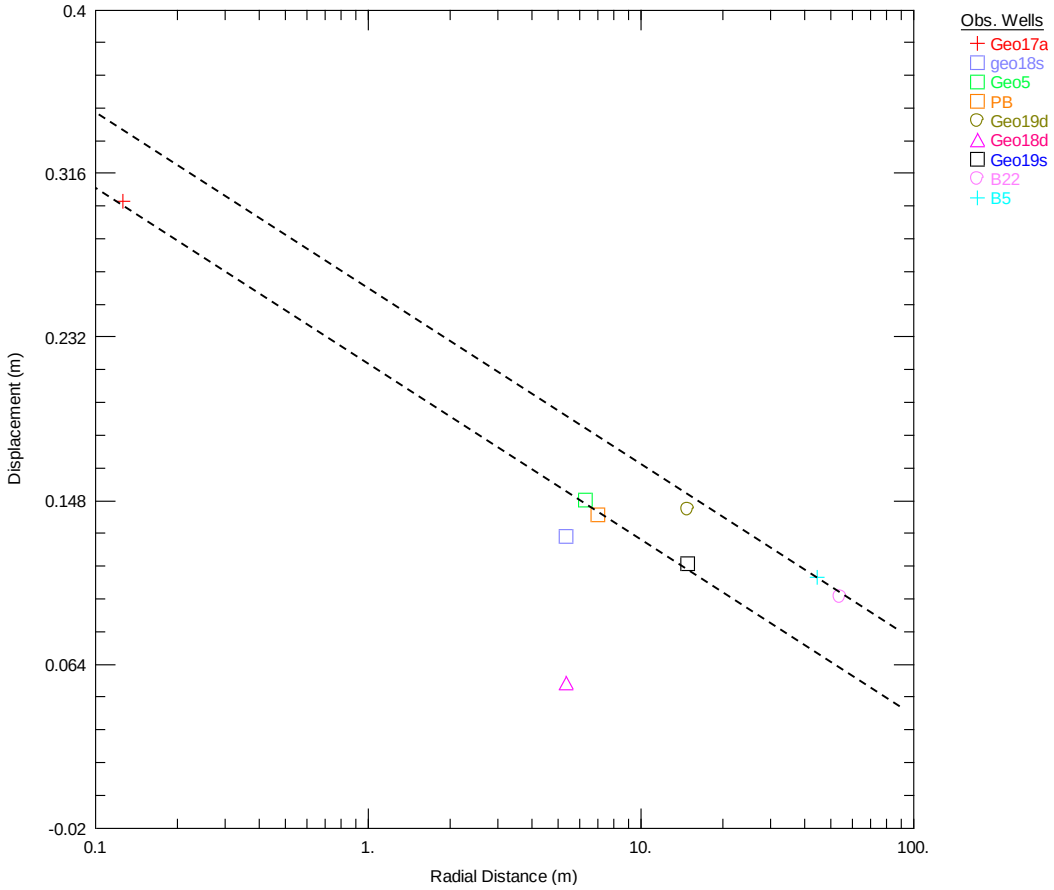

Figure 4.8: Afstands-sænkningsplot fra første pumpeperiode med observationsboringer.

Det observerede knæk på sænkningskurverne fører til at de estimerede værdier for transmissiviteten bliver for store, når der benyttes en Theis-løsning. For at estimere den faktiske transmissivitet kan man benytte de sene data eller de meget tidlige data. De tidlige data er i dette forsøg påvirkede af borehuls effekt og pumpestart, så en Theis løsning er tilpasset de sene data, her er der valgt en løsning der passer til både pumpe- og stigningsdata. De estimerede parametre er repræsentative for den totale transmissivitet, der er domineret af sprække-transmissiviteten samt det totale magasintal (storativitet), der er domineret af matrix. Parametrene benyttes som indledende estimater for sprække-transmissiviteten og den specifikke magasinkapacitet i de efterfølgende tolkninger med dobbeltporøse modeller.

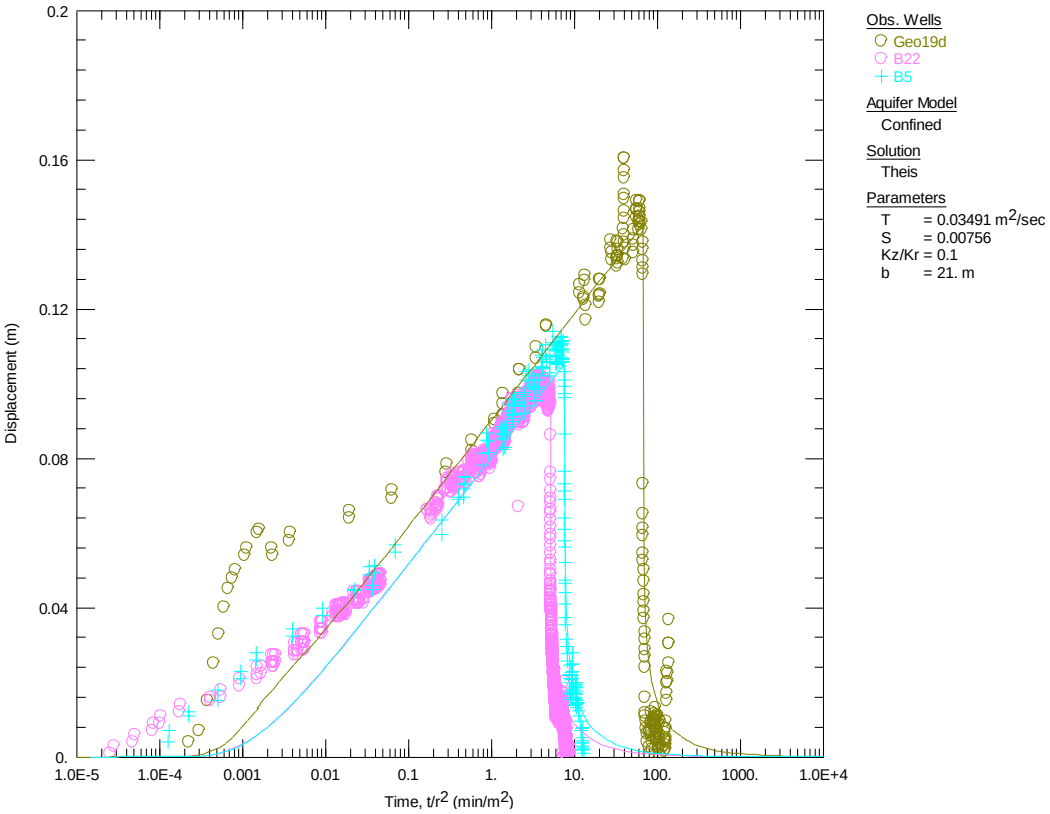

Figure 4.9: Sænkningskurver i semilogaritmisk plot for boringerne B5, B22 og Geo19d (dybt filter). Til tidlige tider, mindre en 0,001 (her vist som t/r^2) ses den tidlige strømning i sprækker, der også er influeret af borehulseffekt. Herefter en transitionsperiode, hvor udviklingen i sænkningen går langsommere. Til sidst ses den fuldt udviklede strømning, der er tilpasset en lineær løsning. Den viste løsning (optrukne linjer) er en Theis løsning der er tilpasset den sidste del af pumpeforsøget, hvor der antages at være strømning i både matrix og sprækker. Transmissiviteten er repræsentativ for sprækkerne, mens magasintallet (storativiteten) er domineret af matrix.

Der er benyttet to forskellige dobbeltporøse modeller til at tolke pumpeforsøget, Moench og Barker. Data blev først tilpasset en Moench model, men den kan ikke i alle tilfælde beskrive sænkningsforløbet til tidlige tider (Figure 4.10). Dog kan der i (næsten) alle tilfælde findes en løsning der beskriver den sidste del af transitionsperioden, dvs. modellen beskriver kurvens knæk. Kurvens knæk bestemmes primært af parametrene Ss, K' og Sf, men de andre parametre har også indflydelse på den tidlige del af sænkningsforløbet. Parametrene virker i fællesskab og der er flere parameterkombinationer som giver samme grad af fit. Der er derfor foretrukket "normale" værdier og kun valgt "unormale" værdier når det ikke kunne undgås. Under fitningen er K og Ss' generelt justeret først (hvis nødvendigt i forhold til Theis-løsning) og herefter de andre parametre.

For at opnå en bedre tilpasning til de tidligere data er der også benyttet en Barker løsning (Figure 4.10). Barker løsningen beskriver de tidlige data bedre end Moench modellen, men den tager ikke højde for den partielle filtersætning i magasinet. De estimerede parametre for Barker løsningen er meget lig de estimerede parametre for Moench løsningen (Table 4.3).

Parametrene for de enkelte tilpasse løsninger er opsummeret Table 4.3 og grafer for alle tolkninger er vedlagt i Appendix G. For løsninger, hvor Theis-modellen er benyttet, er transmissiviteten, T og magasintallet (magasinkapacitet), S omregnet til ledningsevne, K og specifik magasinkapacitet (for matrix) Ss', ved at dividere

med magasintykkelsen, b, der er fastsat til 21 m. Resultaterne kan så sammenlignes direkte med resultaterne fra de egentligt dobbeltporøse modeller (Moench og Barker).

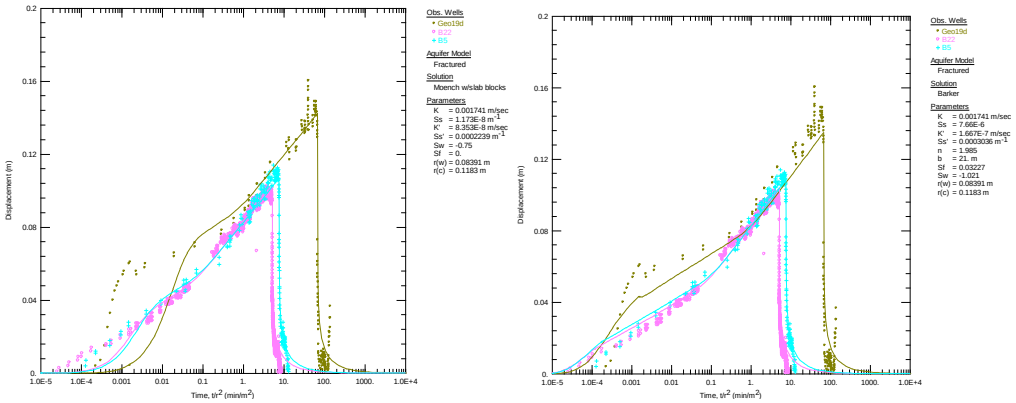

Figure 4.10: To forskellige dobbeltporøse modeller, tilpasset data fra boringerne B5, B22 og Geo19d (dybt filter).

K kunne i alle tilfælde bestemmes med rimelig sikkerhed. Generelt er modellerne følsomme overfor alle parametre, og de er derfor estimeret med en rimelig sikkerhed. Normalt kunne kun en øvre grænse for Ss bestemmes. Typisk ændrede det ikke på fittet at sænke Ss under en vis grænse, og der er derfor valgt den højeste værdi som kunne passe. Sf kan i nogle tilfælde hjælpe med at få modellen til at fitte meget tidlige data men i andre tilfælde ikke. For Geo18d kunne modellen kun tilpasses tidlige data med meget lav Ss'. I disse tilfælde kan K' ikke bestemmes. De enkelte observationsgrupper giver forskellige løsninger, og det kan ikke lade sig gøre at bestemme magasinets hydrauliske parametre med mindre usikkerhed, end hvad de forskellige løsninger indikerer.

Resultaterne fra Geo17 er påvirket kraftigt af at denne boring er pumpeboringen. Således er resultaterne for den specifikke magasinkapacitet i Theis løsningerne påvirkede og kan ikke regnes for at være repræsentative for magasinet.

Resultaterne fra Geo18d er påvirkede af at dette filter liggere dybere end pumpeboringen og magasinets horisontale/vertikale anisotropi for meget stor indflydelse. Anisotropien er desuden meget afhængig af sprækkesystemets geometri, og på grund af den lille afstand mellem pumpeboringen og Geo18d er de enkelte sprækkers placering i forhold til boringerne også afgørende for sænkningens forløb. Sammenholdt med de opnående resultater af tolkningerne, må det konkluderes at Geo18d ikke giver repræsentative værdier for magasinets hydrauliske egenskaber. Resultaterne (den meget lille sænkning) indikerer dog en kraftig anisotropi i magasinet hvilket kan indikere at sprækkesystemet er domineret af vandrette sprækker.

De tolkede specifikke magasinkapaciteter for boringerne Geo5, PB og Geo19s er væsentlig højere end for boringerne Geo19d, B5 og B22. Fælles for boringerne Geo5, PB og Geo19s er, at de er filtersat helt eller delvist i den øverste opknuste zone af kalken. Den højere specifikke magasinkapacitet kan således både være et udtryk for andre egenskaber i den opknuste kalk, men den kan også være et udtryk for magasinets frie grundvandsspejl.

Boringer/ filtre	Parameter	Theis (sænkning)	Theis (stigning)	Theis (sene tider)	Moench	Barker
Geo17	K [m/s]	2.64×10^{-3}	2.97×10^{-3}	2.16×10^{-3}	1.71×10^{-3}	1.45×10^{-3}
	Ss [1/m]				2.68×10^{-7}	1.92×10^{-6}
	K' [m/s]				8.35×10^{-8}	5.15×10^{-10}
	S/Ss' [1/m]	1.31×10^{-3}	1.69×10^{-5}	1.59	2.24×10^{-4}	5.15×10^{-5}
	n					2
	Sf				0	1.15
	Sw				-2.175	0.6027
	r(w) [m]				0.127	0.127
	r(c) [m]				0.1276	0.1267
Geo5, PB, Geo19s	K [m/s]	1.84×10^{-3}	2.65×10^{-3}	1.27×10^{-3}	1.46×10^{-3}	1.60×10^{-3}
	Ss [1/m]				4.60×10^{-6}	0.000208
	K' [m/s]				5.91×10^{-7}	4.19×10^{-7}
	S/Ss' [1/m]	1.54×10^{-4}	4.18×10^{-5}	5.15×10^{-3}	1.78×10^{-3}	1.59×10^{-3}
	n					2
	Sf				0.2	0.2
	Sw				-0.725	-0.725
	r(w) [m]				0.127	0.127
	r(c) [m]				0.1267	0.1267
Geo19d, B5, B22	K [m/s]	2.02×10^{-3}	2.21×10^{-3}	1.66×10^{-3}	1.74×10^{-3}	1.74×10^{-3}
	Ss [1/m]				1.17×10^{-8}	7.66×10^{-6}
	K' [m/s]				8.35×10^{-8}	1.67×10^{-7}
	S/Ss' [1/m]	4.18×10^{-5}	7.62×10^{-5}	3.60×10^{-4}	2.24×10^{-4}	3.04×10^{-4}
	n					1.985
	Sf				0	0.03227
	Sw				-0.75	-1.021
	r(w) [m]				0.08391	0.08391
	r(c) [m]				0.1183	0.1183
Geo18s	K [m/s]	2.69×10^{-3}	2.69×10^{-3}	2.00×10^{-3}	2.57×10^{-3}	1.86×10^{-3}
	Ss [1/m]				2.34×10^{-4}	1.04×10^{-5}
	K' [m/s]				3.73×10^{-5}	9.37×10^{-6}
	S/Ss' [1/m]	5.76×10^{-4}	5.76×10^{-4}	1.43×10^{-2}	6.31×10^{-4}	6.31×10^{-4}
	n					2
	Sf				0	0
	Sw				-2.652	-2.85
	r(w) [m]				0.127	0.127
	r(c) [m]				0.05531	0.05531
Geo18d	K [m/s]	4.90×10^{-3}	5.31×10^{-3}	2.14×10^{-3}	2.85×10^{-3}	
	Ss [1/m]				2.53×10^{-2}	
	K'				1.67×10^{-8}	
	S/Ss' [1/m]	1.28×10^{-3}	4.74×10^{-3}	4.76×10^{-2}	3.98×10^{-17}	
	n					
	Sf				0.45	
	Sw				-2.55	
	r(w) [m]				0.127	
	r(c) [m]				0.05531	

Table 4.3: Opsummering af tolkninger af første pumpeperiode.

Data fra tredje periode

Generelt har det været vanskeligt at tilpasse en dobbeltporøs Moench model til data fra tredje periode.

Parametrene virker i fællesskab og der er flere parameterkombinationer som giver samme grad af fit. Der er derfor foretrukket "normale" værdier og kun valgt "unormale" værdier når det ikke kunne undgås.

Under fitningen er K og Ss' generelt justeret først og herefter de andre parametre. Filtertabet er holdt på 0 i alle tilpasninger og generelt er det også forsøgt at holde Sf på 0. Filterrørsradius og boringsradius er holdt på nominelle værdier.

K kunne i alle tilfælde bestemmes med rimelig sikkerhed. Normalt kunne kun en øvre grænse for Ss bestemmes. Typisk ændrede det ikke på fittet at sænke Ss under en vis grænse. Der er derfor valgt den højeste værdi som kunne passe. Sf kan i nogle tilfælde hjælpe med at få modellen til at fitte meget tidlige data men i andre tilfælde ikke. I nogle tilfælde kunne modellen kun tilpasses tidlige data med meget lav Ss'. I disse tilfælde kan K' ikke bestemmes.

Data fra en del af observationsboringerne kunne fittes meget godt med en almindelig Theis løsning. I nogle tilfælde dog kun hvis magasinet antages at være meget tykkere end de 21 meter som ellers er brugt som udgangspunkt. Tilsvarende kunne en Neumann løsning for et frit magasin i nogle tilfælde fittes langt bedre end en Moench. Når en Theis eller Neumann model fitter data lige så godt eller bedre end Moench dobbeltporøs vurderes det at de dobbeltporøse parametre er dårligt bestemt. Der er ikke benyttet Barker-løsning til data fra tredje periode, da de dobbeltporøse egenskaber ved magasinet generelt ikke er særligt tydelige i data.

Tolkningerne er opsummeret i Table 4.4 og grafer for alle tolkninger er vedlagt i Appendix G.

Table 4.4. Fortsættes på næste side.

Boringer/ filtre	Parameter	Theis (sænkning)	Theis (stigning)	Moench (sænkning)	Moench (stigning)	Note
B22, B5	K [m/s] Ss [1/m] K' [m/s] S/Ss' [1/m] n Sf Sw r(w) [m] r(c) [m]	$3{,}2\times10^{-3}$ $4{,}0\times10^{-5}$	$3{,}2\times10^{-3}$ $4{,}0\times10^{-5}$			Perfekt fit til Theis løsning, der kan ikke observeres et knæk og Moench kan ikke fittes.
Geo19s	K [m/s] Ss [1/m] K' [m/s] S/Ss' [1/m] n Sf Sw r(w) [m] r(c) [m]			$6{,}75\times10^{-3}$ $1{,}81\times10^{-8}$ $9{,}37\times10^{-9}$ $1{,}12\times10^{-8}$ - 0 0	$5{,}36\times10^{-3}$ $6{,}33\times10^{-7}$ usikker $6{,}31\times10^{-6}$ 0 0	Kan kun fittes rimeligt med meget lav Ss'. K' kan ikke bestemmes. Godt Theis fit, men kun med øget (90 m) magasintykkelse.

Boringer/ filtre	Parameter	Theis (sænkning)	Theis (stigning)	Moench (sænkning)	Moench (stigning)	Note
Geo17	K [m/s] Ss [1/m] K' [m/s] S/Ss' [1/m] n Sf Sw r(w) [m] r(c) [m]			$2{,}55\times10^{-3}$ $2{,}21\times10^{-5}$ $3{,}73\times10^{-7}$ $1{,}41\times10^{-4}$ - 0 0	$2{,}55\times10^{-3}$ $6{,}42\times10^{-5}$ $2{,}35\times10^{-7}$ $2{,}24\times10^{-3}$ - 0 0	
Geo18s, Geo5	K [m/s] Ss [1/m] K' [m/s] S/Ss' [1/m] n Sf Sw r(w) [m] r(c) [m]	$2{,}4\times10^{-3}$ $1{,}7\times10^{-4}$				Meget hurtig reaktion på pumpning. Øget (40 m) magasintykkelse Kan fittes med Neumann (frit).
Geo18d	K [m/s] Ss [1/m] K' [m/s] S/Ss' [1/m] n Sf Sw r(w) [m] r(c) [m]	$9{,}0\times10^{-3}$ $9{,}5\times10^{-4}$		$1{,}14\times10^{-2}$ $1{,}14\times10^{-4}$ $2{,}10\times10^{-6}$ $2{,}51\times10^{-4}$ 0 0	$1{,}01\times10^{-2}$ $1{,}14\times10^{-4}$ $1{,}32\times10^{-6}$ $2{,}51\times10^{-4}$	
Geo19d	K [m/s] Ss [1/m] K' [m/s] S/Ss' [1/m] n Sf Sw r(w) [m] r(c) [m]					Kan fittes med Theis, men kun med øget magasintykkelse (100m) Kan fittes rimeligt med Neumann frit magasin.
PB	K [m/s] Ss [1/m] K' [m/s] S/Ss' [1/m] n Sf Sw r(w) [m] r(c) [m]	$1{,}5\times10^{-3}$ $7{,}1\times10^{-5}$	$1{,}5\times10^{-3}$ $7{,}1\times10^{-5}$			Der kan ikke observeres noget knæk. Kan fittes med Neumann frit magasin. Kan fittes med Theis, men kun med øget (95 m) magasintykkelse

Table 4.4 Fortsat. Opsummering af tolkninger af tredje pumpeperiode. Transmissivitet (T) og magasintal (S) er omregnet til ledningsevne (K) eller specifik kapacitet (Ss) ved hjælp af magasintykkelsen, b = 21 m, med mindre en anden værdi er angivet ved den enkelte tolkning.

4.4.4 Resultater fra pumpeforsøg

De to tolkede pumpe- og stigningsperioder giver nogenlunde ensartede oplysninger om magasinets egenskaber, i det omfang disse egenskaber kan bestemmes med rimelig sikkerhed (Table 4.5). Data fra den første pumpeperiode giver desuden oplysninger om magasinets dobbeltporøse egenskaber. Det bedste estimat på den opsprækkede kalks ledningsevne i sprækkerne er estimeret til mellem 1.5×10^{-3} m/s og 2.1×10^{-3} m/s. Den specifikke magasinkapacitet for sprækker er estimeret til ca. 1×10^{-6} 1/m, men kan variere mellem 1×10^{-8} 1/m og 1×10^{-5} 1/m. Den hydrauliske ledningsevne i matrix kan estimeres til ca. 1×10^{-7} m/s, men kan variere mellem 8×10^{-8} m/s og 6×10^{-7} m/s. Ud fra de tidligere udførte porøsitetslogs og permeabillitetsforsøg på borekerner (Geo, 2015) kan man estimere en lednings evne for matrix på mellem $1{,}6 \times 10^{-8}$ m/s og $1{,}3 \times 10^{-7}$ m/s, hvilket er i god overensstemmelse med resultaterne af pumpe-forsøget. Den specifikke magasinkapacitet for matrix kan bestemmes til ca. 2.5×10^{-4} 1/m, men kan variere mellem 5×10^{-5} 1/m og 5×10^{-3} 1/m. Samlet er den opsprækkede kalks egenskaber opsummeret i Table 4.6, der er opdateret fra Geo (2015).

Pumpeperiode	Sprække-permeabilitet	Magasin-kapacitet, sprække	Matrix-permeabilitet	Magasin-kapacitet, matrix	Samlet permeabilitet
1. pumpeperiode (lang)	Ja	Ja	Ja	Ja	Ja
3. Pumpeperiode (kort)	Ja	Delvist	Nej	Delvist	Ja (hvis sprækker dominerer)
Poroperm og logs	Nej	Nej	Ja	Nej	Nej

Table 4.5. Oversigt over de opnåede resultater fra pumpeforsøget samt hvad poroperm og logs kan bidrage med. Farverne indikerer den vurderede usikkerhed ved resultaterne. Blå: meget sikker, grøn: sikker, gul-orange: usikker, rød: meget usikker.

Der er benyttet to forskellige tolkningsmodeller til dobbeltporøse grundvandsmagasiner, Moench og Barker. Den største forskel på de to er at Barker ikke kan tage højde for delvis filtersætning af magasinet. På data fra første periode tilpasser Barker-løsningen de tidlige data bedst, og da strømningen er domineret af vandrette sprækker, og dermed er meget anisotrop, kan det være en rimelig antagelse at filtersætningen dækker hele grundvandsmagasinets tykkelse. Dette kan muligvis forklare noget af forskellen mellem de to tolkningsmodeller.

Under pumpeforsøget reagerede vandstanden i observationsboringerne ikke udelukkende som forventet ud fra de teoretiske modeller, benyttet under tolkningen. Denne varierende respons danne grundlag for inddelingen i grupper, og kan tolkes som et udtryk for sprækkesystemets indflydelse på grundvandsstrømningen under pumpeforsøget. Således reagerede boringerne Geo5, PB og Geo18 forskelligt, selvom de er placeret i ca. samme afstand til pumpeboringen. En del af forskellen skyldes sandsynligvis at filtrene ikke er placeret i samme dybder og en del af filtrene i Geo5 og PB er placeret i den opknuste zone, øverst i kalken. Andre boringer reagerede relativt ens, selvom deres afstand til pumpeboringen var mere varierende (f.eks. Geo19d, B5, B22). Det er ikke umiddelbart muligt at udlede mere præcis viden om sprækkernes indbyrdes

forbindelser ud fra disse forskelle, men de viser at sprækkerne kan have en afgørende indflydelse på grundvandsstrømningen (retning, niveau mv.).

Kommune: Høje-Taastrup Område: Akacievej	Datagrundlag: Denne undersøgelse samt Geo (2015)	Udført af: MMR Dato: 2016-07-13	
Parameter	**Knust/opsprækket kalk**	**Kalksandskalk**	**Bryozokalk**
Porøsitet	10 % - 30 %, sprækkeporøsitet, 1 % - 1,5 %	7,2 % - 46,1 %, sprækkeporøsitet, 1 % - 1,5 %	7,2 % - 46,1 %, sprækkeporøsitet, 1 % - 1,5 %
Grundvandsstrømning	Overvejende mod ØNØ	Overvejende mod ØNØ	Overvejende mod ØNØ
Grundvandsspejl	Delvist umættet, ca. 18,5 m DVR90	ca. 18,5 m DVR90	ca. 18,5 m DVR90
Samlet permeabilitet	$0{,}8 \times 10^{-3}$ m/s til 8×10^{-3} m/s	1.5×10^{-3} m/s til 2.1×10^{-3} m/s	1.5×10^{-3} m/s til 2.1×10^{-3} m/s
Sprækkepermeabilitet	$0{,}8 \times 10^{-3}$ m/s til 8×10^{-3} m/s	1.5×10^{-3} m/s til 2.1×10^{-3} m/s	1.5×10^{-3} m/s til 2.1×10^{-3} m/s
Matrixpermeabilitet	$0{,}05 \times 10^{-8}$ m/s til 1×10^{-8} m/s	$0{,}01 \times 10^{-8}$ m/s til 100×10^{-8} m/s Gns.: 8×10^{-8} m/s til 6×10^{-7} m/s	$0{,}01 \times 10^{-8}$ m/s til 100×10^{-8} m/s Gns.: 8×10^{-8} m/s til 6×10^{-7} m/s
Anisotrop strømning og stoftransport	Ukendt	Horisontal/vertikal, styret af sprækker	Horisontal/vertikal, styret af sprækker
Forkastninger	Ingen	Ingen	Ingen
Lodrette sprækker	Subvertikale, afstand ca. 0,1 m	Subvertikale, højde ca. 0,2 m, afstand 1,5 m, NNV-SSØ	Subvertikale, højde ca. 0,2 m afstand 1,5 m, NNV-SSØ
Vandrette sprækker	Subhorisontale, afstand ca. 0,1 m	Lagparallelle, afstand ca. 2-3 m, udstrækning 1000 m til 1500 m	Lagparallelle, afstand ca. 2-3 m, udstrækning 1000 m til 1500 m
Glacialt forstyrret kalk	Ja, knust / opsprækket	Nej	Nej
Kalkens struktur	Knust	Bænket, muligvis med gennemgående flintlag	Bænket, med gennemgående flintlag
Kalkens hårdhed	Ukendt	H1-H5,	H1-H5
Kalkens litologi	Knust kalksandskalk og bryozokalk	Kalksandskalk	Bryozokalk
Kote / Dybde	ca. +15 m til +20 m	ca. +12 m til+ 20 m	ca. 0 m til +12 m

Table 4.6: De vigtigste geologiske og hydrauliske parameter for kalken. Farverne indikerer den vurderede usikkerhed ved resultaterne. Blå: meget sikker, grøn: sikker, gul-orange: usikker, rød: meget usikker.

Ved dette forsøg er der benyttet både lange (f.eks. Geo5 og Geo18s) og korte (f.eks. Geo19s og Geo19d) filtre i observationsboringerne, og filteret i pumpeboringen var langt. Derved pumpes påvirkes et stort dybdeinterval af grundvandsmagasinet ensartet, og det er ikke muligt at uddrage informationer om enkelte sprækker.

Det udførte pumpeforsøg gav, på trods af nedbrud, de ønskede hydrauliske parametre. Sænkningen i boringerne skete inden for få minutter og det er derfor vigtig at opsamle data med høj frekvens for at kunne analysere forløbet. Samtidigt er det vigtigt med stor sænkning, helst over 1 m, for at minimere ydre påvirkninger (barometereffekt, borehulseffekt m.v.). I det udførte forsøg var det tilstrækkeligt med en pumpeperiode på 10 dage for at kunne udlede både sprække og matrix parametre, og det må forventes at en pumpeperiode på 10 til 15 dage vil være tilstrækkeligt i de fleste tilfælde.

Sprækkernes hydrauliske egenskaber kan bestemmes med pumpeforsøg af få timers varighed. Dette kan være en fordel, hvis det ikke er nødvendigt i forhold til undersøgelens formål at finde lokalspecifikke parametre for matrix. Matrix permeabiliteten kan f.eks. bestemmes med poroperm-forsøg på kerneprøver. I matrix kan der være en meget stor variation af ledningsevnen (op til ca. en faktor 10.000), så disse værdierm skal opfattes som punktforsøg, og kan ikke direkte benyttes til at beregne et bulk-gennemsnit for matrix. Til dette kræves stor datatæthed, men ved hjælp af sekundære (kontinuerte) data som hårdhed (fra kerneprøver) eller værdier fra geofysiske logs, kan der beregnes en bulkværdi.

Andre resultater fra pumpeforsøg som anisotropi, kan bestemmes med er også afhængig af observationsboringernes placering og afstand. Den optimale placering af observationsboringer er afhængig af det enkelte pumpeforsøg, men de skal generelt placeres så ensartet fordelt som muligt i den forventede (målbare) sænkningskegle. Den optimale filtersætning af pumpe- og observations-boringer afhænger af formålet med pumpeforsøget. Skal de generelle hydrauliske parametre bestemmes fordi resultaterne benyttes til dimensionering af afværge-anlæg er sprækkernes konnektivitet afgørende (med henblik på spredningsveje). Dette kan være afgørende for om filtrene skal placeres i samme niveau eller flere niveauer, eller om filtrene skal være korte eller lange.

5. Results: Tracer tests

In conjunction with the pumping test, six tracer tests in four different wells were successfully conducted. The pumping test induced gradients in the flow field that were important for the tracer test. The pumping defines the flow field, speeds up the tracer breakthrough considerably and increases the likelihood of recovering injected tracers. The pumped well was also used for tracer detection. Figure 5.1 provides an overview of the tracer injections and the employed tracers.

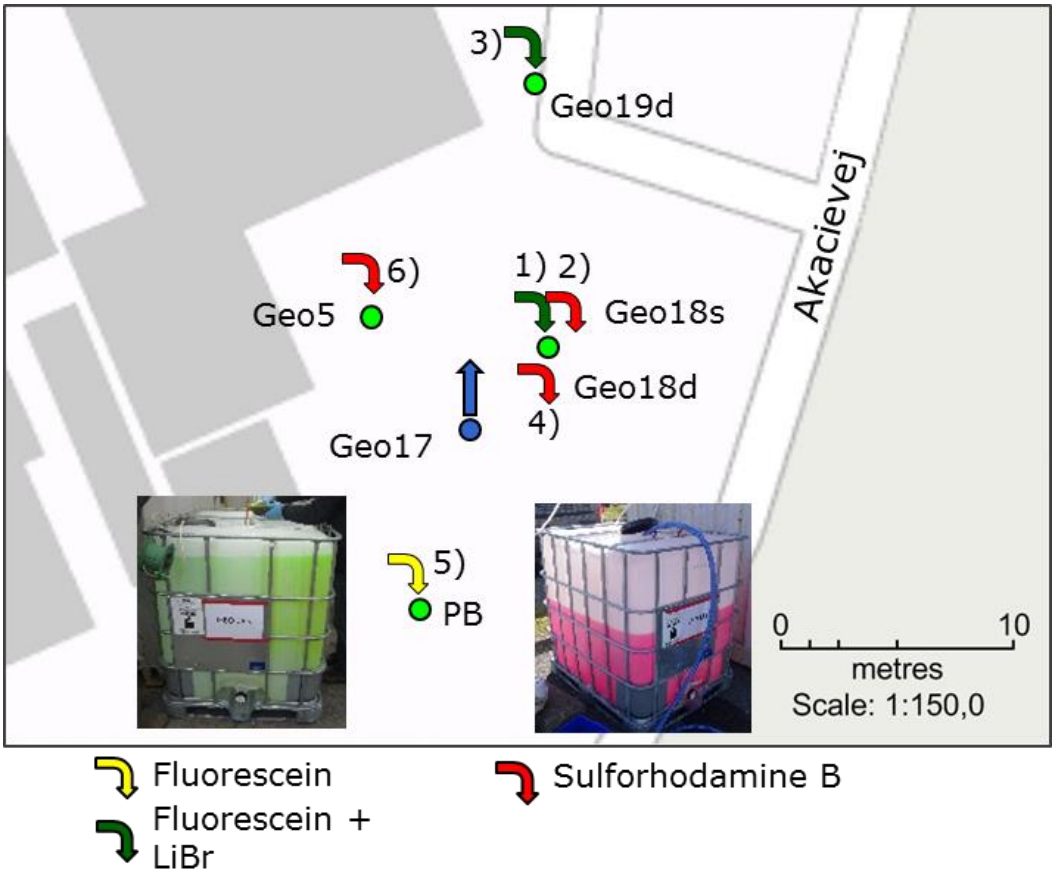

Figure 5.1: Overview of injection wells and injected tracers.

This chapter describes the tracer tests and evaluates the observed tracer breakthrough curves for each of the six injections. The tracer breakthrough graphs in the following sections show measured tracer concentrations in the pumped water divided by the injection concentration. Time 0 is usually when the injection was started. The breakthrough curves with the absolute concentrations can be found in Appendix J.

5.1 Tracer injections

Tracer was injected in five wells located in the surrounding of the pumping well (Geo17): Geo18s, Geo18d, Geo19d, Geo5 and the remediation well (PB). Table 5.1 lists the objectives and the employed tracer(s) for each injection.

No.	Type	Wells	Tracer(s)	Objective / idea
1	Injection of a tracer mixture 4 days before pump was started	Geo18s	LiBr + fluores-cein	tracer diffusion into matrix → transport properties for fracture-matrix system
2	Second injection of a tracer at the same location while pumping	Geo18s	sulfo-rhodamine	tracer break-through curve representing mainly fracture transport
3	Injection in shallow well	Geo19d	LiBr + fluores-cein	further distant injection – more interaction with matrix
4	Injection in deep well	Geo18d	sulfo-rhodamine	vertical transport properties
5	Injection in long screen	Geo5	sulfo-rhodamine	different direction → heterogeneity/anisotropy
6	Injection in remediation well	PB	fluores-cein	tracer injection mainly in crushed limestone

Table 5.1: Overview of tracer injections and objectives of each injection.

Geo18 has two well screens and was used for three tracer injections in total:

1) injection in the shallow screen (Geo18s) four days before the starting to pump,
2) injection of a different tracer in the same screen while pumping,
3) injection in the deep screen (Geo18d) while pumping.

Apart from the first injection in Geo18s, all other tracers were injected while the pumping well was active.

Multilevel sampling prior to the tracer test in Geo18d showed that the PCE concentrations below approximately 30 m bgs. are minimal (Figure 5.2). To avoid pushing contaminated water deeper into the aquifer due to the tracer injection, a packer was installed in the borehole at 30 m bgs. The flow logging in Geo18d showed only little flow below 37 m bgs. Hence, a tracer injection at this depth would was avoided.

Geo19 has also two well screens: the shallow screen Geo19s (mainly in the crushed layer) and the deep screen Geo19d (mainly in the fractured limestone). Initially, it was planned to use the shallow screen for a tracer injection. However, slug tests and the interpretation of the drawdown caused by the remediation system showed that, contrary to expectations, the hydraulic conductivity in the crushed limestone was lower than in the fractured limestone. Model simulations with realistic conductivity values indicated that with the lower conductivity in the crushed limestone, tracer would likely be lost, because it is not drawn to the

pumping well, at least not within a reasonable time frame. As a consequence, tracer was only injected into Geo19d, which is in the fractured limestone at a similar depth as the screen of the pumping well (Geo17).

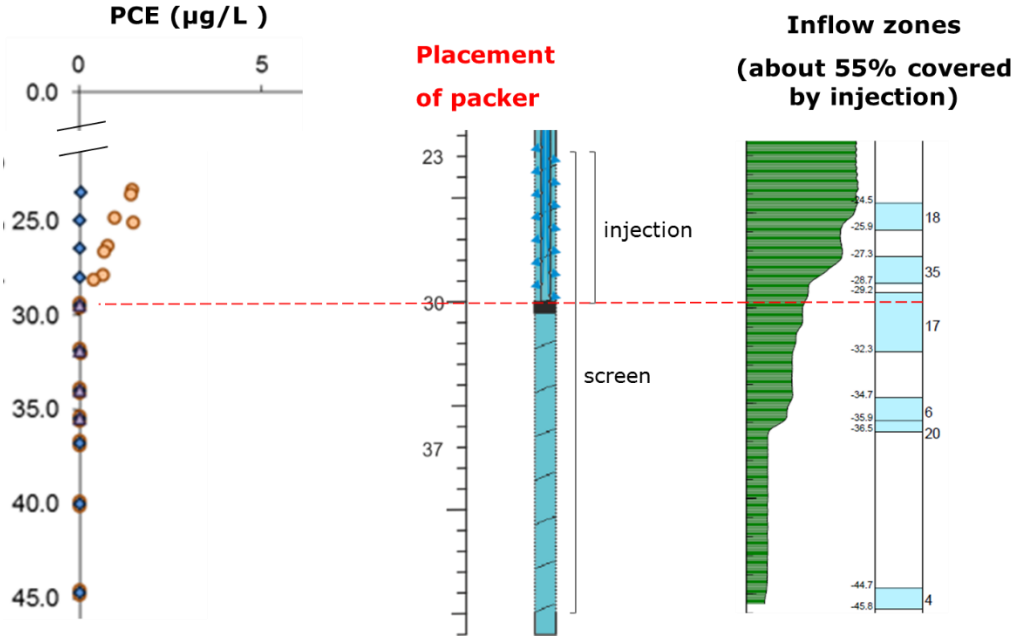

Figure 5.2: PCE distribution in the borehole with no contamination below 30 m bgs., flow log showing the high-flow zones (changes of flow rate) and placement of packer in Geo18d.

The mass recoveries of the injected tracers were calculated as the product of the pumping rate, concentration and time. As concentration, the average concentration value for each time interval without background concentration was used. The pumping rate was Q_{pump} =19.6 m^3/h and the recovered mass was determined by:

$$m_{recovered} = \sum_i Q_{pump} * (c_{i+1} + c_i)/2 * (t_{i+1} - t_i)$$

5.1.1 Injection in Geo18s while pumping

Tracers: 2.99 g Sulforhodamine B on approximately 1000 L groundwater.

Objective: Determine transport parameters mainly for horizontal fractures

Figure 5.3 shows the measured tracer breakthrough curve. The tracer arrived within few minutes. Relatively high peak concentrations of 3.5 % of the injected concentration were observed.

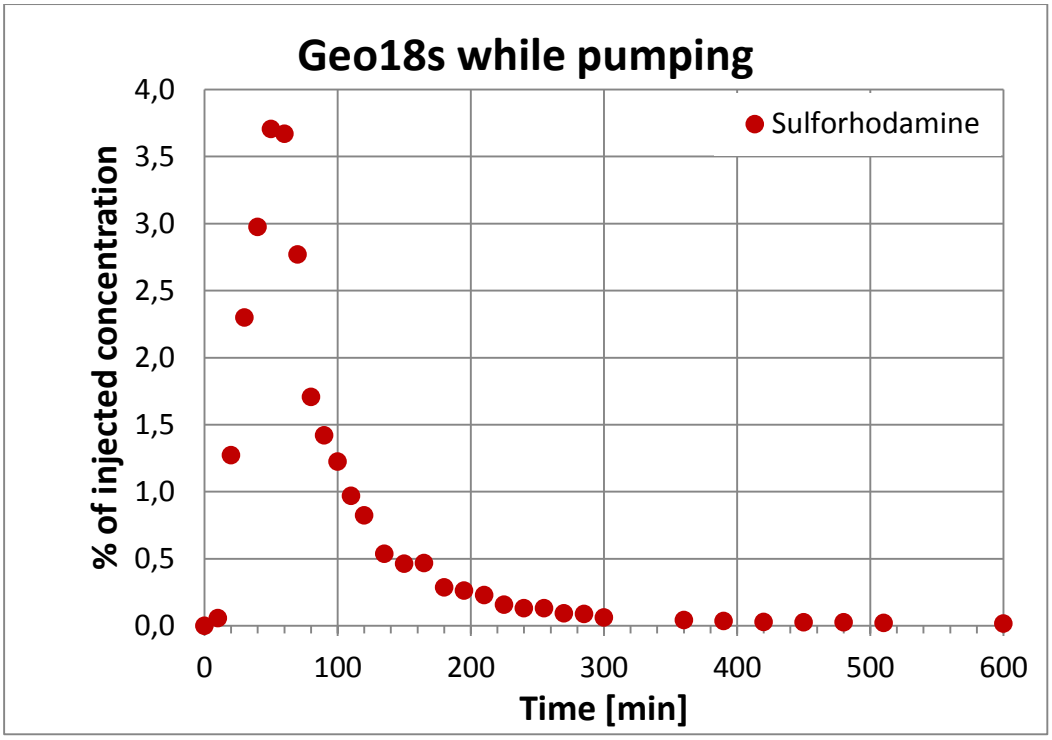

Figure 5.3: Tracer breakthrough curve for the injection in Geo18s while pumping. Time 0 is when the tracer was injected. Fast tracer arrival and high peak concentrations, followed by a tailing in the breakthrough curve. This is characteristic of flow and transport dominated by fractures.

This tracer test shows a typical response for a fractured aquifer, with the fast tracer arrival, high breakthrough concentrations and some tailing (for about 5 hours). For a fractured aquifer, the tailing is relatively short. This indicates that the tracer transport occurs very quickly through the fractures and the time to diffuse into the matrix is short due to the short distance between injection and extraction wells. The tracer arrived earlier and with higher peak concentrations at the pumping well than expected based on modeling prior to the pumping and tracer test. This demonstrates the strong influence of fractures on the transport behavior.

2.98 g sulforhodamine were recovered (recovery of approx. 99 %).

5.1.2 Injection in Geo18s before pumping (Geo18s_pre)

A mixture of lithium bromide and fluorescein was injected 4 days before pumping: 401.8 g LiBr (369.7 g Br, 32.1 g Li) and 4.35 g Fluorescein in approximately 1000 L groundwater.

Objective: Tracers diffuse partly into the limestone matrix → determine transport parameters more characteristic for matrix

Tracer	Injected	Recovered	Recovery
Lithium	32.1 g	(1.3 g)	(4 %)
Bromide	369.7 g	75.7 g	20.5 %
Fluorescein	4.35 g	1.3 g	17.8 %

Table 5.2: Injected and recovered amounts of tracer for the injection before pumping in Geo18s. Note that the measured lithium concentrations were very close to the background concentrations. Thus, the measured concentrations are not very accurate and the recovery rate is probably underestimated.

The tracer mixture was injected 4 days prior to the start of the pumping well over a time period of approximately 1 hour. In the 4 days after injection, the tracers migrated with the natural groundwater gradient (away from the pumping well) and diffused into the matrix.

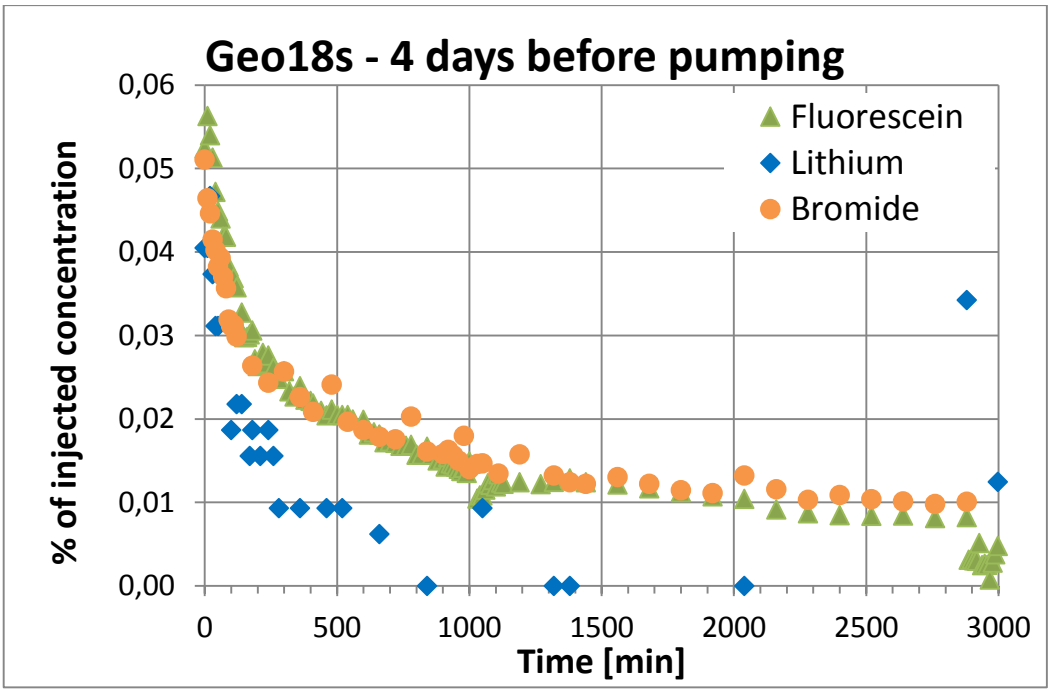

Figure 5.4: Tracer breakthrough curves for the injection in Geo18s four days before the pump was started. The time axis starts with 0 when the pump was started. Low peak concentrations and long tailing of the breakthrough curve.

When the pump was switched on, the flow field changed considerably and the tracers are drawn towards the pumping well. The measured breakthrough curves are shown in Figure 5.5. The expectation based on modeling was that it would take several hours before the tracer arrival. However, despite Geo18 being located downstream of the pumping well, the tracers were detected at the pumping well as soon as the pump was switched on. This showed that the tracers were primarily injected into the high conductive zones (fractures), where they spread also against the dominating groundwater flow direction and diffused from the fractures into the limestone matrix. Moreover, parts of the tracers remained in the injection well and the surrounding sand pack or were transported back to the well with the natural groundwater flow. When the pumping well was started, the tracers in the fractures and in the injection well were quickly drawn towards the pumping well.

The tracer breakthrough behavior is markedly different from that observed for the tracer tests with injection during pumping. All three tracers show low peak concentrations at the beginning of the pumping period, which decrease

continuously and have a very long tailing. The tailing is due to the back-diffusion of tracer from the matrix. A lot of the injected tracer had already migrated further downstream with the fast fracture flow (under natural gradient conditions) or diffused into the matrix. Hence, only part (17-20 %) of the injected tracer was recovered (Table 5.2). The lithium concentrations are very low and very close to the background concentrations. With this, the analytical error is high and the lithium tracer data is not considered further. The increase in the concentration after 2900 minutes is due to the start of the next injection (Geo18s while pumping). The tracer injection mobilized some of the tracer that remained in the aquifer and the gravel/sand pack of the injection well and pushed it away from the injection well.

The three tracers have different diffusion coefficients (Table 2.5). Lithium has in principle the highest one. However, in contrast to bromide, lithium is mostly in a hydrated form making the molecule bigger and the diffusion coefficient lower. With the highest diffusion coefficient of the three tracers (approximately 4 times higher than for fluorescein), bromide tends to diffuse strongest into the matrix.

Within the 4 days between injection and pump start, more bromide has diffused into the matrix than lithium or fluorescein. This is reflected in the slightly higher concentrations in the pumped water during the tailing period: bromide diffused further into the matrix and less migrated downstream with the flow in the fractures beyond the point where it cannot be retrieved, and more back-diffusion from the matrix can be observed.

5.1.3 Injection in Geo19d

Tracers: 1000 g LiBr, 20 g Fluorescein

Objective: Injection from a further distance, more fracture-matrix interaction than for Geo18s.

Tracer	Injected	Recovered	Recovery
Lithium	79.9 g	90.7 g	113.4 %
Bromide	920.1 g	526.4 g	57.2 %
Fluorescein	20 g	17.5 g	87.4 %

Table 5.3: Injected and recovered tracer amounts in Geo19d.

Figure 5.5 shows the tracer breakthrough curves for the tracer test in Geo19d. The tracer breakthrough is characterized by an early arrival of the tracer - almost as fast as from Geo18s despite being considerably further away from the pumping well. This indicates a very good connection between Geo19d and the pumping well (Geo17), possibly by horizontal fractures with a large aperture. The good connectivity is confirmed by a similar drawdown in Geo19d and Geo18s during the pumping test. This emphasizes the importance of the preferential flow paths (fractures) on the transport of substances. It also shows that it is not trivial to determine the well capture zones in fractured limestone, because they can be strongly influenced by a few major fractures.

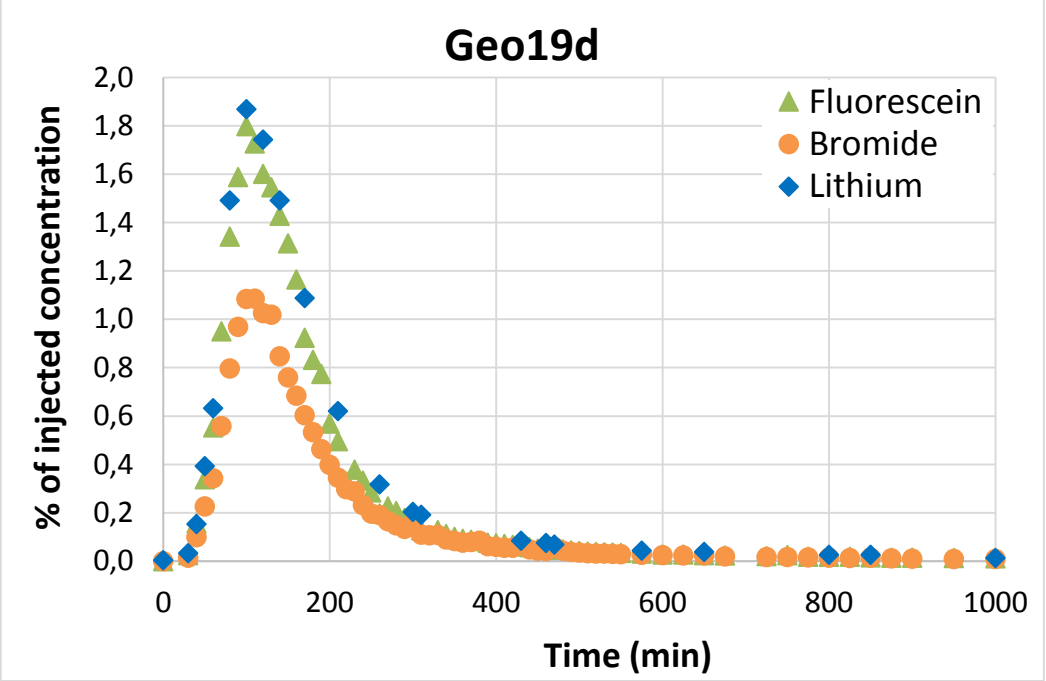

Figure 5.5: Tracer breakthrough curves for the injection into Geo19d. Lithium and fluorescein have higher relative peak concentrations due to a different diffusion behavior.

A breakthrough curve for each injected tracer was recorded. Lithium and fluorescein had a similar breakthrough behavior, whereas bromide had the lowest peak concentration. This can be attributed to the higher diffusion coefficient of bromide (approx. 4 times higher than for fluorescein and hydrated lithium), so more bromide had diffused into the matrix on its way to the pumping well. Lithium shows a longer tailing than the other tracers.

The recovery rate was relatively high for all tracers (Table 5.3). With about 57 %, bromide had the lowest recovery. This can be attributed to matrix diffusion. The calculated recovery for lithium is slightly higher than 100 percent. However, this is still within the analytical error at the low concentration level. Almost all fluorescein was retrieved.

5.1.4 Injection in Geo18d

Tracer: 9 g Sulforhodamine B, 1.3 g recovered (14.8 %)

Objective: Determine vertical transport parameters, test vertical connectivity.

Figure 5.6 shows the measured breakthrough curve for the tracer test in the deep screen of Geo18. The measured tracer concentrations at the pumping well had a low peak concentration and a long tailing. Relatively little tracer could be recovered. Geo18d is located deeper in the aquifer than the screen of the pumping well. The horizontal fractures at the site seem to be the main flow paths for the tracers and the vertical connectivity of the deep screen of Geo18 and the extraction well appears to be limited. The vertical hydraulic gradient could pull some tracer to the extraction well, but much of the tracer was transported further downstream with the local groundwater flow (unaffected by the pumping) in a deeper part of the aquifer.

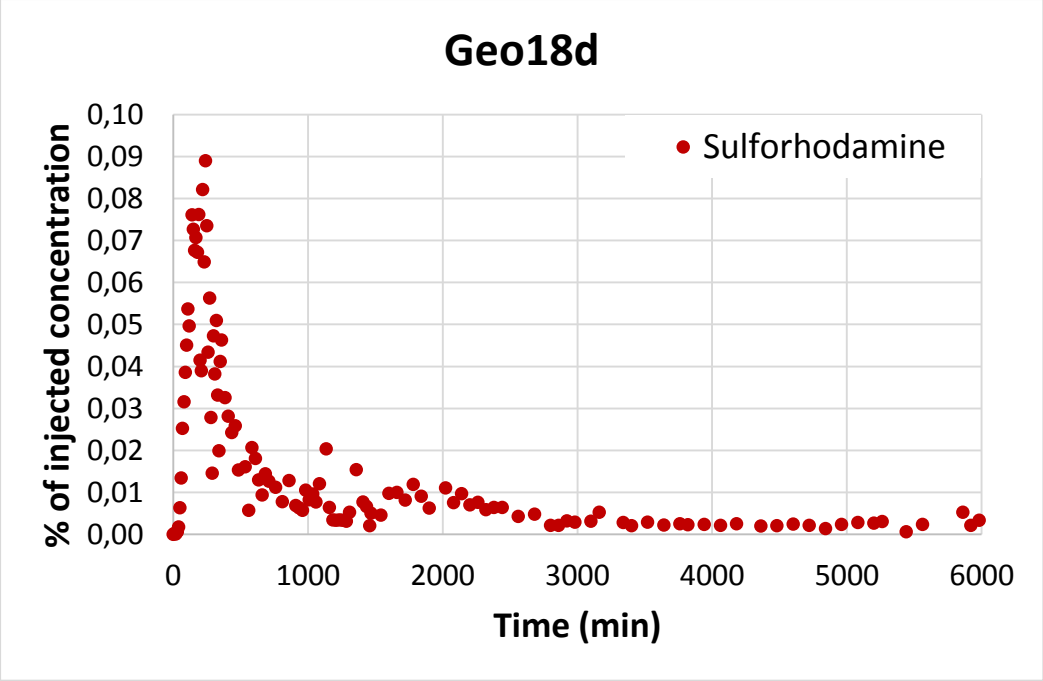

Figure 5.6: Tracer breakthrough curve for the injection in the deep screen of Geo18. Note the low peak concentrations, the long tailing and the long duration of the tracer breakthrough, indicating a poor connectivity of Geo18d and the pumping well.

5.1.5 Injection in the existing remediation well (PB, 207.4059)

Tracer: 4.99 g Fluorescein, recovered 3.6 g (72.7 %).

Objective: Injection mainly in the crushed limestone. Determine vertical transport behavior and partly crushed limestone parameters, analyze connectivity between crushed and fractured limestone.

The measurements from the flow-through spectrophotometer showed a good agreement with filtered samples (Figure 5.7) and were used for the tracer test evaluation. The lab analysis of the unfiltered samples gave very noisy results as described in section 2.5.1. Since no lithium bromide was injected in this tracer test, only a few samples at the beginning of the tracer test were filtered and available for the lab analysis.

The tracer arrived after about 40 minutes at the pumping well and had a relatively low peak concentration. The breakthrough curve shows a considerably longer tailing than the tracer tests in screens located in the fractured limestone. The screen of PB is more shallow than the screen of the pumping well and is located predominantly in the crushed limestone with a lower hydraulic conductivity than in the fractured limestone. Hence, vertical head gradients are relevant for the transport of the tracer. Furthermore, the aquifer is in general anisotropic with a higher conductivity in the horizontal than in the vertical direction. The observed behavior can be attributed to a mixture of crushed and fractured limestone properties.

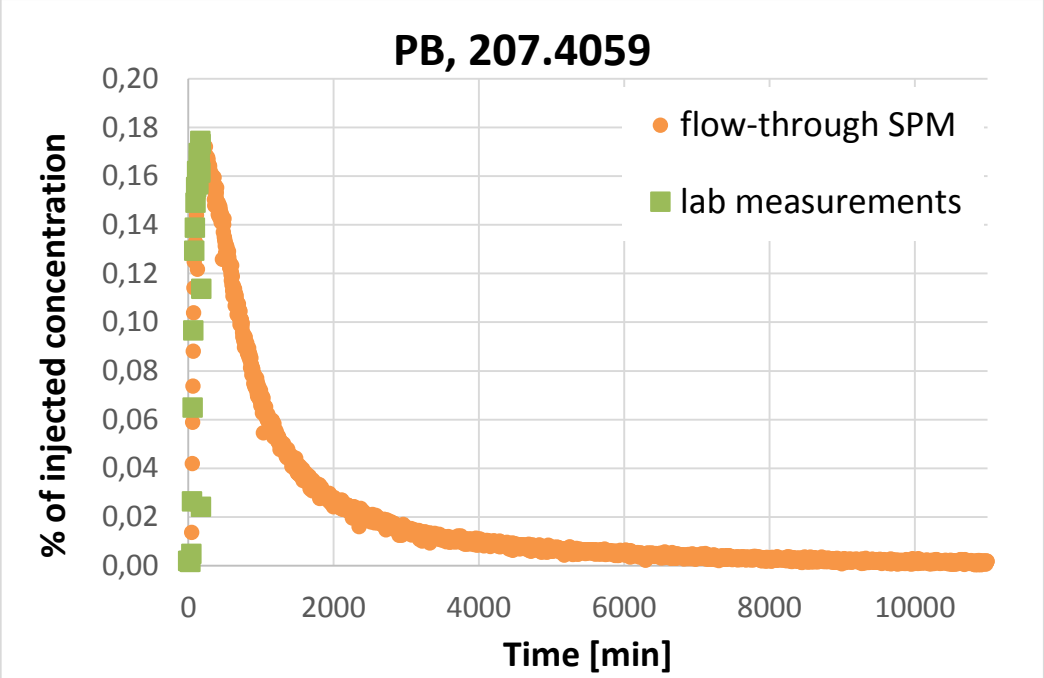

Figure 5.7: Tracer breakthrough curve for the injection in the remediation well (207.4059). The tracer breakthrough takes long with relatively low peak concentrations and a long tailing. This can be partly attributed to the shallower position of the well screen of PB compared to the extraction well Geo17 and to the location in the crushed, less hydraulically conductive limestone.

5.1.6 Injection in Geo5

Tracer: 2.5 g Sulforhodamine B, 3 g recovered (121 %)

Objective: Injection from a different direction. Determine aquifer heterogeneity.

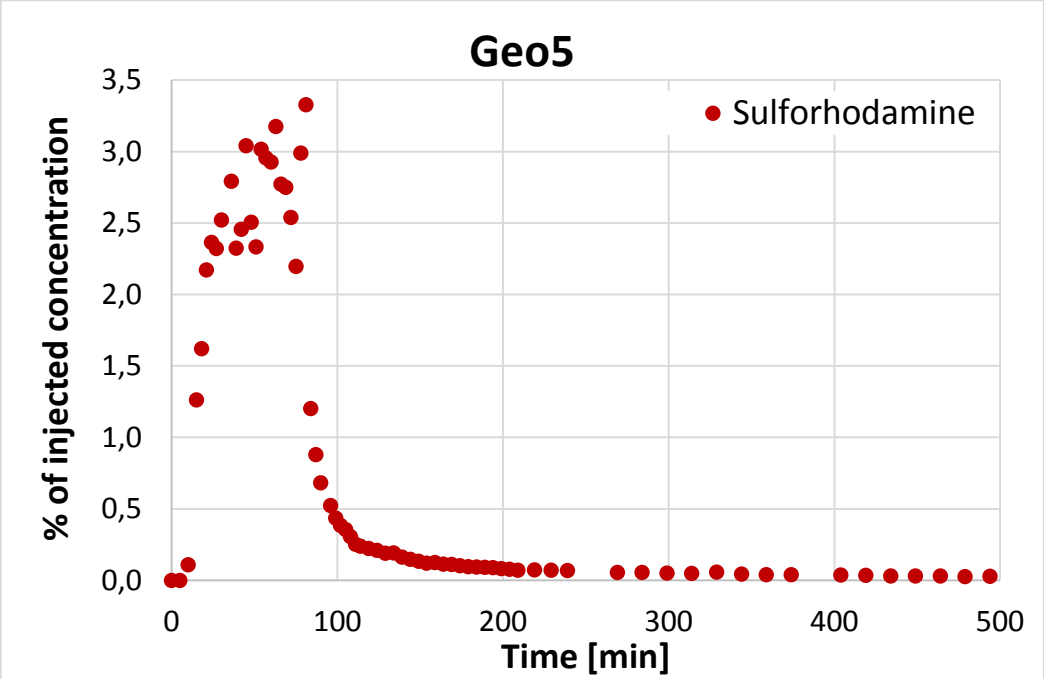

Figure 5.8: Tracer breakthrough curve for the injection in Geo5 with very high breakthrough concentrations and little tailing, showing a very good connectivity between Geo5 and the pumping well.

Geo5 has the longest screen of the injection wells (10 m, partly in crushed and fractured limestone). The tracer breakthrough from this well (Figure 5.8) is the fastest of all tracer tests and shows only very little tailing. This indicates a very good connection of Geo5 and the extraction well, probably with several horizontal fractures connecting them. The tracer is transported mainly within the fractured limestone which provides a fast flow path. Within the short travel time from injection to extraction well, only very little sulforhodamine diffuses into the aquifer matrix and most tracer could be retrieved. The calculated recovery was 121 % which is too high, but is still within the bounds of analytical accuracy. It can be assumed that almost all tracer was retrieved.

5.1.7 Overview and discussion of all injections

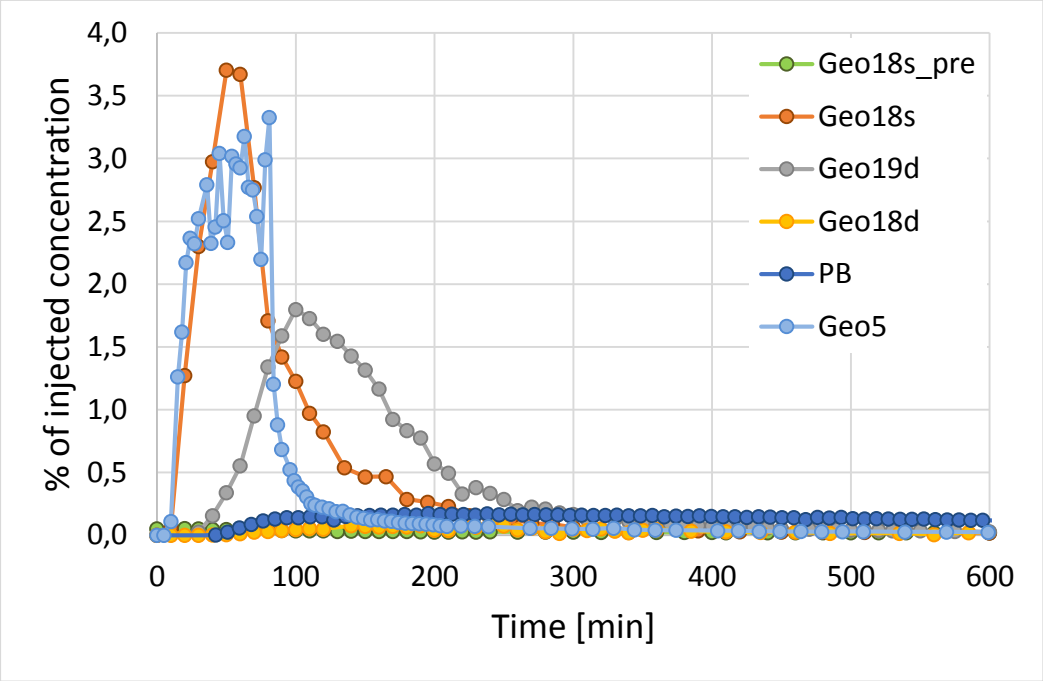

Figure 5.9: Breakthrough curves for all six tracer injections. If multiple tracers were injected at the same time, the values of fluorescein are displayed. Time 0 is when the tracer was injected. For Geo18s_pre, the time shown is from when the pump was started.

The measured tracer breakthrough curves differ considerably (Figure 5.9). They can be subdivided into two major groups:

1) fast breakthrough and high recovery (Geo18s, Geo5, Geo19d)
2) slow breakthrough and low recovery (Geo18s_pre, Geo18d, PB)

The breakthrough curves in group 1 are characterized by a good connectivity to the pumping well Geo17. They all have screens in a similar depth and it is very likely that horizontal fractures provide a direct connection to the pumping well. The tracer transport is clearly dominated by fractures connecting extraction and injection well.

The breakthrough curves in group 2 (Figure 5.10) have less connectivity and the location of the screens of PB and Geo18d is shallower (PB) or deeper (Geo18d) than the screen of the pumping well. Presumably there are only few thin vertical fractures, which have little influence on the tracer transport. For PB it is questionable whether the observed breakthrough behavior is consistent with the crushed limestone being considered as non-fractured.

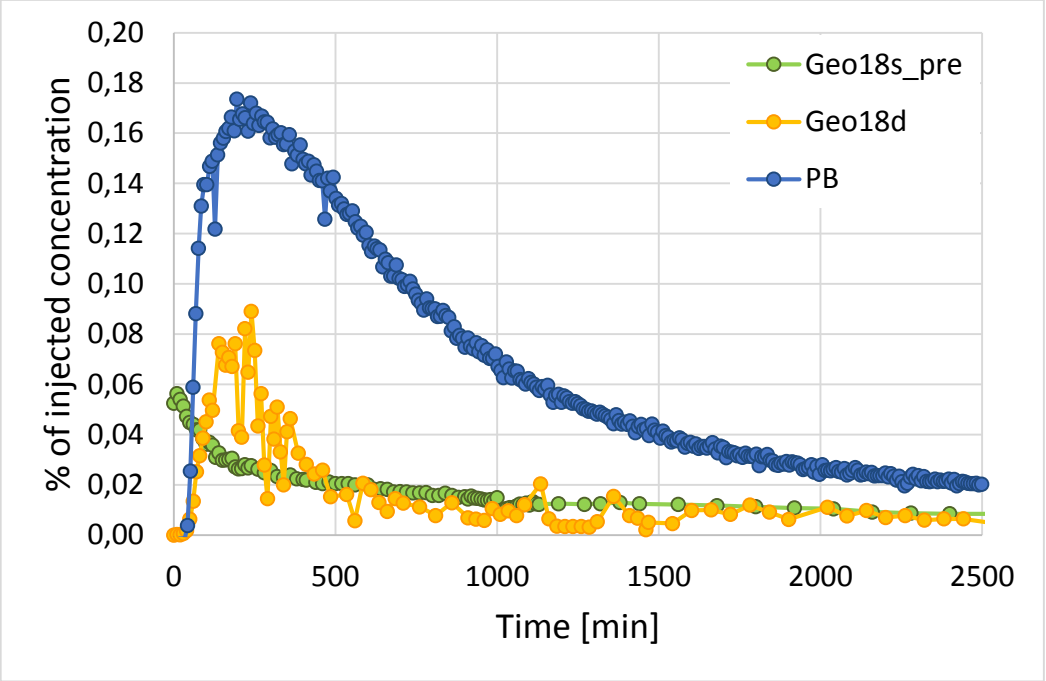

Figure 5.10: Breakthrough curves for the tracer tests with low peak concentrations (group 2). For Geo18s_pre the breakthrough curve of fluorescein is shown and time zero is when the pump was started (4 days after the injection). For Geo18d and PB time 0 is when the tracer was injected. Note that the scales for the concentrations and time considerably differ to those of Figure 5.9.

The breakthrough curve for Geo18s_pre (injection 4 days before the pump was started at a location downstream of the pumping well) is different from all the other tracer breakthrough curves. During the injection, a hydraulic gradient towards the pumping well lead to an upstream transport of a part of the tracer within the fractures and an early arrival of the tracer. The main reason for the low peak concentrations and recovery is that most of the tracer was transported downstream through the fractures with the natural-gradient groundwater flow or diffused into the matrix in the time period before pumping. The recovered tracer is mainly from back-diffusion from the matrix and from some tracer that was still in the sand pack around the injection well.

5.2 Findings from the pumping and tracer test

The pumping test yielded information on the hydraulic properties of the limestone aquifer. It was difficult to determine parameters for the fractures and the matrix because of the high bulk conductivity, which is dominated by the high conductivity of the fractures. The drawdown due to the pumping was fully developed after 7 to 10 days. It was possible to apply specialized pumping test analysis methods for the interpretation of the pumping test (like the Moench or the Barker solution using Aqtesolv). This meant that the hydraulic parameters for both the fractures and matrix could be estimated. A very strong hydraulic conductivity contrast between the fractures and matrix was observed.

From slug testing, from the similar drawdown created by the remediation well (PB) and the new pumping well, and from the tracer breakthrough curves from PB and other injections, it can be deduced that the crushed limestone has a lower bulk hydraulic conductivity than the upper fractured limestone.

The results of the tracer tests with the fluorescent tracers (fluorescein, sulforhodamine) and lithium bromide were good with the chosen setup. The tracer tests provided breakthrough curves to which models can be fitted to obtain aquifer parameters and to improve the conceptual understanding of transport in fractured limestone aquifers.

The tracer tests revealed the importance of fractures on the flow and transport behavior. A few large horizontal fractures seem to dominate the transport behavior between the well screens of injection and extraction wells, leading to a fast tracer arrival at the extraction well, high peak concentrations and little tailing. The very fast arrival of tracers contrasts sharply with the slow expansion of the PCE contaminant plume years after the spill.

The (sub-)vertical fractures provide vertical connections between the horizontal fractures, but seem to have less influence on the overall transport. The tracer injections in screens located at shallower depth or deeper down in the aquifer than the screen of the extraction well showed the vertical connectivity to be limited and the preferential flow direction to be predominantly horizontal.

Despite having a low recovery, the tracer test prior to pumping in Geo18s is most influenced by matrix diffusion and gives valuable information about the transport properties in the limestone matrix.

6. Model interpretation of the pumping and tracer test

Modeling fractured limestone aquifers poses a big challenge, because there are at least two interconnected continua – the fractures, which act as main flow pathways and the matrix with only little flow but extensive storage capacity for dissolved species. The distribution of fractures or the geometry of the fracture network is usually unknown.

For the model comparison, three concepts of different complexity were selected and 3D models were setup to simulate the pumping and tracer test: an equivalent porous medium model (EPM), a dual-continuum model (DCM) and a discrete fracture model (DFM), as illustrated in Figure 6.1. They are described and compared in the following section.

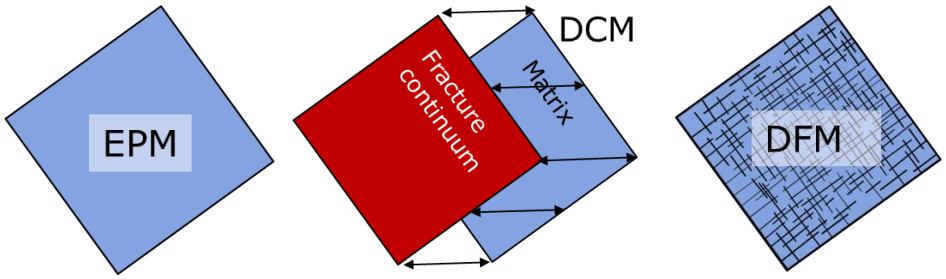

Figure 6.1: Overview of three different model concepts used for flow and transport modeling in fractured media: Equivalent porous medium model (EPM), dual-continuum model (DCM) and discrete-fracture model (DFM).

6.1 Model types

6.1.1 Equivalent porous medium model (EPM)

The equivalent porous medium model is a basic model concept and simulates a porous medium with parameters averaged over control volumes containing both fractures and limestone matrix. The model consists of a flow model and a transport model. The fractures are not explicitly modelled, instead being accounted for in a bulk or average hydraulic conductivity. Due to its simplicity and its low computational effort, the EPM model is widely used.

The steady-state *flow equation* is given by:

$$\nabla \cdot q = \nabla \cdot (-K \nabla h) = 0$$

with the water flux q, the hydraulic conductivity K and the hydraulic head h.

The *transport equation* is given by:

$$(n + \rho_b k_d) \frac{\delta c}{\delta t} + \nabla \cdot n(\boldsymbol{v} c) - \nabla \cdot n(\boldsymbol{D} \nabla c) = 0$$

with the porosity n, the bulk density ρ_b, the sorption coefficient k_d, the concentration c and the hydrodynamic dispersion tensor $\boldsymbol{D}$.

6.1.2 Dual-continuum model (DCM)

This concept is described in detail in, e.g., Gerke and van Genuchten (1993), and accounts for fractures by using two coupled continua, a matrix continuum and a fracture continuum. Both continua are resolved with the same dimensionality (2D-2D or 3D-3D). Two coupled flow equations and two coupled transport equations are usually employed. Dual-continuum models involve additional variables compared to the EPMs. The two continua are coupled via an exchange term, which is usually specified as source / sink in the flow and transport equations.

Equation for steady-state matrix flow (subscript m):

$$-\nabla \cdot (w_{\mathrm{m}} k_{\mathrm{m}} \nabla h_{\mathrm{m}}) = \Gamma_w$$

Equation for steady-state fracture flow (subscript f):

$$-\nabla \cdot (w_{\mathrm{f}} k_{\mathrm{f}} \nabla h_{\mathrm{f}}) = -\Gamma_w$$

Involving a transfer coefficient for water α_w, the exchange fluxes $\Gamma_w$between fracture and matrix continuum can be defined as:

$$\Gamma_w = \alpha_w (h_f - h_m)$$

Equation for matrix transport:

$$w_{\mathrm{m}} \left(n_{\mathrm{m}} + \rho_{\mathrm{b}} k_{\mathrm{d,m}}\right) \frac{\delta c_{\mathrm{m}}}{\delta t} + \nabla \cdot (w_{\mathrm{m}} n_{\mathrm{m}} \boldsymbol{v}_{\mathrm{m}} c_{\mathrm{m}}) - \nabla \cdot (w_{\mathrm{m}} n_{\mathrm{m}} \mathbf{D}_{\mathrm{m}} \nabla c_{\mathrm{m}}) = \Gamma$$

Equation for fracture transport:

$$w_{\mathrm{f}} \left(n_{\mathrm{f}} + \rho_{\mathrm{b}} k_{\mathrm{d,f}}\right) \frac{\delta c_{\mathrm{f}}}{\delta t} + \nabla \cdot (w_{\mathrm{f}} n_{\mathrm{f}} \boldsymbol{v}_{\mathrm{f}} c_{\mathrm{f}}) - \nabla \cdot (w_{\mathrm{f}} n_{\mathrm{f}} \mathbf{D}_{\mathrm{f}} \nabla c_{\mathrm{f}}) = -\Gamma$$

Different approaches for the definition of the coupling term Γ have been developed. It can be defined as (e.g. Gerke and van Genuchten, 1993):

$$\Gamma = (1 - d) \Gamma_{\mathrm{w}} n_{\mathrm{f}} c_{\mathrm{f}} + d \Gamma_{\mathrm{w}} n_{\mathrm{m}} c_{\mathrm{m}} + \alpha_s w_{\mathrm{m}} n_{\mathrm{m}} (c_{\mathrm{f}} - c_{\mathrm{m}})$$

This concept involves weighting functions for the fracture and matrix continuum, w_{f} and w_{m}, the transfer coefficient α_s, and the coupling term of the advective water fluxes between fractures and matrix Γ_{w}. This term is only important, when the pressures in the fracture continuum and the matrix continuum differ locally, otherwise the exchange is governed by diffusive exchange (last term in the equation).

6.1.3 Discrete-fracture model (DFM)

The discrete-fracture model is the most detailed approach to fracture flow and transport modeling. It is described in detail, e.g., in Chambon et al. (2011). In the DFM the discretized fractures are explicitly described and are embedded in the porous matrix domain. Usually, the fractures are resolved with one dimension less than the matrix (e.g. matrix in 3D, fractures in 2D).

The equations for matrix flow and transport are the same as in the EPM model with an additional exchange term on the right hand side. The fractures and the matrix are coupled via the continuity of fluxes across the fracture-matrix interface and by continuity of the primary variables (usually hydraulic head and concentration). In addition to the porous media flow and transport equations (also used in the EPM model), an equation for the flow and the transport in fractures with the aperture *b* is needed:

$$b\frac{\delta c_{\mathrm{f}}}{\delta t} + \nabla \cdot b(\boldsymbol{v}_{\mathrm{f}} c_{\mathrm{f}}) - \nabla \cdot b(\mathbf{D}_{\mathrm{f}} \nabla_{\mathrm{T}} c_{\mathrm{f}}) = -\mathrm{Q}_{\mathrm{m,i}}$$

If the flow velocities in the fractures are moderate, Darcy's law is used to compute the flow in the fractures, and the hydraulic conductivities in the fractures are approximated with the cubic law:

$$k_f = \frac{b^2\, \varrho_{\mathrm{w}}\, g}{12\mu}$$

and

$$\boldsymbol{v}_f = -k_f \nabla h$$

Since the flow in the fracture depends on the aperture cubed, larger fractures contribute much more to the flow than smaller ones.

The exchange to the matrix happens via the continuity of fluxes between fractures and matrix and is usually specified as source and sink term in the fracture and the matrix transport equations. The exchange flux of a component is defined as sum of diffusive and advective exchange

$$\mathrm{Q}_{\mathrm{m,i}} = -n_{\mathrm{m}}\, D_{\mathrm{m},i} \frac{\partial c}{\partial n_{\mathrm{f}}} + n\, v_{\mathrm{m},i}\, c$$

where the advective exchange between fractures and matrix (last term in the equation above) is often neglected.

If their geometry and location is known (based on measurement data and observations), the fractures can be directly included in the model. However, knowledge about the exact fracture geometry is generally limited. Often, a representative fracture network is generated. Therefore, fracture statistics can be used to generate a random fracture network.

By including highly conductive fractures into a low-conductive matrix, strong gradients of the hydraulic heads and concentrations can occur close to the fractures. This makes a high grid resolution close to the fractures necessary to approximate the gradients accurately and poses a challenge for numerical solvers.

6.2 Flow and transport modeling results

The principal setup of the different simulations of the tracer test at the Akacievej site is shown in Figure 6.2. For all models, a domain with 100 x100 m^2 was employed, consisting of different horizontal layers (crushed limestone, fractured limestone). It was checked if the effect of the domain size on the modeling results was negligible. The crushed limestone was always considered as a porous medium without fractures.

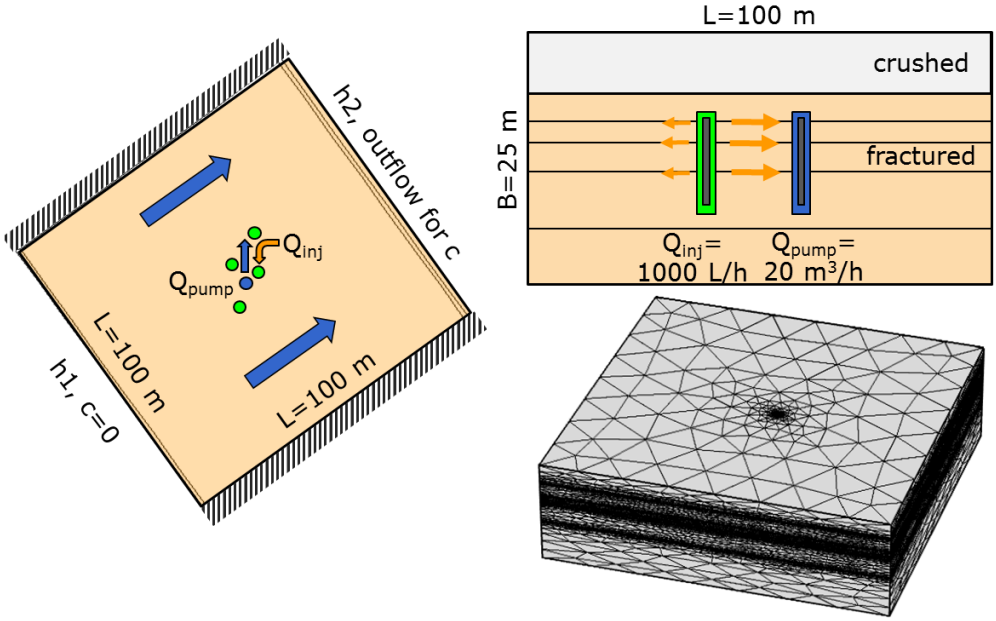

Figure 6.2: Setup of the model simulations with boundary conditions (left), vertical section showing fractures and an exemplary injection and pumping well (top right) and computational mesh for the discrete fracture model (bottom right).

Constant head boundaries are set at the inflow (left) and outflow (right), and no-flow conditions were specified on the other sides (Figure 6.2). The head gradient between the two constant-head boundaries was set to (h1-h2)/L=1/1200 in accordance with the flow field shown in Figure 1.7.

For the transport model, a concentration of 0 µg/L was set at the inflow, an outflow (zero-gradient) boundary on the outflow and no-flow conditions elsewhere. The injection and extraction of water and tracer was set as flux boundary condition on the lateral surface of a cylinder at the location of the well screen. To distribute the flow from a well into the aquifer according to the hydraulic conductivity (water flows mainly in the highly conductive zones or fractures), a cylinder around the well corresponding to the gravel/sand pack was included in which a very high hydraulic conductivity (10 m/s) was set. In Figure 6.2 (bottom right), the computational mesh for the discrete fracture model is shown. The mesh used in the discrete-fracture model consists of more than 1 million grid elements and is

highly refined at the fractures and the wells to obtain a good approximation of the hydraulic head and concentration gradients.

In all simulation runs, stationary flow fields were used during the injection time (1 h) and when flushing with freshwater. A different flow field was used when the injection was over, accounting for the influence of the injection on the flow field. The flow models were first calibrated to the observed drawdown created by the pumping test in the respective wells based on the hydraulic conductivities determined in the pumping test. To improve the approximation of the flow field, the hydraulic parameters (hydraulic conductivity, fracture aperture etc.) were varied to match the heads measured in the pumping and observation wells. Additional information was provided by the data from borehole flow logs. This was used to identify high-flow zones and to place horizontal fractures in the DFM. Data from the remediation well (PB, mainly located in the crushed limestone) and from the slug tests provided information about the conductivity contrast between fractured and crushed limestone.

Once the flow field was calibrated and set, the transport parameters were adjusted (diffusion coefficient, porosity, exchange coefficients) to match the tracer breakthrough behavior. The measured tracer breakthrough curves were used to analyze the processes that can be reproduced by the models. They are discussed in Section 6.2. The calibrated model parameters fitted to the breakthrough curve for the injection in Geo18 while pumping are shown in Tables 6.1, 6.2, and 6.3.

Parameter	Value	Comments
K_m	2×10^{-3} m/s	bulk conductivity
$K_{crushed}$	5×10^{-4} m/s	crushed limestone conductivity
K_{casing}	10 m/s	Casing conductivity next to the wells
n_m	0.5-2 %	matrix porosity
K_{xx}/K_{zz}	10	vertical anisotropy
D_m	13×10^{-10} m^2/s 3.2×10^{-10} m^2/s	molecular diffusion coefficient bromide and fluorescein
Q_{pump}	19.6 m^3/h	pumping rate
α_L	0.1 m	longitudinal dispersivity
α_T	0.02 m	transversal dispersivity
α_V	0.01 m	vertical dispersivity

Table 6.1: Parameters used in the EPM model (fitted to Geo18s while pumping).

Parameter	Value	Comments
K_{matrix}	10^{-7} m/s	matrix conductivity
$K_{fractures}$	0.13 m/s	fracture conductivity
$K_{crushed}$	5×10^{-4} m/s	crushed limestone conductivity
n_{matrix}	0.07 %	matrix porosity
$n_{fractures}$	90 %	fracture porosity
n_{total}	8.3 %	total porosity
a	0.1 m	matrix block size
w_f	1.5 %	volume fraction of fracture system
K_{xx}/K_{zz}	10	vertical anisotropy
D_w	10^{-7} m^2/s	augmented diffusion coeff. Water
D_{eff}	6.5×10^{-8} m^2/s	effective diffusion coefficient
D_{fm}	6.5×10^{-8} m^2/s	diffusion coefficient for fracture-matrix exchange

Table 6.2: Additional parameters used in the DCM and parameters differing from the EPM . The concept presented in Gerke and Van Genuchten (1993) was used.

Parameter	Value	Comments
K_{matrix}	10^{-7} m/s	matrix conductivity
$K_{fractures}$	2.4 m/s	fracture conductivity (aperture 2 mm), 5 horizontal fractures
$K_{crushed}$	5×10^{-4} m/s	crushed limestone conductivity
n_m	20 %	matrix porosity
K_{xx}/K_{zz}	10	vertical anisotropy
D_m	7.5×10^{-7} m^2/s	augmented diffusion coefficient

Table 6.3: Additional parameters used in the DFM (fitted to Geo18s while pumping) and parameters differing from the EPM.

6.2.1 Geo18s while pumping

To test the models and to illustrate differences, each model was fitted to the breakthrough data for the tracer test in GEO18s while pumping. Model parameters were varied in order to match the measured breakthrough curve as well as possible. The calibrated parameters are shown in Tables 6.1 – 6.3. The tables show that different parameters are required for the different models. The output of the three model types differed considerably (Figure 6.3).

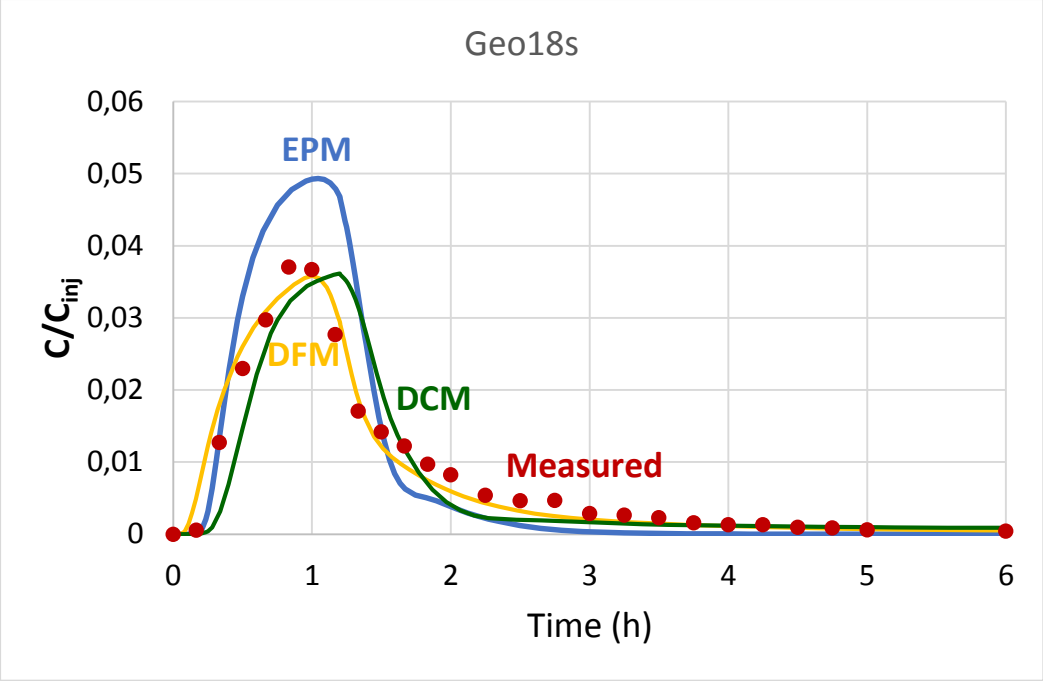

Figure 6.3: Comparison of simulated breakthrough curves for the injection in Geo18s while pumping. A discrete fracture model (DFM), a dual-continuum model (DCM) and an equivalent porous medium model (EPM) were compared with the measured breakthrough data.

The EPM model can match the early breakthrough only by using an unrealistically low porosity of 0.5 %. The value is in the order of the fracture porosity (volume fraction of the fracture system). However, the simulated peak concentrations are too high and the tailing of the breakthrough curve cannot be matched in the low-porosity case. Higher porosities lead to a late tracer arrival and lower peak concentrations.

The DCM model can be better fitted to the measured data. Peak concentrations are in the correct range and the tailing of the breakthrough curve can be reasonably well reproduced. Therefore, the matrix porosity was 8 % and the fracture porosity 90 % (total porosity of 8.3 %), which is already closer to measured matrix values from poroperm tests (see Table 2.3). The diffusion coefficient between fractures and matrix is relevant for the exchange fluxes and was fitted to 6.5×10^{-8} m^2/s. The volume fraction of the fracture system was determined as 1.5 % with a matrix block size of 0.1 m.

In the DFM, the location and characteristics (aperture) of the fractures was changed to improve the model fit. The flow logs showed several significant horizontal fractures connecting the different boreholes. This information was used to include five horizontal fracture planes, but vertical fractures were not included (see Figure 6.5). The matrix hydraulic conductivity was set to 10^{-7} m/s, a value that was within the range determined by the pumping test interpretation and by poroperm tests of some intact limestone cores. A matrix porosity of 20 % was used. The fracture aperture that matched the tracer breakthrough behavior best was around 2 mm, leading to a computed fracture hydraulic conductivity of about 2.4 m/s and a very strong conductivity contrast to the matrix. The diffusion coefficient was augmented to 7.5×10^{-7} m^2/s to account for neglected fractures and channeling within the fracture network.

Simulation results showed that for the breakthrough curves from Geo18s, the highly conductive horizontal fractures between the injection and the extraction borehole dominated the flow field (see Figure 6.4) and the breakthrough behavior (Figure 6.5). Vertical fractures provide connectivity, but testing of various model setups showed that they are less important for the tracer migration in this tracer test. With the strong conductivity contrast between fractures and matrix (seven orders of magnitude), the advective transport in the matrix is negligible and transport into the matrix happens mainly by diffusion from the fractures.

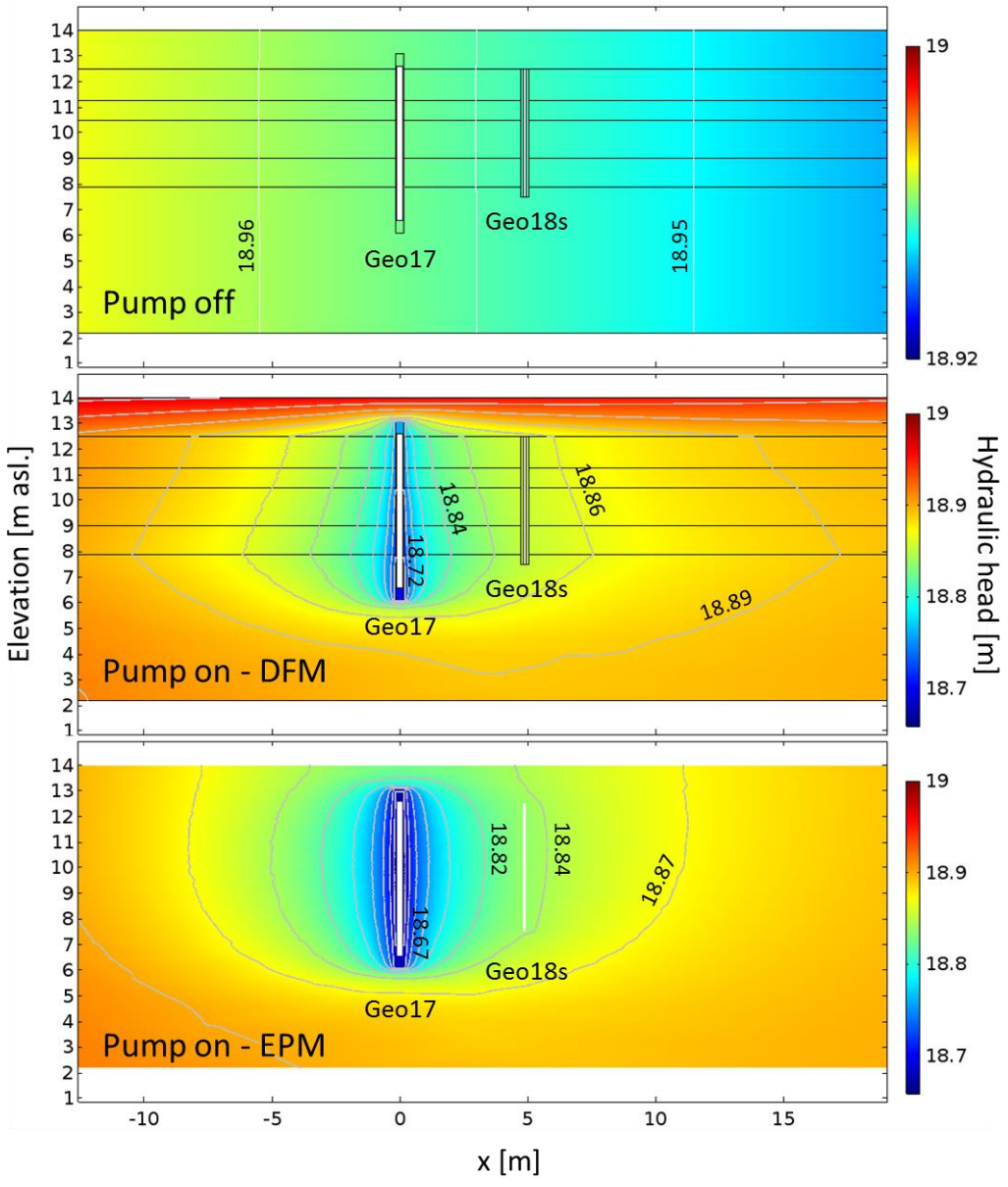

Figure 6.4: Hydraulic heads around the pumping well (left) and an injection well (Geo18s, right), without pumping (top) and with pumping in Geo17, simulated with DFM (middle) and EPM model (bottom). The gray lines are isopotential lines. The horizontal fractures have a strong influence on the head distribution and are dominating the flow. The head distributions simulated with the EPM model and the DFM differ considerably.

The DFM matched the observed data very well, even with this relatively simple setup with five horizontal fractures (Figure 6.3). The peak and the tailing could

both be described. Besides the diffusion coefficient, the parameters were in a reasonable range compared to measured data (from poroperm tests and slug and pumping tests).

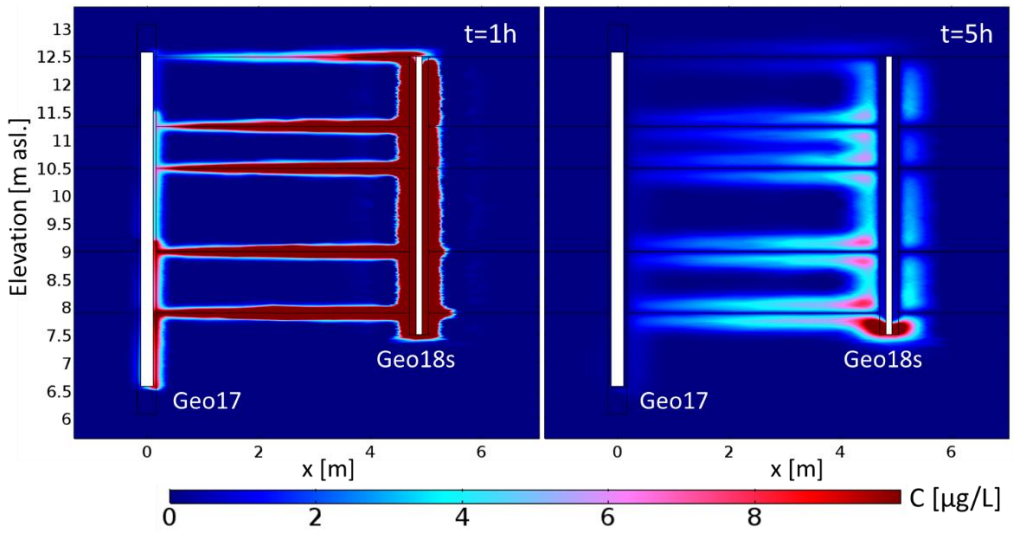

Figure 6.5: Simulated tracer distribution at the end of the injection (left) and 4 hours after the injection (right). The tracer is quickly drawn from the injection towards the pumping well. A part of the tracer diffuses from the fractures and the wells (gravel and sand pack) in the limestone matrix.

6.2.2 Injection in Geo18s 4 days before pump start

It is evident that both the EPM and DCM fail, when the model with parameters from the Geo18s test (while pumping) is applied to the pre-injection test (injection in Geo18s 4 days before pumping) in the same well (Figure 6.6). It can be seen that the equivalent porous medium model deviates strongly from the observations with far too high peak concentrations and hardly any tailing of the breakthrough curve. The dual-continuum model fits better, but also leads to overly high peak concentrations. However, this model may potentially be fitted to the observations if the parameters are adjusted properly.

The differences between the model results are pronounced because different transport mechanisms dominate in the preinjection test than in the other tracer tests. In the preinjection test, the tracer is injected and at first spreads in the fractures. Due to the pressure gradient induced by the injection, the tracer is also pushed upstream within the thin fractures. Figure 6.7 illustrates the behavior of the tracer over time after the tracer has been injected. In the four days before the pump is started, some of the injected tracer flows very fast through the fractures in the downstream direction with the groundwater flow and cannot be drawn back to the extraction well. Hence, the breakthrough curve mainly represents tracer that diffuses back from the matrix close to the fractures and from the sand packs around the borehole.

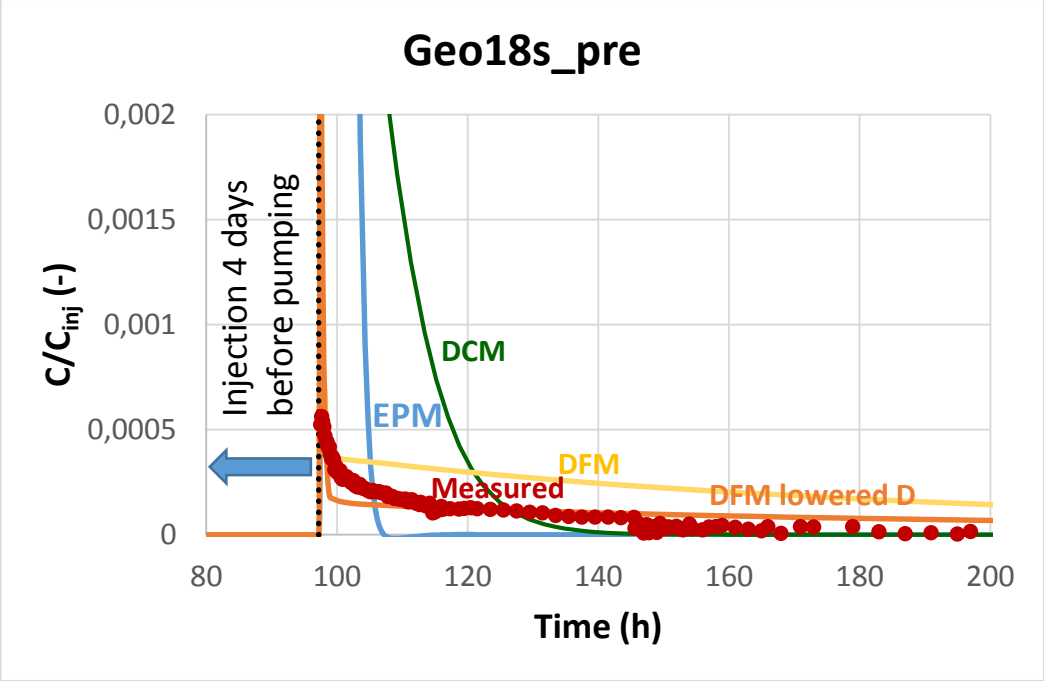

Figure 6.6: Comparison of different models applied to the tracer injection in Geo18s before the pump was started.

The discrete-fracture model leads to the best results of the three models. Without modification of the model setup obtained by calibration to the dataset from the test with tracer injection in Geo18s while pumping, the values were only slightly higher than the observed ones. If the effective diffusivity is lowered to 10^{-7} m^2/s, the breakthrough curve can be matched relatively well.

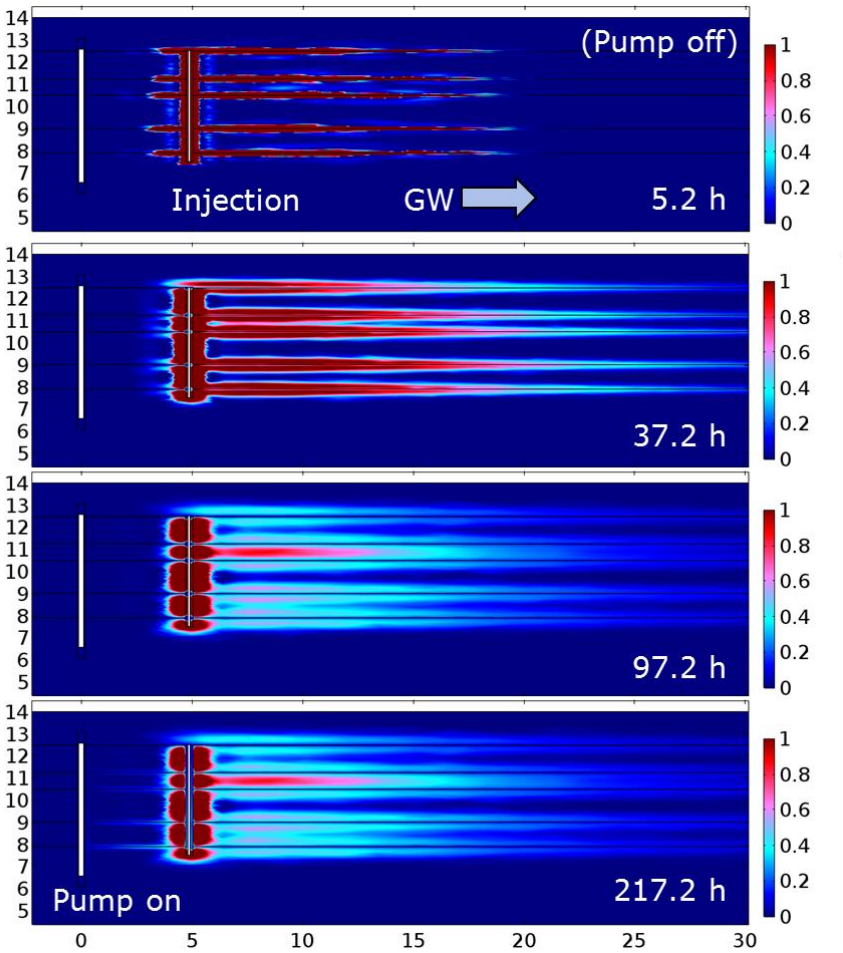

Figure 6.7: Simulation results with the discrete-fracture model showing the spreading of the tracer in the aquifer after the injection in Geo18s before pumping. The tracer propagates quickly in the fractures and then diffuses into the matrix. A considerable part of the tracer diffuses into the matrix around the injection well. After 97.2 hours, the pump (left) is switched on and draws tracer back.

6.2.3 Injection in Geo19d

Figure 6.8 demonstrates the large differences between the modeling results obtained when using a simple EPM model and a DFM. The discrete-fracture model is better able to reproduce the observed breakthrough behavior. While the EPM model shown in the figure fits reasonably well, the porosity needed (Table 6.1) is far below measured values.

Figure 6.9 shows that the EPM model can only match the fast tracer arrival using a very low porosity (0.5 %). An alternative suggested in the literature is to introduce heterogeneity in the EPM (Pedretti et al. 2013, Sanchez-Vila and Carrera, 2004). Heterogeneity can play the same role as fractures by introducing fast and slow transport zones. This can be seen in Figure 6.9, where results are shown for a model with a random statistical distribution of hydraulic conductivities with a variation of three orders of magnitude between highest and lowest conductivity. Such a model can potentially reproduce the tailing seen in the experimental data and in the DFM modeling results.

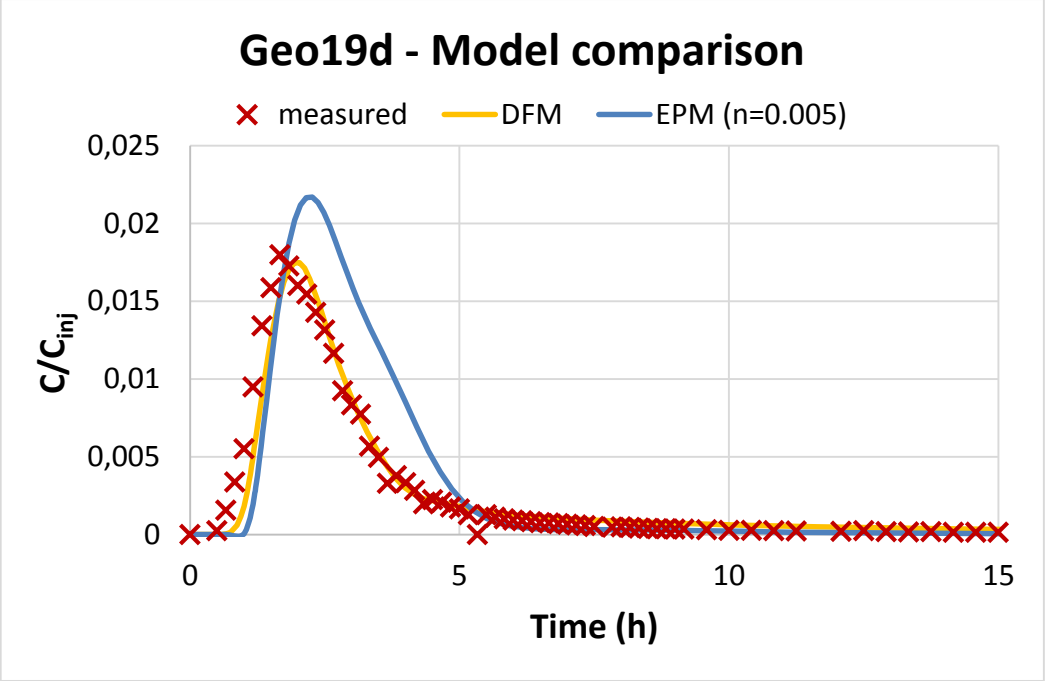

Figure 6.8: Comparison of the best fit for the tracer test in Geo19d using the equivalent porous medium model and the discrete-fracture model. The DFM can better reproduce the observed breakthrough curve. The EPM model predicts a higher peak concentration and gives a wrong approximation of the tailing of the breakthrough curve.

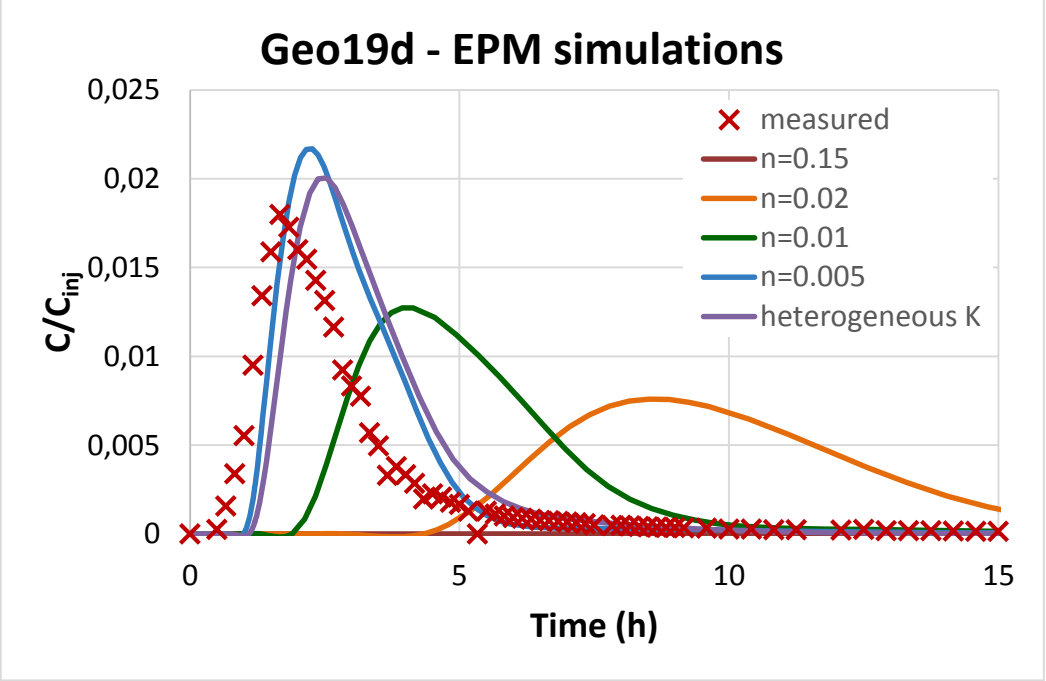

Figure 6.9: Comparison of observed and simulated tracer breakthrough curves for the tracer test in Geo19d using the equivalent porous medium model with different porosities n. Furthermore, the effect of a heterogeneous distribution of the hydraulic conductivity is shown. The same setup as for n=0.005 was used. For a porosity of 0.15, the tracer has not arrived at the pumping well after 15 h.

6.2.4 Other injections (Geo5, PB, Geo18d)

Discrete-fracture models were setup for all tracer tests. For the tracer test in Geo5, the discrete fracture model had to be slightly adjusted (not shown here). Two of the five fractures were deactivated to improve the match with the measured breakthrough curve. This indicates that the aquifer is heterogeneous and the

fracture connectivity between Geo5 and Geo17 is different to Geo18. It can also indicate a dominating orientation of vertical fractures.

It was difficult to match the breakthrough curves for the tracer tests in PB and Geo18d (results not shown here). In these tests, the vertical connectivity and vertical gradients are important, because the well screens are located at a different depth than the pumping well screen. Hence, a more complex fracture network would be required. Field information about vertical fractures was, however very limited. In the vertical boreholes, very few (sub-)vertical fractures could be observed and their aperture was small compared to the major horizontal fractures.

6.3 Choice of models for fractured limestone systems

Three model concepts have been tested for their applicability in fractured limestone systems. The pumping and tracer test data provided the unique possibility to compare the concepts with field data and to get an improved understanding of flow and transport processes in fractured limestone aquifers.

6.3.1 Equivalent porous medium model (EPM)

The EPM model is the simplest of the considered models and is widely used in practice. Compared to the other two models, it has low computational costs. It can be used for a rough approximation of the transport behavior of a substance, but must be used with care. The homogeneous equivalent porous medium model could only be fitted to the early arrival of the tracer by lowering the (effective) porosity. Very low porosity values (below 1 %) had to be chosen to fit the fast tracer arrival.

The peak concentrations were higher than those observed, because diffusion of tracer into the matrix is neglected by the model. This also leads to an earlier decrease of the tracer concentrations, and the tailing observed in measurements due to fracture-matrix interaction cannot be reproduced.

It is possible to obtain a tailing in the simulated breakthrough curve if a heterogeneous parameter distribution in the porous medium is included (Figure 6.9), introducing very conductive structures and less conductive structures that are less penetrated by flow (Pedretti et al. 2013). However, the variation of the hydraulic conductivity must be of a similar order of magnitude to the contrast between fracture and matrix conductivity and have a similar connectivity of the highly conductive zones (fractures). Note that a different vertical placement of the screens for injection and extraction can also lead to a tailing in the breakthrough curves. However, this does not account for fracture-matrix interaction and the storage effect of the matrix.

It is preferable from the point of view of the actual physics to describe fractures as discrete features. However, a very high grid resolution is required to account for thin fractures, so many smaller fractures cannot be included in a model. This can be accounted for by increasing the effective diffusion coefficient.

The use of an EPM model for the simulation of plume migration is not recommended, because exchange processes between fractures and matrix are generally neglected and model results may be misleading for risk assessment or

remedial planning. For example, remediation times can be greatly underestimated because the effect of back-diffusion from the matrix cannot be reproduced.

6.3.2 Dual-continuum model (DCM)

The dual-continuum model matches the observations better than the EPM model. The second continuum represents the matrix and the coupling of the two continua allows an exchange of tracer between fractures and matrix. With this model, the breakthrough behavior can be reproduced by fitting the fracture and matrix porosities and conductivities and the parameters governing the exchange behavior between fractures and matrix (D_{pm}, α, a). However, this concept has many degrees of freedom, and it is not clear how to determine the required parameters governing the fracture-matrix exchange experimentally. It is also reported in the literature to be a "black-box" model (Riley et al. 2001). The computational effort required to run this model type is usually moderate. It is not known whether the model is capable of consistently simulating contaminant plume behavior at both small (site) and larger (catchment) scales.

6.3.3 Discrete-fracture model (DFM)

The discrete-fracture model aims at representing the actual physics and yields the best results. Drawbacks are the often-limited knowledge of the fracture geometry and parameters and the large computational costs. The computational costs limit the amount of fractures that can be included. The diffusion coefficient must be augmented to account for neglected fractures and channeling within the fissures, increasing the diffusive exchange between fractures and matrix. This was already reported in the literature (Riley, Ward, and Greswell, 2001, DeDreuzy et al., 2013).

When setting up the model for the tracer tests in Geo18s, Geo19d and Geo5, it was sufficient to include just a few horizontal fractures to provide preferential flow paths for the tracer. The fractures were located to match flow log observations in the boreholes. The real medium is likely to have many more fractures on different scales, providing a bigger specific surface area for the exchange between fractures and matrix. This can be accounted for by adjusting the matrix diffusivity, which controls the exchange between fractures and matrix. In the simulations presented here, it had to be increased by a factor of 100 to 1000 in order to fit the observed breakthrough behavior.

6.3.4 Recommendations on model choice

The tracer tests and model applications have clearly shown that a crucial aspect of the transport of a substance in fractured limestone cannot be reproduced with a simple equivalent porous medium model: the diffusion and back-diffusion of a substance between fractures with strong flow and low-conductive matrix. In a fractured aquifer, this should be accounted for, or the propagation of a substance will not be realistically simulated. Hence, the use of a traditional equivalent porous medium model is not recommended for fractured limestone aquifers.

The dual-continuum model can describe the exchange between fractures and matrix while keeping computational efforts low. However, the specification of the exchange terms between fracture and matrix continuum has a crucial influence on

the modeling results and a physically-based choice is often challenging. It is not clear how to determine the exchange parameters by measurements. Further, it is questionable if a model, once calibrated, can be employed at a different scale without modifying the used parameters. A requirement for the use of a dual-continuum model is a fracture network with many connected fractures with a relatively uniform distribution, since the fractures are represented as averaged quantities in the fracture continuum.

The use of a discrete-fracture model comes with the cost of being the most complex and numerically demanding model described here. However, it represents the actual physics best and can, depending on the knowledge of the fracture system, lead to the best results. Usually, only few details about the fracture network are available. In this study, the information provided by flow logs could successfully be used to setup a representative network containing the major horizontal flow paths. But such a model does not contain smaller fractures and to compensate for that the diffusion coefficient governing the exchange between fractures and matrix had to be greatly increased. With that, the measured breakthrough curves from the tracer tests could be reproduced. The tracer test in Geo18s before pumping clearly shows that the discrete-fracture model best reproduced the observed data (see Figure 6.6).

Since matrix and fractures are both included in the model and the exchange between the two happens naturally (continuity of fluxes, concentrations and heads at the fracture-matrix interface), the discrete-fracture model is the recommended approach in cases were fractures dominate the transport behavior. Even a simple analytical tool (such as Chambon et al. 2011) or a dual-continuum model should be preferred to an equivalent porous medium model, which neglects the influence of the fractures.

6.4 What does this mean for plume behavior and remedial actions?

In terms of solute transport, the results have substantial ramifications. The neglect of fracture-matrix interaction can have several consequences including: errors in determining plume speeds; underestimation of contaminant remediation times; and poor estimation of well capture zones. These are described in the following sections.

6.4.1 Effect on plume travel speeds

Progressive plume attenuation due to matrix diffusion cannot be described by an EPM, hence the propagation speed of a contaminant is overestimated; this is especially important in the early travel times (first couple of months of the plume evolution), where the plume attenuation is most pronounced.

The very fast arrival of tracers contrasts sharply with the relatively slow movement of the PCE contaminant plume observed at the site, which has only moved about 400 m over a period of several decades. This means that contaminant plumes in fractured limestone do not spread with a constant velocity but slow down with time. To show this a 3D discrete-fracture model simulation of the contaminant plume was setup for the Akacievej site with the continuous release of PCE over

30 years into three fractures, which are located at the depths where high-flow zones were observed in the flow logs. Subsequently, a ten-year period without further contaminant release was simulated (removal of most contaminated soil at the site in 2006). An aperture of 1 mm was chosen. If a larger aperture of 2 mm is used (as in the tracer test evaluation), the plume spreads too fast. It is unlikely that fractures with such big aperture are continuous over the entire plume length (several hundred meters).

The simulations demonstrate that the diffusion of contaminant into the matrix leads to a progressive slowing of the plume (Figure 6.10 and Figure 6.11). This is reflected by the concentration isolines, which do not advance at a constant velocity. The advective transport within the fractures happens fast with the fracture flow velocity. However, diffusive exchange between fractures and the almost immobile water in the limestone matrix continuously removes contaminant mass from the fractures. This reduces the concentration along the fracture and slows down the advancement of the contaminant plume front (e.g. the 1 µg/L isoline) to a velocity considerably slower than the fracture flow velocity.

If the fractures are not accounted for by the chosen model concept, the effect of a continuous slowing of the plume propagation cannot be reproduced and plume extent will be overestimated. It is difficult to obtain field data that can show that the contaminant plume at Akacievej slows down. However, after a simulation time of 40 years, the plume simulated with the discrete fracture model had an approximate extent of 500 m. Despite the relatively simple model setup, this is only slightly longer than the observed extent of the plume in 2015 (approximately 400 m, Figure 1.5). For the EPM model with the parameters calibrated to the pumping and tracer test, a plume length of more than 500 meters is reached already after about ten years.

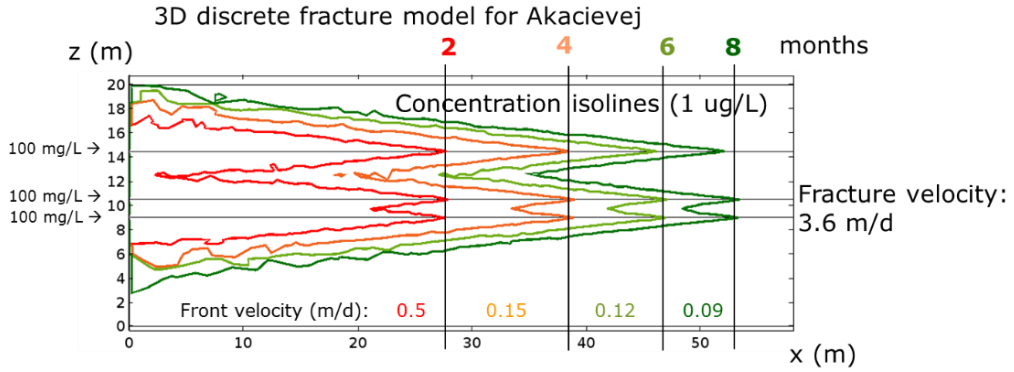

Figure 6.10: Simulated evolution of a plume for a substance continuously injected into three horizontal fractures. This was simulated with a 3D discrete fracture model. The substance enters through the fractures on the left and diffuses continuously into the matrix, leading to a slowing down of the plume propagation and a continuous increase of mass in the matrix.

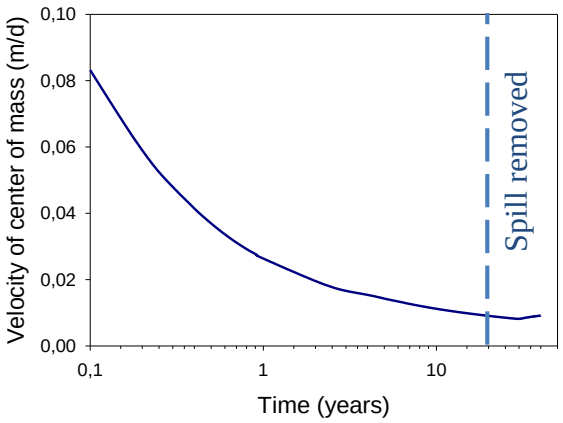

Figure 6.11: The center of mass of the plume slows down with time due to continuous diffusion of the contaminant into the matrix. The spill was removed after 30 years and the plume detaches slowly from the source zone.

6.4.2 Effect on cleanup times

Depending on the exposure time in the aquifer, a substantial part of the contaminant diffuses into the low-conductive matrix, where only little flow penetrates. The contaminant removal with a pump-and-treat system is then limited by back-diffusion from the matrix. In fact, once a contaminant has entered a fractured limestone aquifer it cannot be completely removed. Concentration gradients are not only towards the fractures but also into deeper areas of the matrix. This means that it will take a very long time and it is very difficult to remove the contaminant from the aquifer. With an equivalent porous medium model, the remediation times would be greatly underestimated.

A discrete-fracture model can be used for estimating the cleanup times and the optimization of a remediation strategy. However, it has to be used with care, especially for such heterogeneous systems. The hydromechanical properties of the fractures (e.g. aperture, geometry, spacing, connectivity) may be highly variable in space and an extrapolation of parameters determined by aquifer tests has to be done with care.

6.4.3 Difficulty in capture zone mapping

The complex flow field originating from fractures, flint inclusions and the local geology makes the delineation of the capture zones of pumping wells particularly difficult. Since the fractures are the main flow paths and there is only very little flow in the matrix, an approximation of the capture zone with a standard well capture-zone model may give a wrong approximation. The flow zones are very thin compared to the aquifer thickness and are dominated by flow in the fractures. At the Akacievej site, the fracture systems clearly play a major role in groundwater flow and this means that water is drawn from a much greater upstream distance than a standard EPM model would predict (Figure 6.12). The horizontal extent of the simulated capture zones with the DFM and the EPM model are, however, similar, because both models were fit to observed hydraulic head data and vertical fractures were not included in the DFM. If major vertical fractures were included

or the aperture of the horizontal fractures was spatially variable, then the fractures would direct the flow and the capture zone could have a very different shape.

Major vertical fractures aligned with the overall hydraulic head gradient would have a similar effect on the shape of the capture zone as the horizontal fractures in the cross sections shown in Figure 6.12 (bottom). In case of vertical fractures with a different orientation as the overall head gradient, the capture zone could be widened or have a different direction following the main direction of the fractures. Moreover, the simulated aquifer volume, where the pumping well withdraws water from within one day (red volumes in Figure 6.12), is very compact in the EPM model in contrast to the fracture-dominated volume simulated with the discrete-fracture model. This can be of particular importance for the planning of a pump-and-treat remediation system.

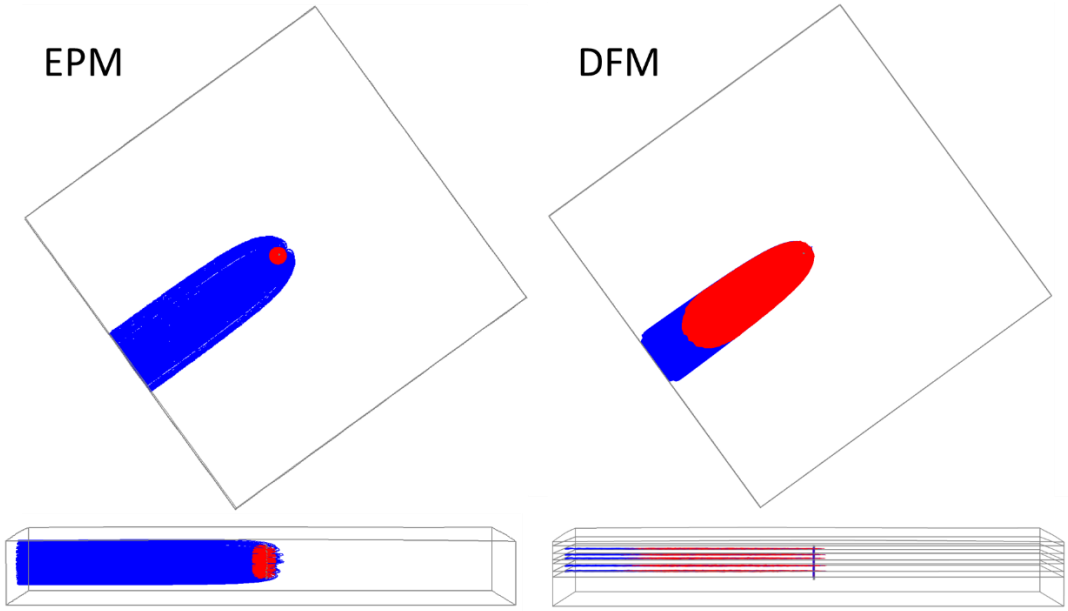

Figure 6.12: Computed capture zones with an EPM model (left) and a DFM (right) with a domain size of 100x100 m^2. The horizontal extent of the capture zone (top view) is similar, whereas the vertical shape differs considerably. The distance, from which water is withdrawn within one day (marked in red) is much longer in the DFM simulations. In a fractured medium with fast flow in the fractures, the water is withdrawn from a much greater distance within the same time as in a standard porous medium.

7. Key findings and conclusions

A combined pumping and tracer test in a fractured limestone has been designed and successfully conducted with a pumping period of almost four weeks. Six tracer tests from different directions with ionic and fluorescent tracers were conducted and PCE contamination data was collected before, during and after the pumping test. The PCE contamination data can be found in Broholm et al. (2016b). These tests allowed for a detailed characterization of the Akacievej site. Moreover, they provided valuable insights on the processes governing the fate and transport of substances in a fractured limestone aquifer. The collected data provided the unique possibility to set up a detailed model for the site and to distinguish different modeling approaches.

7.1 Aquifer parameters

Aquifer parameters could be determined
The *pumping test* yielded average hydraulic parameters for a relatively large volume of the fracture-matrix system (hydraulic conductivity or transmissivity). Information about the fractures (number of fractures, apertures, high flow zones, connectivity) is particularly crucial for the modeling of fractured aquifers. It is very challenging to conduct and interpret pumping tests in fractured limestone aquifers. The bulk hydraulic conductivity in the fractured limestone may be very large and the groundwater flow may be strong. Hence, the drawdown when pumping is initiated is extremely fast. Therefore, it may be difficult to identify different drawdown stages as described in Nielsen (2007). The time intervals for the head measurements have to be set very short (less than 1 s) at the beginning of the pumping test to obtain a good resolution of the drawdown.

The full development of the drawdown was observed within 7-10 days. The corrected drawdown curve was successfully used to estimate hydraulic parameters with standard software for aquifer tests (Aqtesolv). Specialized solution methods developed for fractured aquifers, like the Moench or Barker solution, allowed the estimation of parameters for both the fractures and matrix. The determined values indicate a strong conductivity contrast between fractures and matrix (about 4 orders of magnitude). With this contrast, flow occurs mainly in the fractures and the advective transport in the matrix is negligible. The monitoring of head in several observation wells next to the pumping well also allows for determination of a preferential flow direction (anisotropy) and reveals the connectivity between different wells. The measurements in observation well screens located at a similar depth as the screen of the pumping well are best suited for the determination of hydraulic conductivity values for that aquifer unit. When the well screen of the observation well is located in a different unit as the pumping well (e.g. pumping well in fractured limestone, observation well in crushed limestone), the determined parameters will represent a mixture of the two aquifer units.

Slug-tests are very useful for a quick and cheap analysis of the spatial variability of hydraulic aquifer parameters. Site investigations showed also that the bulk conductivity in the crushed limestone is potentially lower than in the fractured limestone. Slug tests indicate a conductivity of at least a factor 3 to 4 lower in the crushed limestone than in the upper regions of the fractured limestone at Akacievej. The contrast can be even bigger, because the gravel/sand packs around the boreholes influence the observed results. The values determined with slug tests were usually lower than the ones determined with the pumping test, but are within a similar range. The parameters determined with slug tests represent the parameters in a small region around the borehole, whereas a *pumping test* covers a much larger aquifer volume.

For systems with a high hydraulic conductivity, the developed slug test method obtained by placing a vacuum on the water table in the borehole were very useful. The changes of the water table caused by standard slug tests, where a slug of water is poured into the borehole, happen very quickly and it may be difficult to measure the head changes. For vacuum slug tests in a strongly fractured aquifer with a high

hydraulic conductivity, the measurement frequency should be very high (in the performed slug tests: 2 measurements per second; if possible an even higher frequency is recommended) to obtain a good breakthrough curve. Another important consideration is to ensure that the screen is (mostly) below the water table.

Another inexpensive and quick method to determine hydraulic parameters is the *evaluation of waterworks data*, as it was also done in this project. To employ this method, the measurement frequency at the waterworks was increased while pumps were switched on and off. The determined values showed a strong variation (Table 2.4), indicating a very heterogeneous aquifer. Note that the wells used by the water works often have long screens and that the determined values represent average properties over the screen length. The extrapolation of determined parameters to areas outside the well capture zone has to be done with care.

Furthermore, the drawdown caused by the *remediation system* provided information about the hydraulic parameters mainly in the crushed limestone, where the well screen is located. The determined hydraulic conductivity was considerably lower than the conductivity determined with the new pumping well, because the screen of the remediation well is located mainly in the crushed limestone with a lower conductivity than the fractured limestone.

The *poroperm tests* of mainly intact limestone cores were useful to determine the hydraulic conductivity and porosity of the limestone matrix. A very strong contrast between fracture and matrix conductivity was observed, spanning across several orders of magnitudes (between 5 and 8). With such strong contrast, the contribution of advective transport in the matrix to the overall transport is negligible.

The breakthrough curves from *tracer tests* were crucial for the improvement of the conceptual understanding of transport in fractured limestone aquifers. Models could be fitted to the data by adjusting the transport parameters (diffusion/dispersion coefficients). This revealed the dominating influence of the fractures on the transport behavior and allowed the testing of different model concepts. It is, however, clear, that such tracer tests cannot be done at every site. The lessons learned from this tracer test can be transferred to similar sites.

7.2 Specific findings for Akacievej

High-flow zones and the hydraulically active part of the aquifer were determined

Flow logs and geophysical measurements (optical televiewer) provided very valuable information about the location of high-flow zones and fractures. This information was successfully integrated in a discrete fracture model. Furthermore, the flow log in the deep screen of Geo18 showed that there is only a very small flow below a certain depth (36 m bgs.). Hence, the elevation of the bottom of the hydraulically active part of the limestone aquifer at the site could be determined.

Complex three-dimensional flow field is dominated by fractures

The pumping and tracer tests clearly show the importance of fracture flow and transport and of the connectivity of the fracture system. The fractures and the geology lead to a complex three-dimensional flow field. This could be observed in both the pumping test drawdown in observation wells and in the tracer breakthrough curves from injections in different wells. For example, the drawdown in Geo18s and Geo19d was comparable despite Geo19d being almost three times further away from the pumping well (Geo17). However, at shallow depths the drawdown in Geo19s was much smaller. Furthermore, the breakthrough curves from PB and Geo18d, which have their screens in a different depth than the pumping well, have a very different behavior to the injections at a similar depth – the tracer breakthrough took much longer and the recovery was lower, indicating a poor connectivity between the wells.

Fractures dominate the transport behavior
The pumping and tracer test and the flow logs showed that flow occurs primarily through fractures. The tracer breakthrough from Geo18s, Geo19d and Geo5 happened very quickly with very early arrival times, showing the importance of the fracture flow. This dominates also the transport behavior especially at early times and can lead to an unexpected transport of contaminant, even in different directions as the hydraulic head gradients may suggest. Others have observed a similar behavior in natural-gradient tracer tests in fractured aquifer, where the tracer appeared at unexpected observation wells (Bottrell et al. 2010). This has implications on the mapping of capture zones. Standard well capture models will incorrectly estimate the areas affected by pumping.

The transport properties of the crushed limestone are very different to the fractured limestone. The crushed zone had a much lower hydraulic conductivity at the Akacievej site. Indeed, the difference between bryozoan and Copenhagen limestone was far less important than the difference between the crushed and fractured limestone. This may be due to the flat bank structure of the bryozoan limestone in the area and can be different at other sites, where the bank structure is more pronounced leading to longer travel paths for substances.

Vertical plume extent was determined
Multilevel sampling in the deep screen of Geo18d allowed for the vertical extent of the PCE plume to be delineated (see Broholm et al. 2016b). PCE contamination is limited to the upper 20 m of the limestone at the site. The tracer tests and modeling interpretation showed that the vertical connectivity and conductivity is much less than the horizontal one, which limits the vertical plume spreading and also the vertical extent of the aquifer that is affected by remedial pumping.

7.3 General findings, flow and transport

Traditional contaminant transport models do not work
Traditional contaminant transport models do not include the interaction of fractures and matrix and are not recommended for fractured limestone geologies similar to the Akacievej site. An equivalent porous medium model was not able to simulate the breakthrough curve from the tracer injection in the shallow screen of

Geo18s before pumping. There, matrix diffusion is very important, as it is for the propagation of a contaminant plume.

It has been shown that the fractures are also very important for contaminant plume migration. If a traditional contaminant transport model is applied for plume migration and remedial planning, wrong predictions will be obtained; it is better to use a simple analytical model that accounts for fracture transport, or model concepts like the dual-continuum model or the discrete-fracture model.

A dual-continuum model could be fitted to the observed tracer breakthrough curves. However, the determination of the exchange parameters between fractures and matrix is difficult, and it is questionable whether the model can simulate different scales.

The discrete-fracture model was best able to reproduce tracer test data. The effect of plume slowing on a larger scale could be reproduced by such a model. Here, the complexity of the fracture network (how many fractures should be included?) and the choice of the diffusion coefficient are critical.

Use of models at the early stage of a project are beneficial

The combination of fieldwork and modeling was shown to be very beneficial. Models were set up at an early stage based on an initial conceptual understanding and field data. They were used for the planning of further investigations, such as the drilling of new boreholes, the placement of well screens or the choice of the pumping rate. The data obtained from the field investigations improved the conceptual understanding and the models. Using models already at an early stage of a project for the planning of further actions is strongly recommended.

Plume propagation slows with time

The very fast arrival of tracers contrasts sharply with relatively slow movement of a PCE contaminant plume. The matrix diffusion from the fractures leads to a progressive slowing of the plume migration with time (plume attenuation). Initially, a contaminant can propagate very quickly in the fractures. Due to the diffusion of contaminant into the matrix along the fracture, the plume front will continuously slow down with time. The transport velocity of the plume is then considerably lower than the flow velocities in the fractures suggest. The progressive slowing of a contaminant plume can be described using discrete fracture model simulations.

Remediation will take a very long time

The advection-dominated transport occurs mainly through (horizontal) fractures which connect the infiltration and extraction well. Due to strong concentration gradients, a transported substance diffuses into the matrix next to the fractures. Once diffused into the matrix, pump-and-treat remediation removes the contaminant only through back-diffusion from the matrix, which takes a very long time. The transport behavior is dependent on the time scale of the considered processes. Typically, the system is dominated by advective transport in fractures for short time scales, and matrix diffusion-dominated over longer time scales.

Long-term matrix diffusion is very important for the transport and storage of a substance in the aquifer.

Improved planning of remedial activities based on modeling

The vertical location of well screens is very important for the tracer transport and for the success of a pump-and-treat remediation system at the site. The pumping and tracer test and the contamination measurements allowed the aquifer and contaminant plume to be characterized. An advanced model can then be used to evaluate and optimize a remediation system.

Literature

Batu, V., 1998. Aquifer hydraulics. New York: John Wiley and Sons, Inc.

Besora, P.R., 2016. Design and verification of a tracer injection test for contaminant transport characterization of a fractured limestone aquifer. MSc-rapport, DTU Miljø.

Brabæk et al. 2015. Undersøgelsesmetoder af chlorerede opløsningsmidler i sprækkede kalkmagasiner. Fagpakkeprojekt. DTU Miljø.

Britt, S.L. 2005. Testing the In-Well Horizontal Laminar Flow Assumption with a Sand-Tank Well Model. Ground Water Monitoring & Remediation 25 (3): 73–81.

Britt, S.L., Parker, B.L., Cherry, J.A. (2010). A Downhole Passive Sampling System to Avoid Bias and Error from Groundwater Sample Handling. Environ. Sci. Technol. 44 (13): 4917–4923.

Bottrell, S. H. et al. (2010). Assessment of the Use of Fluorescent Tracers in a Contaminated Chalk Aquifer. Quarterly Journal of Engineering Geology and Hydrogeology 43(2): 195–206.

Broholm, M.M., Janniche, G., Mosthaf, K., Fjordbøge, A.S., Binning, P.J., Christensen, A.G., Grosen, B., Jørgensen, T.H., Keller, C., Wealthall, G., Kerrn-Jespersen, H., 2016a. Characterization of chlorinated solvent contamination in limestone using innovative FLUTe® technologies in combination with other methods in a line of evidence approach. Journal of Contaminant Hydrology, 189, 68–85.

Broholm, M.M., Fjordbøge, A.S., Mosthaf, K., Brauns, B., Bjerg, P.L., Binning, P.J., 2016b. Sammenligning af niveauspecifikke prøvetagningsmetoder for vurdering af koncentrationsfordeling i kalkmagasin. Report, DTU Miljø.

Chambon, Julie C, Philip J Binning, Peter R Jørgensen, and Poul L Bjerg. 2011. A Risk Assessment Tool for Contaminated Sites in Low-Permeability Fractured Media." Journal of contaminant hydrology 124(1–4): 82–98.

DeDreuzy, J.-R., Rapaport, A., Babey, T., and J. Harmand. 2013. Influence of porosity structures on mixing-induced reactivity at chemical equilibrium in mobile/immobile Multi-Rate Mass Transfer (MRMT) and Multiple Interacting Continua (MINC) models. Water resources research 49, 8511-8530.

Duffield, G. M., 2007. Aqtesolv for windows ver. 4.50.002, s.l.: s.n.

Geo, 2005a. Høje Taastrup. Fløng. Akacievej 2. Afværgeprogram. GEO projekt nr. 25964. Rapport 2, 2005-02-22

Geo, 2005b. Høje Taastrup. Fløng. Akacievej 2. Skitseprojekt. GEO projekt nr. 25964. Rapport 3.

Geo, 2006. Hydrogeologiske og grundvandskemiske undersøgelser, GEO projekt nr. 28837. Rapport 1.

Geo, 2008. Høje-Taastrup, Fløng. Akacievej 2. Afværgeforanstaltninger. Etablering og indkøring. GEO projekt nr. 29885. Rapport 1, 2008-02-15.

Geo, 2015. Høje-Taastrup. Akacievej 2. Geologisk og hydrogeologisk undersøgelse. Resultater og konceptuelmodel. GEO projektnr. 37952.

Geo, 2016. Unpublished data.

Geo og GEUS, 2014. Strømning og stoftransport i kalklagene på den københavnske vestegn. Geologisk og hydrologisk vidensopsamling og typemodel. 37208. Rapport 1.

Gonthier, G., 2007. A graphical method for estimation of barometric efficiency from continuous data- concepts and application to a site in the piedmont, Air Force Plant 6, Marietta, Geogia, Virginia, USA: U.S Geological Survey.

Hartmann, S., N. E. Odling, and L. J. West, 2007. A Multi-Directional Tracer Test in the Fractured Chalk Aquifer of E. Yorkshire, UK. Journal of Contaminant Hydrology, 94(3–4): 315–31.

Lloyd, J.W. et al. 1996. An Integrated Study of Controls on Solute Transport in the Lincolnshire Limestone. Quarterly Journal of Engineering Geology 29: 321–39.

Moench, A. F., 1984. Double porosity models for a fissured groundwater reservoir with fracture skin. Water Resources Research, 20(7), pp. 831-846.

Mosthaf, K., Binning, P.J., Fjordbøge, A.S., Broholm, M.M., Bjerg, P.L., 2015a. Effect of remedial pump stop for 6 months at the Akacievej site. Short note, DTU Miljø.

Mosthaf, K., Fjordbøge, A.S., Broholm, M.M., Bjerg, P.L., Binning, P.J., 2015b. Risk assessment of the tracer injection at the Akacievej site. Updated 2016. Short note, DTU Miljø.

Mosthaf, K., Fjordbøge, A.S., Broholm, M.M., Bjerg, P.L., Binning, P.J., 2015c. Tracer selection for the pump and tracer test at the Akacievej site. Short note, DTU Miljø.

Nielsen, Kurt Ambo, 2007. Fractured Aquifers. Trafford publishing.

Pedersen, L.C., Vilsgaard, K.D., Broholm, M.M., Bjerg, P.L., 2014. Overblik over lokaliteter i værkstedsområderne. DTU Miljø og Region Hovedstaden, 2014.

Riley, M.S., R.S. Ward, and R.B. Greswell, 2001. Converging Flow Tracer Tests in Fissured Limestone. Quarterly Journal of Engineering Geology and Hydrogeology 34: 283–97.

Salzer, J., 2013. Sorption capacity and governing parameters for transport of chlorinated solvents in fractured limestone. MSc-report, DTU Miljø.

Tanaka, K., and Masao N., 1987. Measurements of Tracer Diffusion Coefficients of Lithium Ions, Chloride Ions and Water in Aqueous Lithium Chloride Solutions. Journal of the Chemical Society, Faraday Transactions 1, 83: 1779–1782.